Altair® AcuSolve® 2022.2

Altair AcuSolve Training Manual

Updated: 11/14/2022

Intellectual Property Rights Notice

This Intellectual Property Rights Notice is exemplary, and therefore not exhaustive, of intellectual property rights held by Altair Engineering Inc. or its affiliates. Software, other products, and materials of Altair Engineering Inc. or its affiliates are protected under laws of the United States and laws of other jurisdictions. In addition to intellectual property rights indicated herein, such software, other products, and materials of Altair Engineering Inc. or its affiliates may be further protected by patents, additional copyrights, additional trademarks, trade secrets, and additional other intellectual property rights. For avoidance of doubt, copyright notice does not imply publication. Copyrights in the below are held by Altair Engineering Inc. or its affiliates. Additionally, all non-Altair marks are the property of their respective owners.

This Intellectual Property Rights Notice does not give you any right to any product, such as software, or underlying intellectual property rights of Altair Engineering Inc. or its affiliates. Usage, for example, of software of Altair Engineering Inc. or its affiliates is governed by and dependent on a valid license agreement.

Altair Simulation Products

Altair® AcuSolve® ©1997-2022

Altair Activate® ©1989-2022

Altair® Battery Designer™ ©2019-2022

Altair Compose® ©2007-2022

Altair® ConnectMe™ ©2014-2022

Altair® EDEM™ ©2005-2022

Altair® ElectroFlo™ ©1992-2022

Altair Embed® ©1989-2022

Altair Embed® SE ©1989-2022

Altair Embed®/Digital Power Designer ©2012-2022

Altair Embed® Viewer ©1996-2022

Altair® ESAComp® ©1992-2022

Altair® Feko® ©1999-2022

Altair® Flow Simulator™ ©2016-2022

Altair® Flux® ©1983-2022

Altair® FluxMotor® ©2017-2022

Altair® HyperCrash® ©2001-2022

Altair® HyperGraph® ©1995-2022

Altair® HyperLife® ©1990-2022

Altair® HyperMesh® ©1990-2022

Altair® HyperStudy® ©1999-2022

Altair® HyperView® ©1999-2022

Altair® HyperWorks® ©1990-2022

Altair® HyperXtrude® ©1999-2022

Altair® Inspire™ ©2009-2022

Altair® Inspire™ Cast ©2011-2022

Altair® Inspire™ Extrude Metal ©1996-2022

Altair® Inspire™ Extrude Polymer ©1996-2022

Altair® Inspire™ Form ©1998-2022

Altair® Inspire™ Mold ©2009-2022

Altair® Inspire™ PolyFoam ©2009-2022

Altair® Inspire™ Print3D ©2022

Altair® Inspire™ Render ©1993-2022

Altair® Inspire™ Studio ©1993-2022

Altair® Material Data Center™ ©2019-2022

Altair® MotionSolve® ©2002-2022

Altair® MotionView® ©1993-2022

Altair® Multiscale Designer® ©2011-2022

Altair® nanoFluidX® ©2013-2022

Altair® OptiStruct® ©1996-2022

Altair® PollEx™ ©2003-2022

Altair® PSIM™ ©2022

Altair® Pulse™ ©2020-2022

Altair® Radioss® ©1986-2022

Altair® romAI™ ©2022

Altair® SEAM® ©1985-2022

Altair® SimLab® ©2004-2022

Altair® SimLab® ST ©2019-2022

Altair SimSolid® ©2015-2022

Altair® ultraFluidX® ©2010-2022

Altair® Virtual Wind Tunnel™ ©2012-2022

Altair® WinProp™ ©2000-2022

Altair® WRAP™ ©1998-2022

Altair® S-FRAME® ©1995-2022

Altair® S-STEEL™ ©1995-2022

Altair® S-PAD™ ©1995-2022

Altair® S-CONCRETE™ ©1995-2022

Altair® S-LINE™ ©1995-2022

Altair® S-TIMBER™ ©1995-2022

Altair® S-FOUNDATION™ ©1995-2022

Altair® S-CALC™ ©1995-2022

Altair® S-VIEW™ ©1995-2022

Altair® Structural Office™ ©2022

Altair®HyperViewPlayer® ©2022

Altair Packaged Solution Offerings (PSOs)

Altair® Automated Reporting Director™ ©2008-2022

Altair® e-Motor Director™ ©2019-2022

Altair® Geomechanics Director™ ©2011-2022

Altair® Impact Simulation Director™ ©2010-2022

Altair® Model Mesher Director™ ©2010-2022

Altair® NVH Director™ ©2010-2022

Altair® NVH Full Vehicle™ ©2022

Altair® NVH Standard™ ©2022

Altair® Squeak and Rattle Director™ ©2012-2022

Altair® Virtual Gauge Director™ ©2012-2022

Altair® Weld Certification Director™ ©2014-2022

Altair® Multi-Disciplinary Optimization Director™ ©2012-2022

Altair HPC & Cloud Products

Altair® PBS Professional® ©1994-2022

Altair® PBS Works™ ©2022

Altair® Control™ ©2008-2022

Altair® Access™ ©2008-2022

Altair® Accelerator™ ©1995-2022

Altair® Accelerator™ Plus ©1995-2022

Altair® FlowTracer™ ©1995-2022

Altair® Allocator™ ©1995-2022

2022.2

September 12, 2022

Technical Support

Altair provides comprehensive software support via web FAQs, tutorials, training classes, telephone, and e-mail.

Altair One Customer Portal

Altair One (https://altairone.com/) is Altair's customer portal giving you access to product downloads, a Knowledge Base, and customer support. We recommend that all users create an Altair One account and use it as their primary portal for everything Altair.

When your Altair One account is set up, you can access the Altair support page via this link: www.altair.com/customer-support/

Altair Community

Participate in an online community where you can share insights, collaborate with colleagues and peers, and find more ways to take full advantage of Altair's products.

Visit the Altair Community (https://community.altair.com/community) where you can access online discussions, a knowledge base of product information, and an online form to contact Support. After you login to the Altair Community, subscribe to the forums and user groups to get up-to-date information about release updates, upcoming events, and questions asked by your fellow members.

These valuable resources help you discover, learn and grow, all while having the opportunity to network with fellow explorers like yourself.

Altair Training Classes

Altair's in-person, online, and self-paced trainings provide hands-on introduction to our products, focusing on overall functionality. Trainings are conducted at our corporate and regional offices or at your facility.

For more information visit: https://learn.altair.com/

If you are interested in training at your facility, contact your account manager for more details. If you do not know who your account manager is, contact your local support office and they will connect you with your account manager.

Telephone and E-mail

If you are unable to contact Altair support via the customer portal, you may reach out to technical support via phone or e-mail. Use the following table as a reference to locate the support office for your region.

When contacting Altair support, specify the product and version number you are using along with a detailed description of the problem. It is beneficial for the support engineer to know what type of workstation, operating system, RAM, and graphics board you have, so include that in your communication.

Location	Telephone	E-mail
Australia	+61 3 9866 5557	anzsupport@altair.com

Location	Telephone	E-mail
Brazil	+55 113 884 0414	br_support@altair.com
Canada	+1 416 447 6463	support@altairengineering.ca
China	+86 400 619 6186	support@altair.com.cn
France	+33 141 33 0992	francesupport@altair.com
Germany	+49 703 162 0822	hwsupport@altair.de
Greece	+30 231 047 3311	eesupport@altair.com
India	+91 806 629 4500 +1 800 425 0234 (toll free)	support@india.altair.com
Israel		israelsupport@altair.com
Italy	+39 800 905 595	support@altairengineering.it
Japan	+81 3 6225 5830	support@altairjp.co.jp
Malaysia	+60 32 742 7890	aseansupport@altair.com
Mexico	+52 55 5658 6808	mx-support@altair.com
New Zealand	+64 9 413 7981	anzsupport@altair.com
South Africa	+27 21 831 1500	support@altair.co.za
South Korea	+82 704 050 9200	support@altair.co.kr
Spain	+34 910 810 080	support-spain@altair.com
Sweden	+46 46 460 2828	support@altair.se
United Kingdom	+44 192 646 8600	support@uk.altair.com
United States	+1 248 614 2425	hwsupport@altair.com

If your company is being serviced by an Altair partner, you can find that information on our web site at https://www.altair.com/PartnerSearch/.

See www.altair.com for complete information on Altair, our team, and our products.

Contents

AcuSolve Training Manual

1

Introduction of background knowledge regarding flow physics and CFD as well as detailed information about the use of AcuSolve and what specific options do.

The AcuSolve training class is to teach engineers or students who have no previous experience with AcuSolve. The training class is intended to be a modular format that allows instructors to choose what topics to cover. Each module contains a detailed explanation of the content in the form of a reference (or training) manual, and comes with a condensed version of the content in the form of a presentation. The presentation material is intended to be used by the instructors for teaching the class, while the training manual is intended to be a resource for those that want additional information on a given topic. The training manual contains the following topics:

- Brief introduction about CFD, its history, applications and advantages
- Basics of flow phenomena, including flow models, governing equations
- Turbulence physics and its modeling
- Introduction to AcuSolve, its background and features
- Hands on training on the use of AcuSolve and its supporting features using tutorials

Introduction to CFD and AcuSolve

2

This chapter covers the following:

Fluid Analysis Overview

This section details the various approaches available for analyzing a general fluid flow problem. It also provides pros and cons for each of these approaches.

Analysis of any physical problem, in general, is governed by a set of basic governing equations. The basic equations governing the motion of fluids are the Navier-Stokes equations, which were developed more than 150 years ago.

Continuity Equation

$$\frac{\partial \rho}{\partial t} + \nabla \cdot (\rho \vec{u}) = 0 \quad (1)$$

Momentum Equation

$$\rho \frac{\partial \vec{u}}{\partial t} + (\rho \vec{u} \cdot \nabla)\vec{u} = -\nabla p + \rho b + \nabla \cdot \tau \quad (2)$$

Energy Equation

$$\rho \frac{\partial h}{\partial t} + (\rho \vec{u} \cdot \nabla)h = \nabla \cdot (k \nabla T) + \nabla \vec{u} : \tau + \frac{Dp}{Dt} + S \quad (3)$$

These equations are a set of coupled partial differential equations which describe the relation among the flow properties like pressure, temperature and velocity. The solution to the above equations is in general complex because of the non-linear terms and coupled nature of the equations. However, in general the following three solution approaches are available:

Analytical Approach

An analytical solution can be obtained by integrating the above boundary value problem, resulting in an algebraic equation for the dependent variables as a function of independent variables. Because of the complexity of the Navier-Stokes equations a general solution for all physical problems is an insurmountable task. However, analytical solution is possible in some simple cases with certain approximations in geometry, dimensionality and compressibility of the flow. A few examples of such flows include Couette flow, Hagen-Poiseuille flow and Parelle flows through straight channels. An obvious limitation of this approach is the practical applications of these flows.

Experimental Approach

This approach uses the physical experiments on the scale down models of the problem at hand and extrapolates the results based on similarity laws. For example, to investigate the flow around an actual aircraft a Reynolds number based miniature model is placed in the wind tunnel and the results are extrapolated to that of the actual aircraft. Although a variety of experimental techniques are available, the choice of the particular type to use depends on capturing the parameter of interest. For example, Particle Image Velocimetry (PIV), Laser Doppler Velocimetry (LDV) and Hot-wire anemometry are used to measure flow velocity. PIV is used to produce 2D or 3D vector fields. Hot-wire anemometry and LDV are used when measuring the rapidly varying velocities at a

point with good spatial and time resolution is important. A few limitations of this approach include the necessity of conducting a large number of experiments for the complete description of flow, cost and the complexity of conducting them.

Numerical Approach (Computational Fluid Dynamics-CFD)

The third approach available for investigating fluid flow is CFD. In this approach, the fluid region of interest is divided into finite regions and the complex governing equations are discretized to obtain a set of algebraic equations that are advanced in time and space using computers. The end result of the CFD analysis is a complete description of the fluid flow within the region of interest.

CFD Brief History

This section details the advancements in CFD research throughout the twentieth century.

Although the study of fluid mechanics is centuries old most of the evolution of CFD took place throughout the twentieth century. By the start of the twentieth century all of the basic governing equations were consolidated. Closed form analytical solution for simple problems were derived putting aside the large set of problems of practical significance that are not suitable for analytical solution. Before the 1950's the main focus was on developing a variety of approximated semi analytical techniques such as perturbation methods for viscous boundary layer calculations, a method of characteristics for compressible flow calculations alongside the numerical solution development. By the mid-century the Finite difference based numerical methods were developed. However, the numerical algorithms until the fifties provided a solution to the single partial differential equations limited by the computation power. With the advent of digital computers the development of numerical simulation was put on an accelerated path. During the fifties and sixties significant developments were made on solution of inviscid compressible flows.

The seventies largely focused on inviscid flows over geometries like airfoils, wings and wing-body combinations. During the eighties intense efforts were made on algorithms for solution of Euler equations which include rotational flows but still inviscid. Research on grid generation was invested in the late eighties which presented a challenge in generating suitable grids for the computational domain of complex geometries. During the late eighties the transonic flow computations with viscous compressible flow over airfoils was made possible. This resulted in designing the super critical airfoils computationally with reduced wave drag. For the first time one could move away from the catalogued airfoil shapes to custom-designed airfoils to suite design end.

In the nineties the power of parallel computing paved the way for turbulence modeling in the flow. Turbulence was incorporated using turbulence modeling techniques such as Reynolds-averaged Navier Stokes (RANS) and Large Eddy Simulation (LES) along with Direct Numerical Simulation (DNS) without any modeling. This period marked the beginning of an era of commercial software capable of impressive visualization of vast numerical data generated by the CFD simulation of flow fields.

CFD Advantages

This section details the diverse advantages of CFD.

Several of the many possible advantages of CFD are listed below:

- Evaluation of performance before modifying or installing a system.

  Without commissioning a real system CFD results can forecast critical regions for improved performance.
- Provides detailed information of the variables on the complete domain.

  CFD simulation can provide all of the information in a single run, unlike the experiments that require multiple runs for evaluating different variables.
- Non-intrusive techniques with powerful visualizing techniques.

  Some of the experiments are intrusive, such as measuring equipment interfering with the flow under consideration, which can be eliminated with CFD.
- The possibility to have a variety of post-processing providing a deeper insight of results.

  CFD can help with evaluating the user-defined variables such as drag and pressure coefficient directly.
- Costs much less than experiments with lesser turnaround times.

  Most of the experimental equipment is costly and requires a large amount of time and expertise in setting up the experiment unlike CFD simulation.

CFD Applications

This section details the few of the numerous industries in which CFD has become indispensable.

CFD has become an indispensable tool in diverse industries for a variety of applications.

Aerospace Industries

The development of CFD in its formative years was mostly driven by the Aerospace industry. From the initial design and development phases of an aircraft the application of CFD is prominent in various modules of aerodynamics design such as configuration design, estimation of aerodynamic loads, estimation of stability derivatives and performance of engines. The design and development of today's state of the art missiles and launch vehicles would be unimaginable without CFD.

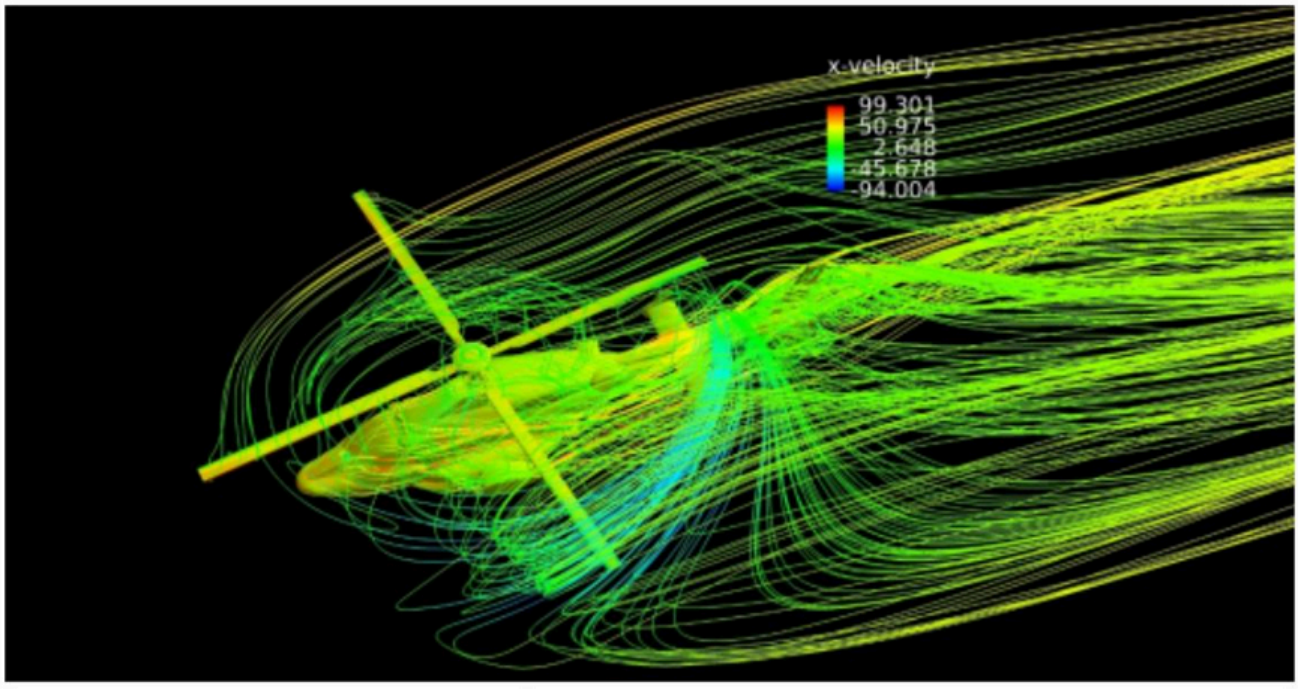

Figure 1:

Automotive Industries

The fuel efficient and stream lined automobiles in today's market are results of extensive use of CFD analysis. For example, CFD tools play a big part in external aerodynamics, the engine coolant jacket, under hood thermal management and passenger comfort.

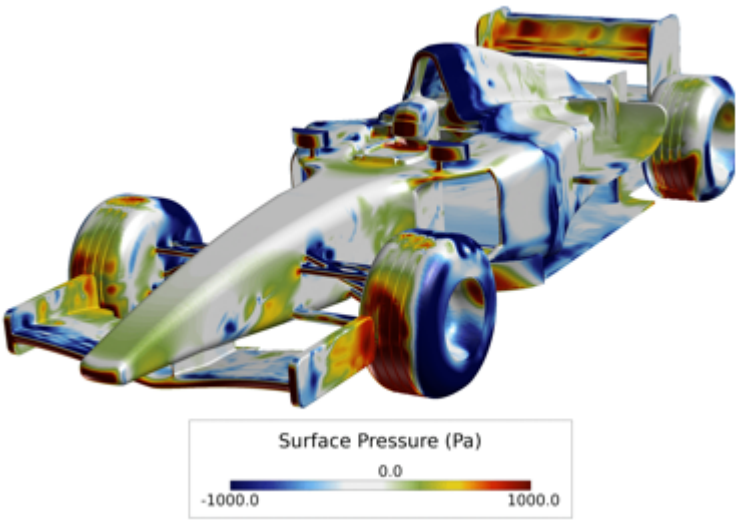

Figure 2:

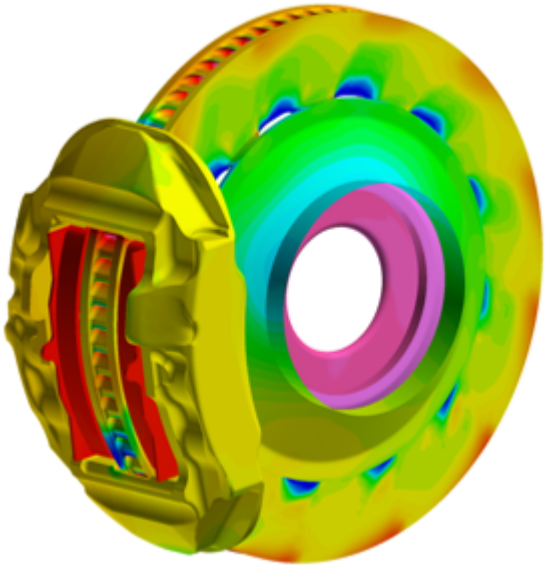

Figure 3:

Civil Engineering

CFD is used for building aerodynamics, hydraulic systems, aeroacoustics, fire and smoke simulation resulting in improved safety features at lower costs.

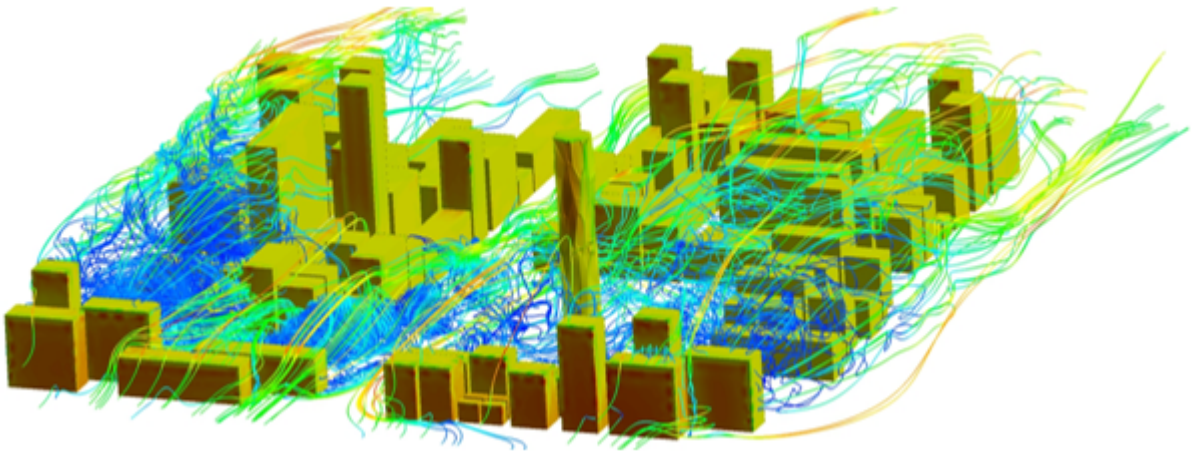

Figure 4:

Naval Engineering

CFD is a major tool in solving hydrodynamic problems associated with harbors, ships, submarines, torpedoes, oil exploration platforms, and so on.

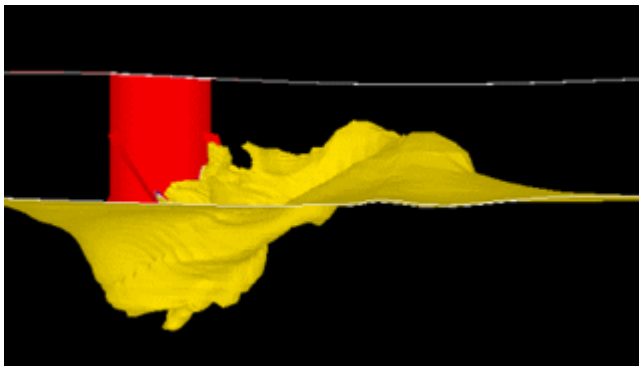

Figure 5:

HVACR Engineering

CFD is used for heating, ventilation, air conditioning and refrigeration applications. CFD analysis gives a detailed description of fluid flow, heat transfer and chemical species transfer in HVAC systems.

Figure 6:

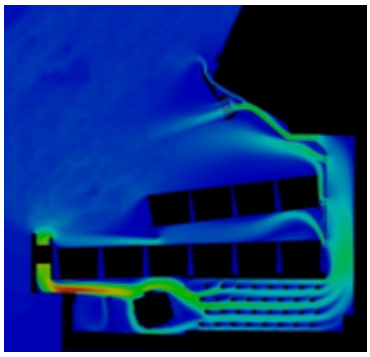

Figure 7:

Heavy Engineering

Heavy engineering is another industry that has a strong presence of CFD applications. CFD provides greater insight for the design of products, such as earth moving machinery, cranes and excavators

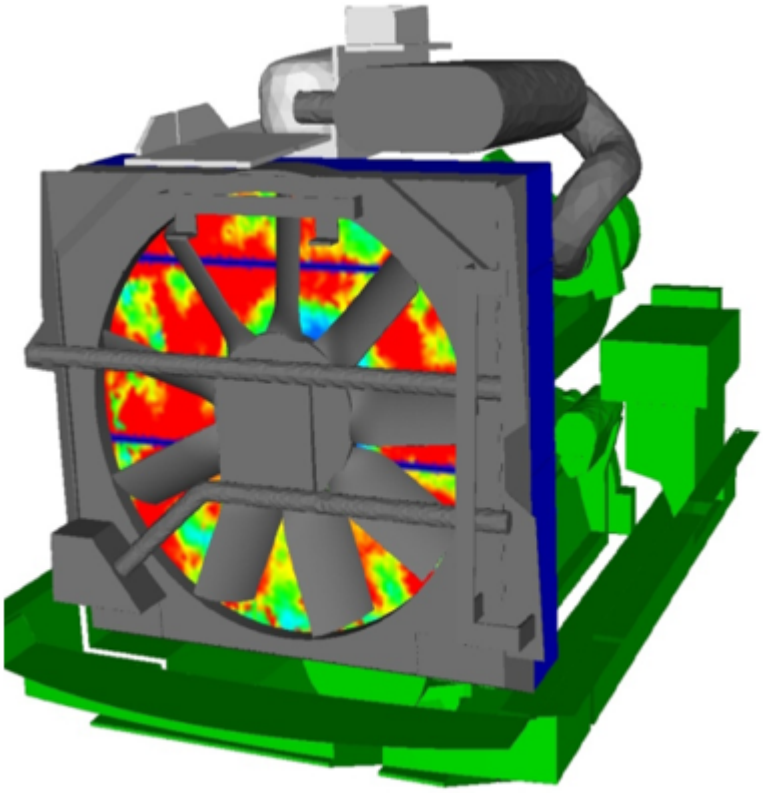

Figure 8:

.

Chemical Industries

CFD applications in the chemical industry involve combustion, mixing, multiphase flows and cavitation for evaluating the accurate heat/mass transfer parameters.

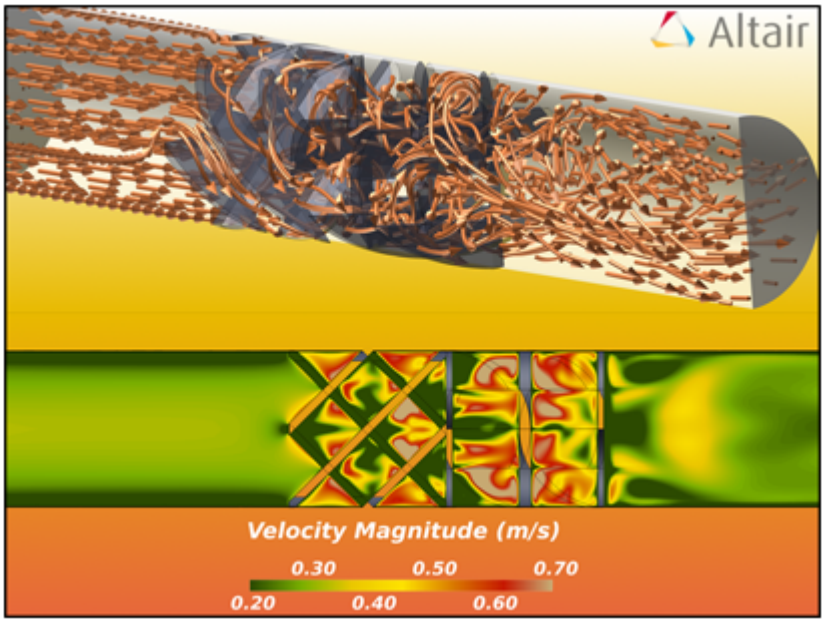

Figure 9:

Electronic Industries

CFD analysis can provide great value in predicting temperature distribution over a chip and the deposition rate therefore reducing the number of experiments.

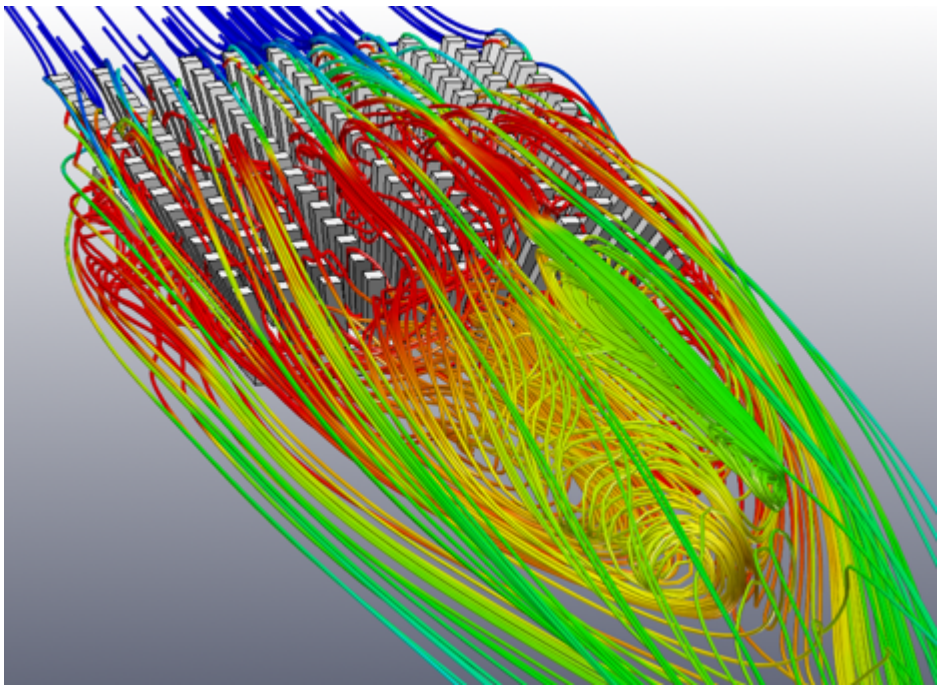

Figure 10:

Medical Industries

The application of CFD in the medical industry includes analysis of blood circulation, impact of artery blockage, air circulation in lungs, and so on.

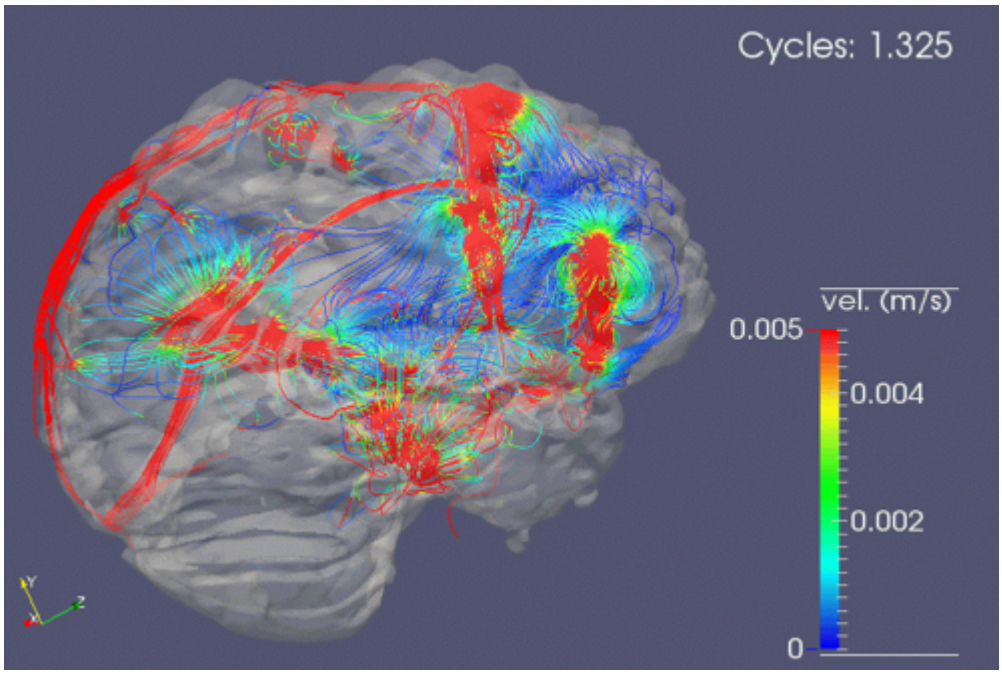

Figure 11:

Aside from the conventional industries mentioned above, CFD is also making strides into newer platforms, such as movies, computer graphics and food processing.

Altair Simulation- AcuSolve: Background

This section gives a brief background of Altair Simulation- AcuSolve and a brief introduction of AcuSolve.

Altair Simulation products, which include Radioss, OptiStruct, MotionSolve and HyperXtrude to name a few, is a software giant in the Computer Aided Engineering (CAE) Industry.

Apart from CAE products, Altair operates business in product design consultancy and cloud computing services.

AcuSolve is a leading general purpose CFD solver that is capable of solving the most demanding industrial and scientific applications. Based on the Finite Element method, AcuSolve's robust and scalable solver technology empowers users by providing unparalleled accuracy on fully unstructured meshes. Applications ranging from steady Reynolds-averaged Navier-Stokes (RANS) simulations to complex, transient, multi-physics simulations are handled with ease and accuracy. AcuSolve is used worldwide by scientists and engineers to explore applications in a variety of markets including automotive, aerospace, energy, electronics cooling and chemical processing.

The key benefits of AcuSolve include:

- Robustness: Most problems are solved on the first attempt
- Speed: Fully coupled solver on shared memory and distributed parallel systems
- Accuracy: Highly accurate in space and time while globally and locally conservative

Pre and Post-Processing with AcuSolve

This section details the integration of AcuSolve with the industrially accepted pre and post-processing tools.

AcuSolve is smoothly integrated with pre and post-processing HyperWorks CFD or SimLab.

A user of HyperWorks CFD can prepare the model in HyperWorks CFD and then can either export the input files for AcuSolve or launch the AcuSolve CFD solver directly by clicking the **Run** tool from the Solution ribbon.

After the solution is obtained from AcuSolve, HyperWorks CFD or SimLab can be used for various post-processing applications. For example, AcuSolve `.log` files can be directly read from HyperWorks CFD or SimLab by clicking **File** > **Open** > **Results** from the Post ribbon and then choosing the appropriate AcuSolve `.log` file.

Co-Simulations Using AcuSolve

This section details the capabilities of AcuSolve in simulating the multi-physics problems by coupling with structural solvers.

Fluid Structure Interaction (FSI)

One of the rich features of AcuSolve lies in its ability to simulate FSI problems.

AcuSolve simulates these problems using two different technologies:

Practical FSI (P-FSI)	In P-FSI simulations, AcuSolve and the structural code are run separately. The Eigen solution obtained from a structural solver is projected onto the CFD mesh and used as boundary conditions to displace the fluid mesh. The mass, stiffness and damping arrays are also transferred from the structural model to flexible body in the CFD model, completing the inputs necessary to compute the structural deformation. P-FSI is preferred for simulations that have linear structural response (linear material properties and small mesh deformations).
Direct Coupled FSI (DC-FSI)	For applications involving a nonlinear structural response, AcuSolve is coupled at run time to a structural solver using the DC-FSI approach. The codes are run in tandem and exchange forces and displacements at each time step. This technique captures all nonlinearities in the structural model and can exploit the full capabilities of the structural solver. The DC-FSI technology within AcuSolve performs all projection and interpolation between the structural and CFD meshes without the use of any middleware. The supported structural solvers for AcuSolve include OptiStruct, Abaqus and MD-Nastran.

Coupled Multibody Dynamics (MBD) with AcuSolve

AcuSolve can be directly coupled with MotionSolve, a multibody dynamics solver, to solve multi-physics problems that involve both fluid and rigid body dynamics.

The wetted surfaces are paired with rigid bodies and loads. Displacements are exchanged during the run time using AcuSolve's code coupling interface. The coupling is currently supported for rigid body motion only and not for a flexible body. However, AcuSolve supports both one way and two way coupling with MotionSolve. With one way coupling, the displacements are read from a file generated from MotionSolve and projected onto AcuSolve. With two way coupling, the codes exchange forces and displacement at each time step.

Theoretical Background

3

This chapter covers the following:

Mathematical Background

This section on mathematical background covers the various notations and operators used to formulate and define the equations of fluid flow.

Vector or Dyadic Notation

The conservation laws for a continuum medium involve vector and tensor quantities as well as several operators such as gradient and divergence.

In order to have a comprehensive understanding of these equations it is essential to get a good grasp of the notations and operators used in this manual.

In this notation, the governing equation is independent of the choice of the coordinate system. For the purposes of this manual the scalar quantities would be denoted with italicized letters. For example, pressure field is denoted as p. The vector quantities would be denoted with an arrow above the letters, for example velocity field denoted as $\vec{u}$. Tensor quantities are donated with bold face letters, for example stress tensor represented as $\boldsymbol{\tau}$.

Cartesian Tensor Notation

In this notation, an index subscript is written after the quantity which corresponds to a component of the quantity.

Single subscript is used to denote a component of vector, for example u_i for the vector field $\vec{u}$ and two subscripts are used to denote a component of tensor, for example τ_{ij} for the stress tensor $\boldsymbol{\tau}$.

Kroneker Delta

The Kroneker Delta is a second-order isotropic tensor which is defined as: $\delta_{ij} = 1 \quad \text{for} \quad \text{i} = \text{j}$, $\delta_{ij} = 0 \quad \text{for} \quad \text{i} \neq \text{j}$.

Operators

The most frequently used math operator related to flow equations is the ∇ referred to as nabla, grad or del.

The nabla operator operates on the quantity to the right of it and the rules of a derivative of a product still hold. Otherwise the nabla operator behaves like any other vector in an algebraic operation. It is a vector operator and for a Cartesian coordinate system, it is defined as

$$\nabla = \frac{\partial}{\partial x}\hat{i} + \frac{\partial}{\partial y}\hat{j} + \frac{\partial}{\partial z}\hat{k} \tag{4}$$

∇ appears in several different ways when applied to scalar, vector and tensor quantities.

Gradient

When the nabla operator is applied on a scalar quantity φ, it is called Gradient and it gives a vector whose components are the partial derivatives.

$$\nabla\varphi = \frac{\partial\varphi}{\partial x}\hat{i} + \frac{\partial\varphi}{\partial y}\hat{j} + \frac{\partial\varphi}{\partial z}\hat{k} \tag{5}$$

The gradient of φ points to the direction of greatest change of φ and has a magnitude equal to the rate of change of φ with respect to distance in that direction.

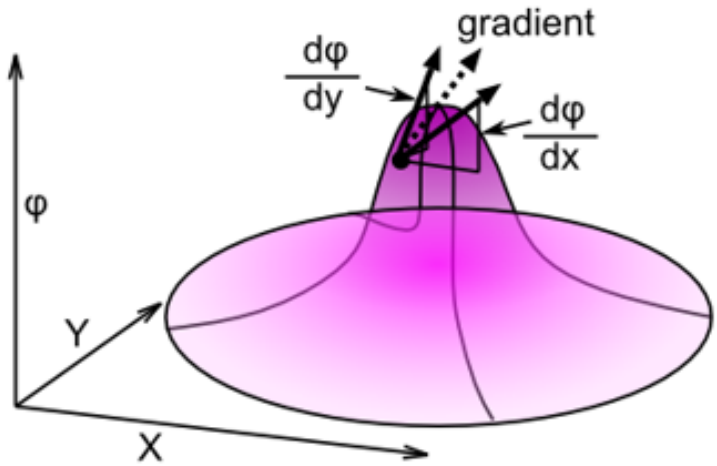

Figure 12: Gradient at a Point

When gradient is applied to a tensor quantity it produces a tensor one rank higher. When applied to a vector quantity $\vec{u}$ it gives a second-order tensor given by

$$\nabla(\vec{u}) = \left(\frac{\partial}{\partial x}\hat{i} + \frac{\partial}{\partial y}\hat{j} + \frac{\partial}{\partial z}\hat{k}\right)\left(\mathrm{u}\hat{i} + \mathrm{v}\hat{j} + \mathrm{w}\hat{k}\right) \equiv \begin{pmatrix} \frac{\partial \mathrm{u}}{\partial x} & \frac{\partial \mathrm{u}}{\partial y} & \frac{\partial \mathrm{u}}{\partial z} \\ \frac{\partial \mathrm{v}}{\partial x} & \frac{\partial \mathrm{v}}{\partial y} & \frac{\partial \mathrm{v}}{\partial z} \\ \frac{\partial \mathrm{w}}{\partial x} & \frac{\partial \mathrm{w}}{\partial y} & \frac{\partial \mathrm{w}}{\partial z} \end{pmatrix} \tag{6}$$

The gradient of a vector quantity represents the gradient of each component of the vector field individually, each of which is a scalar.

Divergence

The divergence of a vector quantity $\vec{u}$ is defined as a scalar quantity given by

$$\nabla \cdot \vec{u} = \frac{\partial \mathrm{u}}{\partial x} + \frac{\partial \mathrm{v}}{\partial y} + \frac{\partial \mathrm{w}}{\partial z} \tag{7}$$

The divergence of a vector field represents the flux generation per unit volume (flux density) at each point on the field.

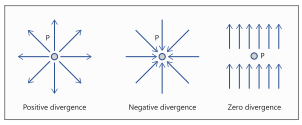

Figure 13: Divergence at a Point

The divergence of a tensor gives a tensor which is one rank lower. When applied to a second-order stress tensor τ it yields a vector field whose ith component is expressed as

$$(\nabla \cdot \tau)_i = \frac{\partial \tau_{ij}}{\partial x_j} \tag{8}$$

Div

The div operator is defined as $\vec{u} \cdot \nabla$ and is expressed as

$$\mathrm{u}\frac{\partial}{\partial x} + \mathrm{v}\frac{\partial}{\partial y} + \mathrm{w}\frac{\partial}{\partial z} \tag{9}$$

It maps a vector quantity to a scalar which can then be applied to a scalar, vector or higher order tensors.

Laplacian

The Laplacian of a scalar quantity φ is a scalar defined as

$$\nabla^2 \varphi = \frac{\partial^2 \varphi}{\partial x^2} + \frac{\partial^2 \varphi}{\partial y^2} + \frac{\partial^2 \varphi}{\partial z^2} \tag{10}$$

Double Dot Product (Scalar Product of Two Tensors)

The double dot product is a doubly contracted product between two tensors. It is expressed as

$$A : B = A_{ij} B_{ji} \tag{11}$$

Total Derivative

The total derivative, also known as material derivative or substantial derivative, describes the rate of change of a physical quantity of a fluid element with time as it moves along a trajectory in a velocity field. The total derivative of a scalar quantity φ is a scalar defined as

$$\frac{D\varphi}{Dt} = \frac{\partial \varphi}{\partial t} + \vec{u} \cdot \nabla \varphi \tag{12}$$

The total derivative of a quantity can be seen as a sum of local time derivative and convective derivative.

Basics of Fluid Mechanics

This section on basics of fluid mechanics covers topics describing the fundamental concepts of fluid mechanics, such as the concept of continuum, the governing equations of a fluid flow, definition of similitude and importance of non-dimensional numbers, different types of flow models and boundary layer theory.

Concept of Continuum

This section introduces the concept of a continuum medium.

Any material, solid, liquid or gas is composed of billions of individual molecules, in a very small region, separated by empty spaces in between them. The continuum assumption considers that matter is continuously distributed and fills the entire region of the space it occupies.

A continuum material can be continually sub divided into infinitesimal elements with properties being those of the bulk material. Properties such as density, pressure, temperature and velocity are taken to be well-defined at infinitely small points.

For a continuum fluid, at each point of the region of the fluid it is possible to construct one volume infinitesimally small enough compared to the region of the fluid and still big enough compared to the molecular mean free path. This condition is mathematically expressed using a non dimensional number known as a Knudsen number.

Describing a fluid flow quantitatively makes it necessary to assume that flow variables, such as pressure and velocity, and fluid properties vary continuously from one point to another. Mathematical description of flow on this basis have proved to be reliable and treatment of fluid medium as a continuum has firmly become established.

Governing Equations

This section describes the definition and formulation of the equations governing the conservations of mass, momentum and energy in a fluid flow and obtaining a closed form solution from these equations.

The equations which govern the motion of a fluid are called the Navier-Stokes equations. These equations refer to the basic governing continuity equations for a compressible, viscous, heat conducting fluid.

They describe the transport of three conserved quantities for a local system: mass, momentum and energy and can be expressed in an integral form when applied to a finite region known as the control volume, or a differential form when applied at an infinitesimally small fluid element.

Continuity Equation

The instantaneous mass conservation equation commonly termed as the continuity equation, is derived by applying mass conservation to a control volume for a general fluid.

Its differential form is written as:

$$\frac{\partial \rho}{\partial t} + \nabla \cdot (\rho \vec{u}) = 0 \quad (13)$$

where

ρ is the fluid density

t is time

$\vec{u}$ is the flow velocity vector

The first term $\frac{\partial \rho}{\partial t}$ describes the rate of change of density with respect to time and the second term $\nabla.(\rho \vec{u})$ describes the divergence of the vector field $\rho \vec{u}$ at a particular point fixed in space. The continuity equation can also be expressed using the substantial derivative and is written as:

$$\frac{D\rho}{Dt} + \rho \ (\nabla \cdot \vec{u}) = 0 \quad (14)$$

Momentum Equation

The momentum conservation equation is derived by applying Newton's second law of motion to the fluid control volume, which applies as the rate of change of momentum of the fluid particle equals the sum of surface and body forces.

The surface forces comprise of viscous forces (Tensile and shear) and pressure (compressive) and the body (volume) forces can be gravity, centrifugal force, Coriolis force, electromagnetic force, and so on.

The momentum equation is written as:

$$\rho \ \frac{\partial \vec{u}}{\partial t} + (\rho \vec{u} \cdot \nabla)\vec{u} = -\nabla p + \rho b + \nabla \cdot \tau \quad (15)$$

where

p is the pressure

b is the source term (generally gravity)

τ is the viscous stress tensor

If the fluid is Newtonian in nature, the viscous stresses are proportional to the time rate at which strain occurs. Stokes hypothesis for a Newtonian fluid simplifies the stress tensor to:

$$\tau_{ij} = \mu\left(\frac{\partial u_i}{\partial x_j} + \frac{\partial u_j}{\partial x_i}\right) - \frac{2}{3}\mu\delta_{ij}\frac{\partial u_k}{\partial x_k} \quad (16)$$

where μ is the dynamic viscosity of the fluid

The general form of the momentum equation can be seen to be comprised of the following terms:

Time derivative + Convection terms = Forcing (Source) terms + Diffusive terms

The momentum conservation equation for the flow velocity vector $\vec{u}$ can be written as three separate equations in an orthogonal system. These equations describe the conservation of momentum in x, y, z directions with flow velocity components u, v and w.

Energy Equation

The energy conservation equation is derived by applying first law of thermodynamics to fluid control volume, which applies as rate of change of energy of a fluid particle equals the sum of rate of heat addition and rate of work done.

The energy of a fluid particle comprises of internal (thermal) energy and kinetic energy. Heat addition generally takes place in the form of conduction due to a temperature difference through sources such as chemical reactions, potential energy, and so on. Work is done on the fluid volume by the surface and body forces.

The energy equation is written as

$$\frac{\partial(\rho E)}{\partial t}+\nabla\cdot(\rho E\vec{u})= \quad \nabla\cdot(k\nabla T)-\nabla\cdot(p\vec{u})+\vec{u}\cdot(\nabla\cdot\tau)+\nabla\vec{u}:\tau+\rho b\cdot\vec{u}+S \tag{17}$$

where

E is the total energy (internal + kinetic)

$k\nabla T$ is the heat flux given by Fourier's Law

S is the heat source

There are different possible versions of the energy equation. The form written above is known as the total energy form. Another form which describes the convection of internal energy and more commonly used is written as:

$$\frac{\partial(\rho e)}{\partial t}+\nabla\cdot(\rho e\vec{u})= \quad \nabla\cdot(k\nabla T)-p\nabla\cdot\vec{u}+\nabla\vec{u}:\tau+S \tag{18}$$

where

e is the internal energy substituted from the relation $E=e+\frac{1}{2}|\vec{u}|^2$

T is the temperature

k is the thermal conductivity of the fluid

$\nabla\vec{u}:\tau$ is the double dot product defined as $\frac{\partial \mathrm{u}_j}{\partial x_i}\tau_{ij}$ describing the irreversible transfer of mechanical energy into heat

Another form known as the enthalpy form is written as:

$$\rho\frac{\partial h}{\partial t}+(\rho\vec{u}\cdot\nabla)h \quad =\nabla\cdot(k\nabla T)+\nabla\vec{u}:\tau+\frac{Dp}{Dt}+S \tag{19}$$

where

h is the enthalpy substituted from the relation $h=e+\frac{p}{\rho}$

$\frac{Dp}{Dt}$ is the energy transfer due to work done by compressive forces, that is, pressure work

The five equation sets described above, one continuity, three momentum and one energy equation contain unknowns: ρ, p, T, e, u, v, w. In order to obtain a closed form solution for this system of

differential equations, two more equations are needed. For a compressible flow these equations come in the form of equations of state. They are stated as:

$$p = p(\rho, T) \tag{20}$$

and

$$e = e(p, T) \tag{21}$$

For an ideal gas, these equations take the form

$$p = \rho RT \tag{22}$$

and

$$e = C_v T \tag{23}$$

These relations give an additional equation for enthalpy given by $h = C_p T$. When substituted into the energy equation it simplifies to:

$$\rho \quad c_p \frac{DT}{Dt} \quad = \frac{Dp}{Dt} + \nabla \cdot (k \nabla T) + \quad \nabla \vec{u} : \tau + \mathrm{S} \tag{24}$$

Similitude and Non–Dimensional Numbers

This section describes the concepts of similitude and non-dimensional numbers and their importance in fluid mechanics.

Similitude is a concept that relates the behavior of an object in a given flow field with its behavior in a different flow field under different operating conditions. This concept allows you to compare any two scenarios (simulations or experiments) and determine the similarities in the flow fields between them.

This concept becomes useful when there is a prototype of a vehicle, aircraft wing or any such application to be tested under laboratory conditions. It is not always feasible to test the full scale prototype owing to the large size or requirement of large scale flow conditions. Scaled models allow testing of a prototype prior to its production which can greatly increase the efficiency of the development process.

The following similarities need to be met in order to achieve similitude.

Geometric Similarity

Geometric similarity refers to similarity relations between the linear dimensions of the test scale model and the prototype. This means the model has the same shape as the prototype. More precisely, the model can be superimposed on the prototype by geometric operations like scaling, translation, rotation and reflection.

Kinematic Similarity

Kinematic similarity refers to the similarity of motion between the model and prototype in a fluid. This means that the flow streamlines are similar for the model and the prototype. More specifically, the

velocities at corresponding points are in the same direction and are related in magnitude by a constant scale factor.

Dynamic Similarity

Dynamic similarity refers to the similarity between the force ratios at corresponding points and boundaries of the model and the prototype. This means that force distributions of the same type on the model and prototype have the same direction and are related in magnitude by a constant scale factor.

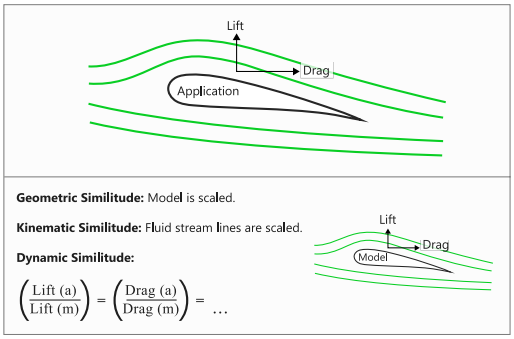

Figure 14: Similitude Between a Model and a Prototype

In order to analyse the above similarities certain non-dimensional numbers are used. The use of these numbers drastically simplifies the task of inferring the experimental data from the model and applying it to prototype design. Another advantage is that these numbers are independent of units of measurement and hence can be interpreted to suit any measurement system.

The most widely used non-dimensional numbers in fluid flow analysis are the following.

Reynolds Number

Reynolds number is the ratio of inertial (momentum) forces to viscous forces. It is an important parameter that can be used to determine the dynamic similarity between two cases of fluid flow or it can be used to characterize the flow regime in a fluid, this is, the laminar or turbulent nature of the flow. It is also used to study the transition between laminar and turbulent flows.

A laminar flow occurs at low Reynolds number when the viscous forces dominate resulting in a smooth velocity and pressure field where as a turbulent flow occurs at high Reynolds number where the inertial forces dominate the flow resulting in instabilities having a large range of time and length scales.

It is defined as

$$\mathrm{Re} = \frac{\rho u L}{\mu} \tag{25}$$

where

ρ is the density of the fluid

u is the mean velocity of the flow

L is the characteristic length

μ is the dynamic viscosity of the fluid

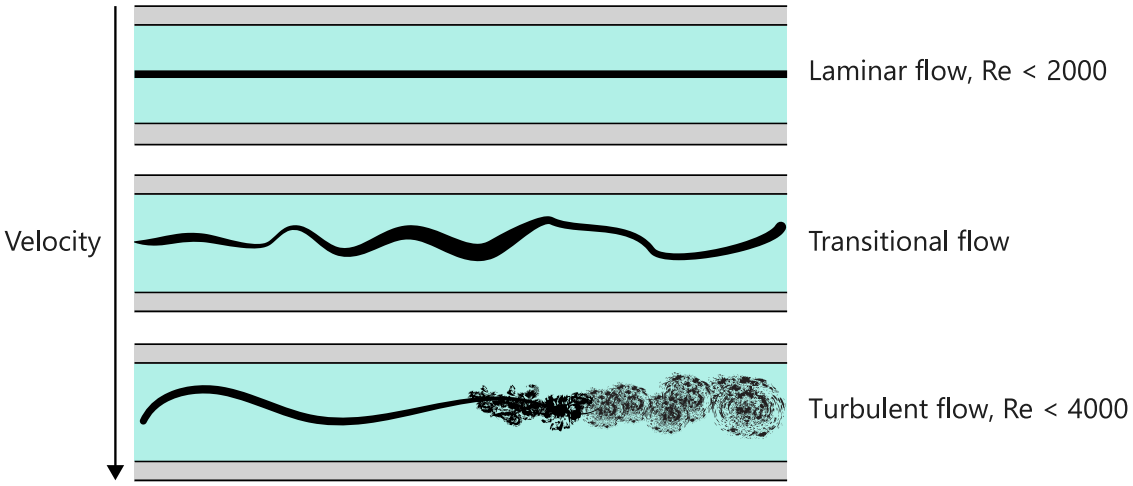

Figure 15: Flow Characterization Based on Reynolds Number

The Reynolds number can also be expressed as the ratio of total momentum transfer to molecular momentum transfer.

The characteristic length is geometry dependent and defines the scale of physical system. For example, the characteristic length for a flow in a pipe with circular, square or annular cross section is taken as the hydraulic diameter of the pipe.

The hydraulic diameter for a pipe is defined as

$$D_H = \frac{4A}{P} \tag{26}$$

where

A is the area of the cross section

P is the wetted perimeter, that is, the perimeter of the pipe in contact with the flow

For a fluid moving between two plane parallel surfaces, where the width is much greater than the space between the plates, the characteristic dimension is twice the distance between the plates.

For an airfoil the characteristic length is considered to be the chord length.

There is no universal definition for a characteristic length. Any geometric length that significantly simplifies the governing equations when converted to their non-dimensional form is considered the characteristic length.

Mach Number

Mach number is the ratio of flow velocity to local speed of sound. It is a key parameter that characterizes the compressibility effects in a fluid flow.

When the Mach number is small (less than 0.3) the inertial forces experienced by the flow can be considered sufficiently small to not cause any changes to the fluid density. Under these conditions the compressibility effects of the fluid can be ignored.

It is written as

$$M = \frac{u}{a} \tag{27}$$

The local speed of sound and hence the Mach number depend on the flow conditions, particularly on temperature and pressure of the fluid.

The Mach number is used to classify the flow regime into subsonic, transonic, supersonic and hypersonic flows, and they are defined as:

Subsonic flow $M < 0.8$

Transonic flow $0.8 < M < 1.0$

Supersonic flow $1.0 < M < 5.0$

Hypersonic flow $M > 5.0$

Knudsen Number

Knudsen number is the ratio of the molecular mean free path length to the representative physical length scale (characteristic length). It is a measure of rarefaction of the flow. Knudsen number determines whether continuum mechanics or statistical mechanics formulation should be used to model the flow.

It is expressed as

$$Kn = \frac{\lambda}{L} \tag{28}$$

where

λ is the molecular mean free path understood as the mean distance travelled by a molecule between two successive collisions with other molecules

L is the characteristic length

Prandtl Number

Prandtl number is the ratio of molecular diffusivity to thermal diffusivity in a fluid. When the Prandtl number is low it means that the heat diffuses quickly compared to momentum and vice versa.

It is written as

$$Pr = \frac{c_p \mu}{k} \tag{29}$$

where

c_p is the molar heat capacity of the fluid at constant pressure

μ is the dynamic viscosity of the fluid

k is the thermal conductivity of the fluid

Nusselt Number

The average Nusselt number is the ratio of convective heat transfer across a chosen boundary or surface to conductive heat transfer within a fluid. The convection heat transfer includes both advection and diffusion heat transfer.

It is defined as

$$Nu = \frac{hL}{k} \tag{30}$$

where

h is the convective heat transfer coefficient

L is the characteristic length

k is the thermal conductivity of the fluid

A Nusselt number close to one is characteristic of a laminar flow whereas a large value corresponds to turbulent flow.

The local Nusslet number at a point at a distance x from the boundary is expressed as

$$Nu_x = \frac{h_x x}{k} \tag{31}$$

Pressure Coefficient

The pressure coefficient is the ratio of pressure difference to the dynamic pressure. It describes the relative pressure across a fluid field. It is expressed as

$$C_p = \frac{p - p_\infty}{\frac{1}{2}\rho_\infty u_\infty^2} \tag{32}$$

where

p is the point at which pressure coefficient is being calculated

p_∞, ρ_∞, u_∞ are the free stream pressure, density and velocity, respectively

Lift and Drag Coefficients

The lift coefficient is the ratio of lift force to the dynamic force experienced by a body in a flow field.

It is expressed as

$$C_L = \frac{L}{qA} = \frac{2L}{\rho_\infty u_\infty^2 A} \tag{33}$$

The drag coefficient is the ratio of drag force to the dynamic force experienced by a body in a flow field. It is expressed as

$$C_D = \frac{D}{qA} = \frac{2D}{\rho_\infty u_\infty^2 A} \tag{34}$$

where

L is the lift force experienced by the body

D is the drag force experienced by the body

q is the dynamic pressure of the fluid defined as $q = \frac{1}{2}\rho_\infty u_\infty^2$

A is the reference area of the body

The reference area depends on the type of coefficient being measured. For automobiles and many bluff bodies the reference area while calculating the drag coefficient is taken as the projected frontal area. For airfoils the reference area is taken as the normal wing area.

The non-dimensional numbers used to determine similitude depend on the type of flow. For example, in a case of incompressible flow (without free surface), the Reynolds number can satisfy the similarity condition. If the flow is compressible, Reynolds number, Mach number and specific heat ratio are required in order to establish similarity.

It is not always possible to achieve absolute similitude between a model and prototype. It becomes even harder as you diverge from the prototype's operating conditions, therefore it becomes important to focus on only the most important parameters.

The following table lists the most frequently encountered non-dimensional number, their description and applications.

Table 1: List of Frequenty Used Non-Dimensional Numbers

Name	Symbol	Numerator	Denominator	Formula	Applications
Reynolds number	Re	Intertial Force	Viscous force	$\frac{\rho u L}{\mu}$	Fluid flow with viscous and inertial forces
Froude number	Fr	Intertial Force	Gravitational force	$\frac{u}{\sqrt{(gL)}}$	Fluid flow with free surfaces
Weber number	We	Intertial Force	Surface force	$\frac{\rho u^2 L}{\sigma}$	Fluid flow with interfacial forces

Name	Symbol	Numerator	Denominator	Formula	Applications
Mach number	M	Local velocity	Local speed of sound	$\frac{u}{a}$	Gas flow at high velocity
Prandtl number	Pr	Viscous diffusion rate	Thermal diffusion rate	$\frac{c_p \mu}{k}$	Fluid flow with heat transfer
Nusselt number	Nu	Convective heat transfer	Conductive heat transfer	$\frac{hL}{k}$	Fluid flow with heat transfer
Grashof number	Gr_L	Buoyancy force	Viscous force	$\frac{g\beta(T_s - T_\infty)D^3}{\mu^2}$	Fluid flow with natural convection
Rayleigh number	Ra_x	(Buoyancy force) * (Viscous diffusion rate)	(Viscous force) * (Thermal diffusion rate)	$\frac{g\beta(T_s - T_\infty)x^3}{\mu\alpha}$	Buoyancy driven flow
Specific Heat ratio	γ	Enthalpy	Internal Energy	$\frac{c_p}{c_v}$	Compressible flow
Pressure Coefficient	C_p	Local pressure	Dynamic pressure	$\frac{p - p_\infty}{\frac{1}{2}\rho_\infty v_\infty^2}$	Pressure drop estimation
Lift Coefficient	C_L	Lift Force	Dynamic Force	$\frac{L}{qA}$	Aerodynamics, Hydrodynamics
Drag Coefficient	C_D	Drag Force	Dynamic Force	$\frac{D}{qA}$	Aerodynamics, Hydrodynamics
Skin friction Coefficient	C_f	Wall Shear Force	Dynamic Force	$\frac{\tau_w}{qA}$	Aerodynamics, Hydrodynamics
Knudsen number	Kn	Molecular mean free path	Characteristic length	$Kn = \frac{\lambda}{L}$	Determination of applicability of continuum mechanics. i.e. suitability of AcuSolve for the application.

Simplification of Governing Equations (Different Types of Flow Models)

This section describes the simplification of the governing equations to various flow models by assumptions on time dependence, density and viscosity of the fluid flow.

Depending on the flow conditions the Navier-Stokes equations, primarily the momentum equations, can be simplified. The simplification of these equations depends on which effects in the flow are significant or insignificant.

The simplified flow models that are most broadly used are the following:

- Steady flow
- Euler flow or Inviscid flow
- Stokes flow
- Incompressible flow

Steady Flow

The time dependence of flow field parameters is an important factor in the analysis of a fluid flow. A majority of flows are not steady but transient in nature. In a steady state flow the flow properties at a point, such as pressure and velocity, do not change with time. Steady state flows are of interest in cases where the flow properties need to be studied after the flow field has stabilized.

This is achieved in simulations by taking a very large time step (Δt) which causes the time derivative of properties in the governing equations to reach to zero.

$$\nabla \cdot (\rho \vec{u}) = 0 \tag{35}$$

$$(\rho \vec{u} \cdot \nabla)\vec{u} = -\nabla p + \rho b + \nabla \cdot \tau \tag{36}$$

$$(\rho \vec{u} \cdot \nabla)h = \nabla \cdot (k \nabla T) + \nabla \vec{u} : \tau + \frac{Dp}{Dt} + S \tag{37}$$

While performing simulations, a steady state flow result gives a preliminary insight into whether the problem is set up correctly or not. If there are a large number of oscillations in the residuals it can be inferred that the flow is transient and not steady. If the residuals show a smooth converge it implies that the flow field becomes stable and steady state is achieved. The results can also be used to fine tune the setup for further simulations or use them as initial conditions for a transient simulation.

Euler Flow or Inviscid Flow

Inviscid flow is a representation of a fluid flow where the dissipative and transport phenomenon of viscosity, mass diffusion and thermal diffusion are neglected. This assumption is valid when the viscous forces are small in comparison to the inertial forces.

Such flow situations can be identified in cases with a high value of Reynolds number, where the viscous effects are concentrated to regions close to solid boundary and can be neglected for the regions far away from the boundary.

The governing equations for such flows are expressed as:

$$\frac{\partial \rho}{\partial t} + \nabla \cdot (\rho \vec{u}) = 0 \quad (38)$$

$$\rho \frac{\partial \vec{u}}{\partial t} + (\rho \vec{u} \cdot \nabla)\vec{u} = -\nabla p + \rho b \quad (39)$$

$$\rho \frac{\partial h}{\partial t} + (\rho \vec{u} \cdot \nabla)h = 0 \quad (40)$$

These equations can form a closed form solution by assuming the equation of state.

Results obtained from these assumptions in the flow field are widely used in designing flying vehicles, rockets and their engines, turbines and compressors. Studies of inviscid flows are carried out in gas dynamics, acoustics, electro and magneto gas dynamics, the dynamics of rarefied gases, plasma dynamics, and so on.

Stokes Flow

Stokes flow is a representation of fluid flow where the viscosity of the fluid is high. In such flows the viscous effects dominate the advective inertial effects.

The Reynolds number in such flows is low, hence, it is also termed as creeping flow or Low Reynolds number flow.

The governing equations for such flows are expressed as:

$$\frac{\partial \rho}{\partial t} + \nabla \cdot (\rho \vec{u}) = 0 \quad (41)$$

$$\rho \frac{\partial \vec{u}}{\partial t} = -\nabla p + \rho b + \nabla \cdot \tau \quad (42)$$

$$\rho \frac{\partial h}{\partial t} = \rho s + \nabla \cdot q \quad (43)$$

This results in the linearization of the governing equations and thus they can be solved by a number of linear differential solvers available.

If the governing equations are non-dimensionalized and the Reynolds number is assumed to be very low, the momentum equation reduces to

$$\mu \nabla^2 u = \nabla p - f \quad (44)$$

where

$$f \quad (45)$$

is the external force.

Incompressible Flow

All fluids (gas or liquid) exhibit some change in volume when subjected to compressive stresses. The degree of compressibility for a fluid can be quantified using the bulk modulus of elasticity, E, defined as

$$E = \frac{dp}{\frac{d\rho}{\rho}} \quad or \quad \frac{dp}{-\frac{dV}{V}} \tag{46}$$

where dp is the change in pressure and $d\rho$ or dV is the corresponding change in volume or density.

A flow can be classified as incompressible if the density within fluid particle does not change during its motion. It is also termed as isochoric flow and implies that under certain conditions a compressible fluid can undergoincompressible flow.

$$\frac{D\rho}{Dt} = \frac{\partial \rho}{\partial t} + \vec{u} \cdot \nabla \rho = 0 \tag{47}$$

Incompressibility is a property of flow and not of the fluid itself. Therefore the density field does not need to be uniform for the flow to be incompressible. When the above equation is combined with the continuity equation the following relation is obtained:

$$\nabla \cdot \vec{u} = 0 \tag{48}$$

which states that in an incompressible flow the velocity field is solenoidal (having zero divergence).

When an incompressibility assumption is made it is important to know under what conditions this assumption is valid. For a steady flow the condition is that the flow velocity must be much smaller compared to the local speed of sound, that is, $u \ll a$.

In case of an unsteady flow there is an additional condition which needs to satisfied, stated as $at \ll 1$. Physically this condition states the distance travelled by a sound wave in time t must be much greater than the distance travelled by the fluid particle. This implies that the propagation of pressure signals (sound waves) is instantaneous compared to the interval over which the flow field changes significantly.

When the limit for maximum relative change in density is set to five percent as the criteria for an incompressible flow, the maximum value of Mach number achieved is 0.3. This criteria states that any flow with a Mach number less than 0.3 (without heat source) can be assumed to be incompressible.

One of the implications of assuming the flow to be incompressible is that there is no equation of state as in a case of a compressible flow. In practice this means that the energy equation is decoupled from the continuity and momentum equations, assuming fluid properties are not a function of temperature. If the fluid properties change with temperature the equations again become coupled as in the case of a compressible flow.

The pressure in such a flow is no longer a thermodynamic quantity and cannot be related to temperature or density through an equation of state and must be obtained from the continuity and momentum equation while satisfying zero divergence for the velocity field. In the continuity equation there is no pressure term and in the momentum equation there are only the derivatives of pressure, but not the pressure itself. This means that the actual value of pressure in an incompressible flow solution is not important, only the changes of pressure in space are important.

Basic Boundary Layer Theory

This section covers concepts such as boundary layer type, flow, separation and transition.

Velocity Boundary Layer

Velocity boundary layer or commonly referred to as boundary layer is a thin layer of fluid formed near a boundary surface where the viscous effects of the fluid are significant.

When a fluid moves past an object or an object moves past a fluid, the fluid molecules right next to the boundary surface stick to it. This causes the molecules just above the surface to slow down because of collision with the molecules sticking to the surface. These molecules consequently slow down the flow just above them. As we move farther away from the surface of the object, the collisions affected by the object's surface reduces. Thus a layer of fluid is created within which the velocity of the flow gradually changes from zero at the object's surface to the free stream velocity at a certain distance away from the surface.

This distance at which the flow velocity inside the boundary essentially reaches the free stream velocity is termed as the boundary layer thickness. Mathematically it is defined as the distance at which the flow velocity is 99 percent of the free stream velocity.

$$\text{At } y = \delta, u = 0.99u_\infty$$

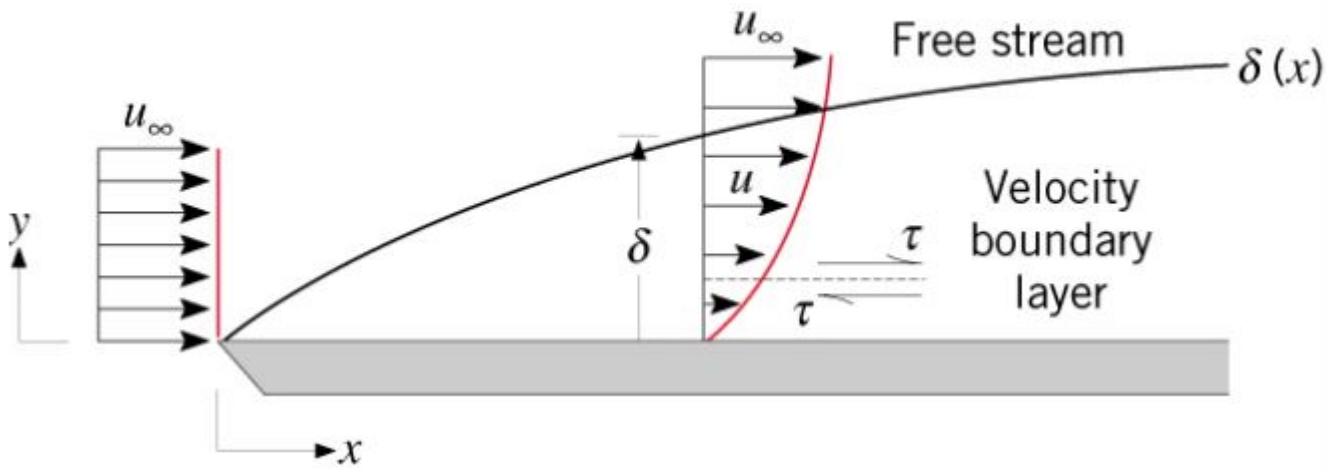

Figure 16: Velocity Boundary Layer

As a result of the loss of velocity, a shear stress is imparted on the object surface defined as

$$\tau_s = \mu \frac{\partial u}{\partial y}\bigg|_{y=0} \tag{49}$$

Thermal Boundary Layer

Thermal boundary layer is a region of fluid flow near a solid surface characterized by temperature gradients and heat fluxes. It is a consequence of heat transfer between the fluid and the solid surface and the fluid temperatures are directly influenced by heating or cooling from the surface wall.

The distance at which the difference between the flow temperatures inside the boundary layer and the boundary surface essentially reaches the difference between free stream temperature and the boundary surface temperature is termed as the thermal boundary layer thickness. It is mathematically expressed as:

At y $=\delta_t$, $\frac{T_s - T}{T_s - T_\infty}$ = 0.99

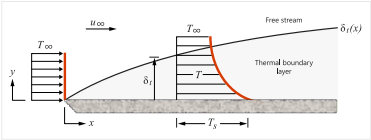

Figure 17: Thermal Boundary Layer

The local heat flux in a thermal boundary layer is analogous to the shear stress in a velocity boundary layer. The heat flux at the surface is proportional to the temperature gradient. It is defined as

$$q''_s = -k_f \left.\frac{\partial T}{\partial y}\right|_{y=0} \quad (50)$$

The flow inside the velocity boundary layer can be classified into two types

- Laminar boundary layer flow
- Turbulent boundary layer flow

Laminar Boundary Layer Flow

The flow inside a laminar boundary layer is smooth and takes place in layers. Each layer slides past the adjacent layers and any exchange of mass or momentum takes place only between these layers on a microscopic scale. Laminar boundary layer is formed when the Reynolds number is low.

The shear stresses associated with this flow can be calculated using the molecular viscosity μ.

Figure 18 depicts the typical velocity profile for a laminar boundary layer.

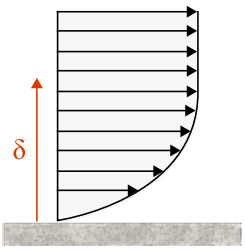

Figure 18: Laminar Boundary Layer

Turbulent Boundary Layer Flow

As the name suggests turbulent boundary layer flow is more chaotic and is characterized by active mixing of the fluid and momentum across several layers. The exchange of mass, momentum and energy takes place on a macroscopic scale with packets of fluid moving across the layers. A turbulent boundary layer is formed only at high Reynolds number.

In this case the scales of mixing cannot be handled by molecular viscosity alone, therefore turbulent or eddy viscosity has to be modeled in order to proceed with the calculations.

Figure 19 depicts the velocity profile for the turbulent boundary layer.

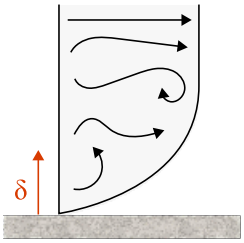

Figure 19: Turbulent Boundary Layer

The velocity profile for a turbulent boundary layer is quite different from a laminar boundary layer. It comprises of three regions or layers:

- Outer layer: This layer is sensitive to the properties of the external flow.
- Inner layer: This layer has turbulent mixing as the dominant physics.
- Laminar or viscous sublayer: This layer is attached to the wall where the no slip condition is applied. The shear stress in this layer is dominated by molecular viscosity.

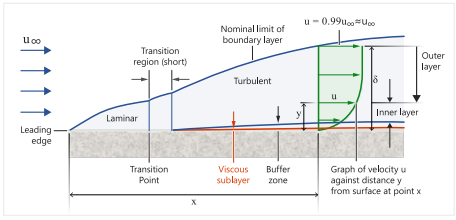

Figure 20: Complete Boundary Layer Profile (Laminar and Turbulent)

These layers blend into each other and the blending region between the inner layer and laminar sublayer is termed as the Buffer Zone.

As a consequence of intense mixing, a turbulent boundary layer has a much steeper gradient of velocity resulting in a larger shear stress and higher skin friction drag at the wall compared to a laminar boundary layer. In addition heat transfer rates are higher for a turbulent boundary layer. The presence

of eddies brings fluid particles at different temperatures into close contact with each other and the heat transfer comes more effective.

Another consequence of mixing is that a turbulent boundary layer has higher momentum near the wall, so it can withstand adverse pressure gradient longer and is less easily driven by the changes in the free stream pressure compared to a laminar boundary layer. This property allows a turbulent boundary layer to be attached to the object surface longer.

Boundary Layer Separation

Boundary layer separation is defined as the detachment of the boundary layer from the surface of the object thus leading to formation of eddies and vortices in the wake. The most important factor which leads to boundary layer separation is an adverse pressure gradient.

The pressure gradient is one of the parameters that greatly influences a flow. The shear stress caused by viscosity, near an object surface, has a retarding effect on the flow. This retardation can be overcome by a implementing a negative pressure gradient in the direction of the flow. A negative pressure gradient is termed as a favourable pressure gradient because it enables the flow.

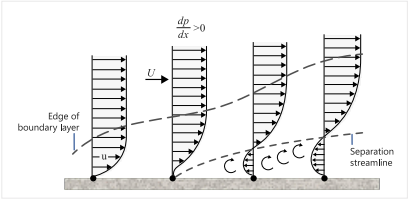

Figure 21: Boundary Layer Separation

A positive pressure gradient, termed as adverse pressure gradient, has the opposite effect on the flow. It further retards the flow leading to a reduction in the velocity near the wall and an increased boundary layer thickness. This continuous retardation causes the shear stress at the wall to drop to zero which then becomes negative causing a reversal in the flow direction near the surface. A region of recirculating flow is developed with formation of large slowly rotating eddies resulting in the flow detaching from the surface of the object. The point at which the velocity gradient and essentially the shear stress reaches zero is termed as the point of separation.

The separation leads to the formation of a large wake of vortices behind the body, where the fluid pressure is much lower compared to the regions where the fluid is attached to the surface since the eddies cannot convert the rotational energy into pressure head. As described in the previous section the flow velocity near the object surface is higher in case of a turbulent boundary layer. This higher fluid momentum means that the fluid separation occurs further downstream than in case of a laminar boundary layer when subject to the same adverse pressure gradient, resulting in a narrower wake and consequently less pressure drag.

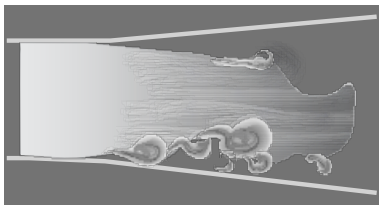

Figure 22: Boundary Layer Separation in a Diverging Channel (source: National committee for Fluid Mechanics Films; http://web.mit.edu/hml/ncfmf.html)

Figure 22 shows the separation of a laminar (top) and turbulent boundary (bottom) layer in a diverging channel.

Depending on the flow conditions, the recirculating flow may reattach to the surface of the body. A number of factors could influence the reattachment. The pressure gradient may turn favourable due to changing flow conditions or the geometry of the body. The other factor is that the boundary layer may transition from laminar to turbulent resulting in a fuller velocity profile that could sustain the adverse pressure gradient and causing the flow to reattach.

Boundary Layer Transition

Boundary layer transition is a very complex process and may be triggered by various types of flow disturbances, which can be due to the following factors:

- Free stream turbulence
- Acoustic Noise (Pressure fluctuations)
- Pressure Gradient
- Surface thermal disturbances
- Surface curvature
- Surface roughness
- Compressibility and high speed flow (transonic, supersonic and hypersonic) transition

These factors along with many other sources of disturbance can cause a smooth laminar flow to break down, enter a transition region and then develop into a turbulent flow. The mechanisms through which a boundary layer transitions can be one of the following:

- Natural transition: This mechanism is prevalent in weak disturbance environments (vibrations, free stream turbulence, adverse pressure gradient, and so on, are absent). The transition occurs gradually and breakdown is reached thorough a linear growth of disturbances. This mechanism is most commonly observed in the flow around a transport aircraft in flight.
- Bypass transition: This mechanism is observed in cases where the initial disturbances in the laminar flow are sufficiently high, caused by factors like surface roughness or high free stream turbulence. The highly non-linear growth of disturbances results in the quick formation of turbulent spots in the flow leading to breakdown, thus bypassing the linear mechanism. This transition

mechanism is observed in flows related to turbomachinery where there is high free stream turbulence present.

- Intermediate mechanisms: Aside from the primary mechanisms of turbulence discussed above, there are additional intermediate mechanisms. They include spanwise modulations in the flow, distortions leading to secondary instabilities and direct bypass.

Importance and Practical Applications of Boundary Layer

The properties associated with boundary layer flow, heat transfer, transition and separation are of great importance. Their application can be found in fields such as aerodynamics, hydrodynamics, meteorology, and so on. The following sub-sections describe the areas of special interest in the various fields which have significant practical applications.

- Flow over an airfoil: In the aerodynamics industry, the boundary layer is particularly important because it is responsible for a considerable amount of drag on the surface. The airfoils are designed to be thin and streamlined in order to keep the boundary layer laminar, thus reducing the skin friction drag. In situations where there are higher chances of flow separation, it is always preferable that the boundary layer separates towards the leading edge of the airfoil and reattaches somewhere downstream. It is dangerous if the separation occurs near the trailing edge in which case the flow would not reattach, resulting in sudden loss of lift and stalling of the aircraft. There are several approaches used to prevent this problem. These approaches include turbulence generation by tripping the boundary layer using vortex generators, boundary layer suction at the leading edge and reenergizing the boundary layer through blowing.
- Heat exchangers: A large number of production facilities in many industries use processes in which heat transfer takes place within the fluid or between different fluids. In such cases it is always preferable to increase the heat transfer and mixing without paying too high a penalty in terms of increased pressure loss. Some of the approaches used for this purpose include use of internal ribs or fins to increase the internal surface area of the domain, deformation in the flow domain to decrease the hydraulic diameter and disruption of the boundary layer to induce turbulence.
- CFD: The approximations obtained from the thin boundary layer theory greatly reduce the complexity of the equations solved. Mathematically the application of boundary layer theory changes the character of the governing Navier-Stokes equation from elliptic to parabolic. This allows marching in the flow direction, as the solution at any location is independent of the conditions farther downstream.

Aside from the topics discussed above, there are numerous cases where the boundary layer and the physics associated with it have significant applications. A few examples are natural boundary layer in the atmosphere, biometrics of marine organisms, automobile aerodynamics and design of sports merchandise such as golf balls.

Turbulence

This section on turbulence covers the topics describing the physics of turbulence and turbulent flow. It also covers the modeling of turbulence with brief descriptions of commonly used turbulence models.

Physics of Turbulent Flows

This section on physics of turbulence introduces a brief history of turbulence and covers the theory behind turbulence generation, turbulence transition and energy cascade in fluid flows.

On a daily basis you encounter turbulent flows in many places including rivers, ocean currents, atmospheric turbulence, bush fires, flows over blunt bodies, for example, cars, aircraft, ships and buildings, cross flows of chimney plumes, internal flows in pipelines, turbines and engines and many other various forms. Despite the prevalence of turbulent flows in your daily life there is no consensus on the definition of turbulence.

The following are several definitions quoted from various sources of literature.

- Bradshaw (1971): “Turbulence is a three dimensional time dependent motion in which vortex stretching causes velocity fluctuations to spread to all wavelengths between a minimum determined by viscous forces and a maximum determined by the boundary conditions. It is the usual state of fluid motion except at low Reynolds numbers.”
- Hinze (1975): “Turbulent flow motion is an irregular condition of flow in which various quantities show a random variation with time and space coordinates, so that statistically distinct average values can be discerned.”
- Launder (1991): “At moderate Reynolds numbers the restraining effects of viscosity are too weak to prevent small, random disturbances in a shear flow from amplifying. The disturbances grow, become non linear and interact with neighboring disturbances. This mutual interaction leads to a tangling of vorticity filaments. Eventually the flow reaches a chaotic, non repeating form describable only in statistical terms. This is the turbulent flow.”
- Pope (2000): "An essential feature of turbulent flows is that the fluid velocity field varies significantly and irregularly in both position and time."

Considering these definitions you can arrive at the following set of characteristic features of turbulent flows:

- Irregularity. Turbulent flow is highly chaotic and irregular in both space and time (Tennekes and Lumley, 1972; Hinze, 1975; Pope, 2000).
- Non-repetition. Turbulent flow is a non-repeating form (Launder, 1991).
- Three dimensional unsteady eddies with different scales. Turbulent flow is always three dimensional and unsteady. Turbulent flow contains eddies with different scales, which extract energy from shear stress of the mean flow and produce fluctuations in the velocity and pressure fields. The eddies also interact with one another and exchange momentum and energy (Bradshaw, 1971; Tennekes and Lumley, 1972).
- Diffusivity. Turbulent flow is diffusive (that is, the spreading of fluctuations) (Tennekes and Lumley, 1972; Pope, 2000). The chaotic eddies (vortices) within the turbulent flow increase the momentum

exchange in boundary layers delaying separation on the surface of curved bodies and increasing the resistance (wall friction) and heat transfer.

- Dissipation. Turbulent flow is dissipative. This suggests that the kinetic energy within small eddies is transformed into thermal energy. The small eddies receive their energy from larger eddies, which receive their energy from even larger eddies, and so on. The largest eddies extract their energy from the mean flow. This process of transferring energy from the larger eddies to the smaller eddies is called the energy cascade process. Turbulence is not self sustainable without a source of energy input.
- Amplification. The flow disturbances amplify when the Reynolds number exceeds critical Reynolds numbers (~2300 for internal flows, ~500000 for external flows).
- Flow property. Turbulent flow is a property of flow, it is not a fluid property.
- Sensitivity. Turbulence is extremely sensitive to flow disturbances (Pope, 2000).

The First Visualization of Turbulent Flow

Leonardo da Vinci was the first one to report the visualization of turbulent flow in his famous sketches from 1510.

He described the existence of whirlpools of water in his notes. He wrote, "Observe the motion of the surface of the water, which resembles that of hair, which has two motions, of which one is caused by the weight of the hair, the other by the direction of the curls; thus the water has eddying motions, one part of which is due to the principal current, the other to random and reverse motion." This notion is a precursor to the Reynolds flow decomposition of velocity into mean and fluctuating parts, which Osborne Reynolds suggested 400 years later. He also noted, "The small eddies are almost numberless, and large things are rotated only by large eddies and not by small ones and small things are turned by both small eddies and large." Nowadays, the "small eddies" and the "large things" refer to turbulence and large-scale coherent eddies, respectively. Leonardo da Vinci utilized his sketches as a flow visualization method, providing clear information of turbulence behaviors and their effects.

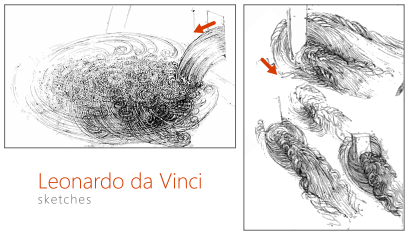

Figure 23: Leonardo da Vinci's Sketches: Whirlpools of the Water (left), Vortices Behind Obstacles (right): Arrows Indicate Flow Directions

The Reynolds Measurement

In 1883, Osborne Reynolds conducted an experiment where dye was injected into a glass tube with water flowing due to gravity.

He studied the conditions of transition from laminar flow to turbulent flow, indicated by the flow patterns in the tube. He analyzed that the flow patterns differed as the flow velocity was changed. At low speed, the dye showed regular straight lines of a laminar flow pattern. When the flow velocity increased, the dye became random (or chaotic) with eddies filling the entire tube, and mixed with water. This random flow pattern is a turbulent flow. He further noticed that the appearance of turbulent flow highly depended on a dimensionless parameter of velocity and length scale, as well as viscosity. This parameter is now known as the Reynolds number.

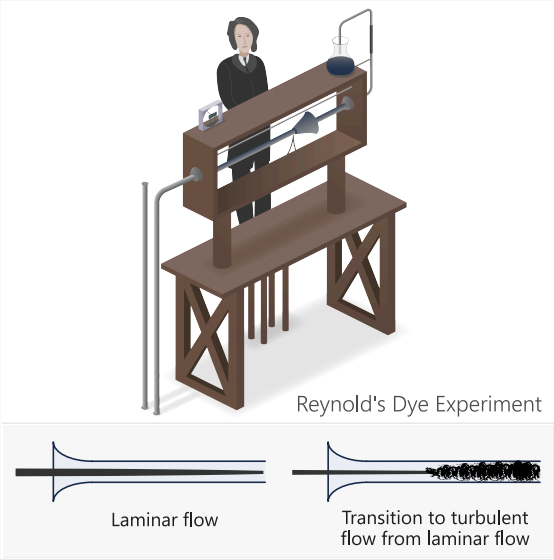

Figure 24: The Dye Experiment Conducted by Osborne Reynolds

The Reynolds Number

The Reynolds number is not only used to characterize the flow patterns, such as laminar or turbulent flow, but also to determine the dynamic similitude between two different flow cases.

The latter is an important concept to ensure valid experimental or computational results of numerous scaled models for industrial applications.

The Reynolds number is the ratio of the inertial force to the viscous force, defined as

$$\mathrm{Re} = \frac{\rho u L}{\mu} \tag{51}$$

where ρ is the fluid density (kg/m3), u the mean flow velocity (m/s), L the characteristic length (m), for example, hydraulic diameter for internal flows, and μ the dynamic viscosity of the fluid (kg/(m-s).

The characteristic length in the Reynolds number can be anything convenient, as long as it is consistent, especially when comparing different geometries. For example, the radius and the diameter are both valid for spheres or circles in flows with the diameter primarily used by convention. When computing the Reynolds number for airfoils and wings, the chord length is often chosen over the span because the

former is a representative function of the lift. For pipes, the diameter is the characteristic length. For rectangular pipes a suitable choice is the hydraulic diameter defined as

$$D_h = \frac{4A}{P} \tag{52}$$

where A is the cross-section area (m2) and P is the wetted perimeter (m). The wetted perimeter is the total perimeter of subject walls in contact with the flow.

Fluid flows are laminar when their Reynolds number is below a certain critical value and they are turbulent when they are larger than this critical value, termed the critical Reynolds number (Recr). This critical Reynolds number is between 2,300 and 4,000 for pipe flows.

The critical Reynolds number is also referred to as the transition Reynolds number. It varies widely depending on the conditions of surface roughness, flow disturbances, flow velocity and geometric considerations. For example, the critical Reynolds number for the boundary layer flow over a flat plate reaches about 500,000 based on the free stream velocity outside of the boundary layer and characteristic length of the distance from the leading edge of the plate.

Turbulent Flow Verses Laminar Flow

At low values of Reynolds number the viscous force is large compared to the inertial force.

In this range, viscous forcing dampens out disturbances in the flow field that are a result of surface roughness or pressure gradients. As the Reynolds number increases, the viscous force becomes relatively smaller and at some point it becomes possible for small perturbation to grow. The flows become unstable and can transition to turbulence where large fluctuations in the velocity field continue to develop.

Figure 25 shows two different flow patterns in pipes for laminar flow and turbulent flow. It is evident in the image that turbulent flow undergoes irregular flow patterns while laminar flow moves in smooth layers while maintaining a constant flow direction. The turbulent flows happen at a high Reynolds number where inertial forces are higher than viscous forces and perturbations can become amplified, whereas the laminar flows occur at a low Reynolds number in which any induced perturbations are damped out due to relatively strong viscous forces.

Figure 25: Flow Patterns

Figure 26 shows the time history of local velocity variations for laminar flows and turbulent flows, respectively. These patterns can be obtained from hot wire anemometer measurements or CFD simulations. For the pipe flow cases, laminar flows have nearly constant velocity, while turbulent flows have random or chaotic velocity fluctuation patterns. For a cylinder in cross flow, laminar flows produce a sine wave velocity pattern at a downstream location of the cylinder, while the turbulent flows have similar wave patterns but with embedded fluctuations.

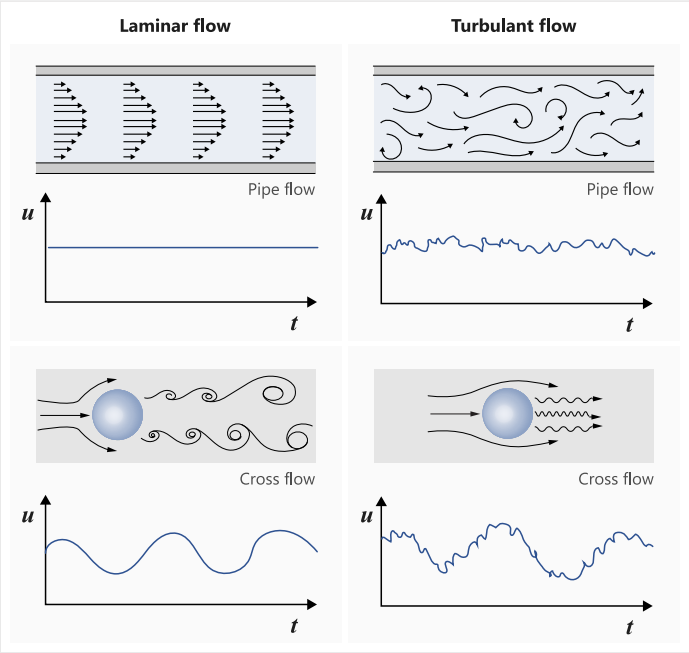

Figure 26: Time History of Instantaneous Velocity at a Local Point

If you consider a flat plate immersed in a flow field with finite viscosity, a thin boundary layer will begin to develop as a function of the distance traveled along the plate (x). The image below shows a comparison of time-averaged velocity profiles for laminar flow and turbulent flow over a flat plate. The time-averaged velocity profile in a turbulent flow appears more uniform than in a laminar flow because the eddy motions in turbulent flow transport momentum more actively from one place to another. This process results in a more uniform profile outside the boundary layer. The velocity gradient near the wall is higher than the one seen in a laminar flow resulting in a larger skin friction coefficient (C_f) than the laminar flow. The skin friction coefficient can be defined as

$$C_f = \frac{\tau_w}{\frac{1}{2}\rho U^2} \tag{53}$$

where $\tau_w = \mu \frac{\partial U}{\partial y}$ is the wall shear stress, μ is the dynamic viscosity, ρ is the density and U is the mean velocity. The local Reynolds number (Re_x) is calculated by using the distance from the leading edge of the flat plate as the length scale. Re_x measures the local ratio of inertial to viscous forcing and provides an indication of the state of the flow regime as it moves from laminar to turbulent.

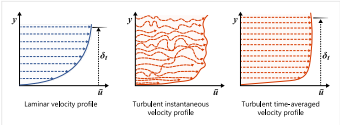

Figure 27: Time Averaged Velocity Profiles for Laminar and Turbulent Flows

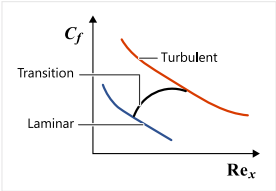

Figure 28: Time Averaged Skin Friction Coefficient for Laminar Flow and Turbulent Flow

The information below includes equations of boundary layer thickness and skin friction coefficient for turbulent flow and laminar flow. These equations where developed through empirical relationships between local Reynolds number and boundary layer characteristics. The information below also provides a summary of general characteristics that are present in turbulent flow and laminar flow.

Table 2: Laminar Flow vs Turbulent Flow: Boundary Layer Thickness and Skin Friction Coefficient

Laminar Flow	**Turbulent Flow**
Boundary layer thickness: $\delta_l = 4.91 \quad x/\sqrt{\mathrm{Re}_x}$	Boundary layer thickness: $\delta_t \cong 0.38 \quad x/(\mathrm{Re}_x)^{1/5}$
Skin friction coefficient: $C_{fl} = \quad 0.664/\sqrt{\mathrm{Re}_x}$	Skin friction coefficient: $C_{ft} \cong \quad 0.059/(\mathrm{Re}_x)^{1/5}$

Table 3: Laminar Flow vs Turbulent Flow

	Laminar Flow	**Turbulent Flow**
Reynolds Number	Low	High
Flow	High degree of orderness	Unsteady three-dimensional flow with random fluctuations

	Laminar Flow	Turbulent Flow
Disturbance	Damped due to high viscous forces	Amplified by inertia forces
Heat transfer	Low heat transfer	High heat transfer because of active mixing
Friction drag (wall shear stress)	Low (low velocity gradient near walls)	High (high velocity gradient near wall)
Separation	Separation can occur at weak adverse pressure gradient	High momentum flow near wall delay flow separation

Transition Flow

In the real world, laminar flow and turbulent flow coexist when obstacles are located inside of a fluid flow.

Industrial examples of the transition from laminar to turbulent flow regimes can be found in many different applications, as shown in Figure 29.

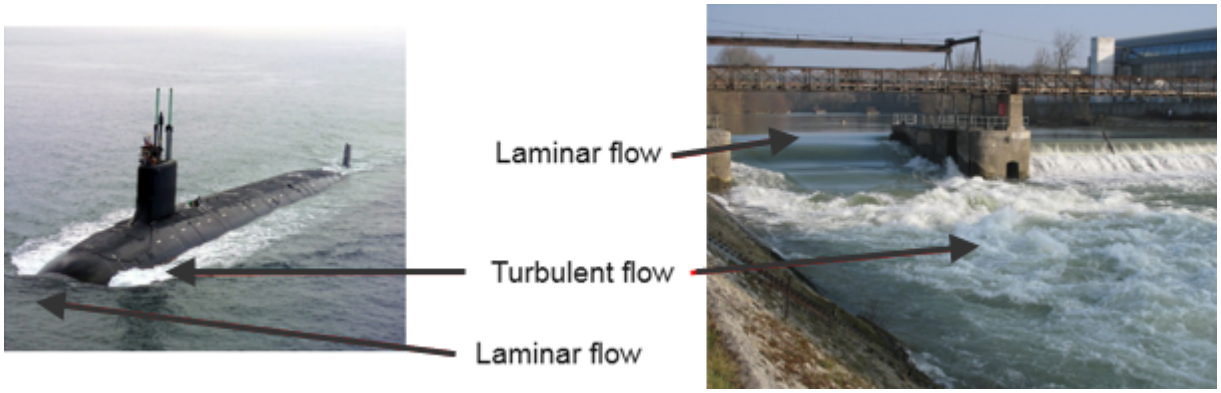

Figure 29: Submarine (left) and Dam (right)

A transition from laminar flow to turbulent flow occurs due to various external factors such as freestream turbulence level (vortical disturbances), sound waves (acoustic disturbances), temperature fluctuations (entropy disturbances), streamwise pressure gradients, surface roughness, surface curvature and vibration. Depending on the external factor or factors, the development of various transition (instability) mechanisms cause the flow to trip from laminar to turbulent. Since transition affects the flow development drag, heat transfer and many other factors it is important to understand the transition phenomena properly. The following section overviews the three main transition processes: natural transition, bypass transition and separation-induced transition.

Natural Transition

In the laminar flow regime viscous forces usually damp out the disturbances.

However, when the free stream turbulence is below one percent and the Reynolds number is higher than the critical Reynolds number, viscous forces destabilize the shear layer such that it becomes unstable two dimensional Tollmien-Schlichting (T-S) waves. These waves develop into three dimensional waves and hairpin vortices, which eventually break down, elongate, and roll up. They then develop into triangular turbulent spots past certain downstream locations. These turbulent spots grow by spreading sideways and burst into a turbulent flow.

Although T-S waves are the main instability mechanisms of the natural transition process for two dimensional boundary layers, such as flows over flat-plates, there are other kinds of instability mechanisms for natural transition. These include Görtler vortices and the crossflow instability.

Görtler vortices generate on any surfaces with concave curvatures from the effects by centrifugal forces. These are counter-rotating pairs of stationary streamwise vortices. Examples of industrial applications with concave surfaces include supercritical airfoils designed for laminar flow control, high speed wind tunnels, as well as forebody compression surfaces ahead of scramjet engine inlets. Details about these vortices are discussed in Saric (1994).

The third instability mechanism is crossflow instability. Crossflow instability develops when the pressure gradient over a swept wing combines with the cross flow from a wing root to a wing tip. It leads to the formation of three dimensional streamwise, co-rotating vortices, inducing transition.

Having an understanding of these instability mechanisms and controlling them with flow controls have received considerable attention over the past decade with the goal of delaying turbulent transition. This is beneficial in reducing the drag of slim bodies, for example wings, by keeping laminar flows as long as possible.

Bypass Transition

Another transition process is bypass transition. When the initial disturbances are high due to surface roughness or freestream turbulence levels higher than one percent, turbulent spots are generated without development of the three initial disturbances, T-S waves, spanwise vorticity and vortex breakdown, observed in the natural transition.

Although the bypass transition phenomena has been investigated in experimental and computational studies it has not been very well understood. A common industrial example of bypass transition is that of turbomachinery. The bypass transition occurs when blades in a gas turbine engine encounter wakes from upstream vanes.

Separation-Induced Transition

The third kind of transition process is separation-induced transition. When a laminar flow experiences adverse pressure gradients, such as airfoil suction surfaces and flow over a sphere, the fluid flow detaches from the wall surface.

If the disturbances are low, separation can cause the generation of structures found in natural transition. Larger disturbances generate Kelvin-Helmholtz instabilities, where vortices roll up before breaking down into turbulence. The process involved in separation-induced transition depends on

the size of the adverse pressure gradient and the presence of additional disturbances, for example obstacles.

Many balls have some type of surface roughness, such as the seams on baseballs and the fuzz on tennis balls. A rough surface can assist in reducing the drag by promoting an early transition.

A number of industrial applications take advantage of this observation for practical design. These include vortex generators on various types of airfoils, such as wind turbine blades, wings and fences on aircraft and automobiles, as well as wings enhanced with surface roughness.

Turbulent Wake

At the low Reynolds number, the downstream flow of the cylinder has a symmetric flow pattern and produces near zero pressure drag.

When flow reaches Re ~ 100,000 vortices begin to shed from each side of the cylinder. This particular shedding pattern is called a Von Kármán vortex street. When the Reynolds number is about 1,000,000 a turbulent wake begins to form behind the cylinder. It is generated by the adverse pressure gradient at the peak position of the cylinder. This forms a large separation region where vortical structures interact and decay downstream. As the Reynolds Number increases the size of the turbulent wake decreases which in turn results in the reduction of the drag. This mainly attributes to the turbulent boundary formation on the cylinder, delaying the flow separation as it has a higher momentum near the cylinder than laminar flow.

As mentioned before, vortex shedding forms behind the cylinder when the Reynolds Number is between 47 and 100,000. This is referred to as a Von Kármán vortex street and is caused by unsteady flow separation around the cylinder (see Figure 30). Since vortices induce low-pressure zones, the cylinder experiences lateral (sideways) forces. When the frequency of lateral forces is close to the natural frequency of the cylinder, unwanted structural vibration will occur. In order to remedy this issue, spirals are sometimes installed on objects subject to wind loading, such as a chimney.

Figure 30: Vortex Shedding Formation Downstream of a Cylinder (left) and Chimney with Spirals (right)

Blunt bodies experience strong pressure drag compared to skin friction. This occurs due to the pressure imbalance between the front cross-section of the blunt bodies and the downstream cross-section. This pressure imbalance is attributed to the formation of downstream turbulent wakes, which reduces the local pressure. The high-pressure drag is a determinant factor of the flying range of a ball. As an example, it is common practice to make dimples on the surface of golf balls so that turbulent boundary

layers form on the surface of a ball. This results in delayed flow separation and consequently reduces the size of the turbulent wake. Since the reduction of turbulent wake induces the smaller pressure drag, the golf ball with dimples should fly for a longer range when compared to the smooth ball.

Compared to the sphere in an airfoil at a low angle-of-attack (AOA) produces a smaller wake size, which results in the reduction of pressure drag. That is why the total drag is smaller for the airfoil than the ball, although the friction (viscous) drag is higher on the airfoil. Consequently, designers focus on the friction drag reduction by employing smooth surfaces. This is contrary to a ball with dimples for long flying range. However, since the turbulent wake size increases for high AOA, designers will shift their focus on reducing wake size by controlling flow on the airfoil suction side where it separates. Several methods are available, including a leading-edge extension, a vortex generator and a flow injection method.

The Navier-Stokes Equations

The physics of turbulent flows have been discussed by presenting experimental observations and comparing it to laminar flows. In this chapter, the focus will shift to the governing equations of these flow fields.

The Navier-Stokes (NS) equations were named after Claude-Louis Navier and George Gabriel Stokes. These equations govern the flow motion of a fluid and usually consist of the mass conservation equation and the momentum conservation equation. Sometimes, the momentum conservation equations alone represent the Navier-Stokes equations. The NS equations govern the behavior of a viscous fluid by balancing the forces with Newton's second law and assuming that the stress in the fluid is the sum of a diffusing viscous term. In the case of incompressible Newtonian fluid the instantaneous continuity equation is the mass conservation equation, which reads in vector notation as:

$$\nabla \cdot \vec{u} = 0 \tag{54}$$

where $\vec{u}$ is the velocity vector.

In tensor notation, the continuity equation is expressed as $\frac{\partial u_i}{\partial x_i} = 0.$

The instantaneous momentum equation using vector notation is written as

$$\frac{\partial \vec{u}}{\partial t} + \vec{u} \cdot \nabla \vec{u} = \frac{-\nabla p}{\rho} + \frac{\nabla \cdot \tau}{\rho} \tag{55}$$

where ρ is the fluid density, p is the pressure and τ is the viscous stress tensor. In tensor notation, the incompressible momentum equation is given by

$$\frac{\partial u_i}{\partial t} + u_j \frac{\partial u_i}{\partial x_j} = \frac{-1}{\rho}\frac{\partial p}{\partial x_i} + \frac{1}{\rho}\frac{\partial \tau_{ij}}{\partial x_j} \tag{56}$$

The left-hand side of the equation describes acceleration, which includes the unsteady term and convective term. The right-hand side of the equation represents the summation of pressure and the shear-stress divergence terms. The convective term is non-linear due to an acceleration associated with the change in velocity over position. This term can be disregarded in one-dimensional flow and Stokes flow (or creeping flow). For the Newtonian fluid, the viscous shear stress is assumed to be proportional to the shear strain rate. Thus, viscous stresses can be obtained by

In vector notation, $\tau = \mu\left(\nabla\vec{u} + (\nabla\vec{u})^T\right) = \mu\nabla^2\vec{u}$

In tensor notation, $\tau_{ij} = \mu\left(\frac{\partial u_i}{\partial x_j} + \frac{\partial u_j}{\partial x_i}\right)$

Vorticity Transport Equation

Since turbulent flows contain eddies that are rotational, a transport equation of local rotation (vorticity) of the fluid is briefly discussed.

The vorticity vector, $\vec{\omega}$, is the curl of the velocity vector and is defined as follows:

$$\vec{\omega} = \nabla \times \vec{u} \tag{57}$$

or

$$\omega_i = \epsilon_{ijk}\frac{\partial u_k}{\partial x_j} sa \tag{58}$$

The vorticity transport equation can be obtained by taking the curl of the momentum conservation equation:

$$\underset{U}{\nabla \times \frac{\partial \vec{u}}{\partial t}} + \underset{C}{\nabla \times (\vec{u} \cdot \nabla\vec{u})} = \underset{P}{-\nabla \times \frac{\nabla p}{\rho}} + \underset{V}{\nabla \times \left(\frac{\mu\nabla^2\vec{u}}{\rho}\right)} \tag{59}$$

The U term becomes $\nabla \times \frac{\partial \vec{u}}{\partial t} = \frac{\partial}{\partial t}(\nabla \times \vec{u}) = \frac{\partial \vec{\omega}}{\partial t}$

The P term vanishes as $\nabla \times \nabla \cdot \mathrm{p} = 0$

The V term becomes $\nabla \times \left(\frac{\mu\nabla^2\vec{u}}{\rho}\right) = \frac{\mu}{\rho}\nabla^2\vec{\omega}$

The convective term in C can be written as:

$$\vec{u} \cdot \nabla\vec{u} = \frac{1}{2}\nabla(\vec{u} \cdot \vec{u}) - \vec{u} \times (\nabla \times \vec{u}) = \frac{1}{2}\nabla(u^2) - \vec{u} \times \vec{\omega} \tag{60}$$

The C term becomes $\nabla \times (\vec{u} \cdot \nabla\vec{u}) = \nabla \times \frac{1}{2}\nabla(u^2) - \nabla \times (\vec{u} \times \vec{\omega}) = \nabla \times (\vec{\omega} \times \vec{u})$

The C term can be rearranged as $\nabla \times (\vec{\omega} \times \vec{u}) = (\vec{u} \cdot \nabla)\vec{\omega} - (\vec{\omega} \cdot \nabla)\vec{u}$

After substituting above terms, the vorticity transport equation can be obtained as:

$$\frac{\partial \vec{\omega}}{\partial t} + (\vec{u} \cdot \nabla)\vec{\omega} = (\vec{\omega} \cdot \nabla)\vec{u} + \frac{\mu}{\rho}\nabla^2\vec{\omega} \tag{61}$$

Using tensor notation, it is given by:

$$\frac{\partial \omega_i}{\partial t} + u_j\frac{\partial \omega_i}{\partial x_j} = \omega_j\frac{\partial u_i}{\partial x_j} + \frac{\mu}{\rho}\frac{\partial^2\omega_i}{\partial x_j \partial x_j} \tag{62}$$

The vortex stretching term, $\omega_j \frac{\partial u_i}{\partial x_j}$, on the right-hand side of the equation corresponds to the enhancement of vorticity ω_j when a fluid element is stretched $\frac{\partial u_i}{\partial x_j}<0$. In other words, when the cross section of the fluid element is decreased, the vorticity is increased. The image below shows the concept of vortex stretching. In the image, there are two cylindrical fluid elements within the streamwise fluid flow. The concept shows that compared to a thick element a thin element has stronger vorticity due to the angular momentum conservation.

In two-dimensional flow, the vortex stretching term $\omega_j \frac{\partial u_i}{\partial x_j}$ vanishes since $\omega_x = 0$, $\omega_y = 0$ and $\frac{\partial}{\partial z} = 0$. Therefore, the vortex stretching term is essential to the energy cascade for three-dimensional turbulent flow.

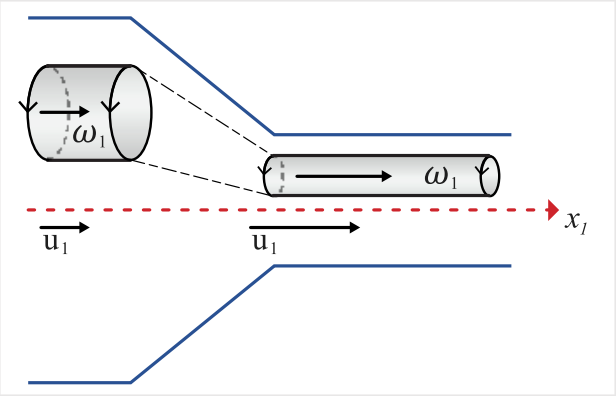

Figure 31: Vortex Stretching

Turbulence Scales and Energy Cascade

Turbulence is composed of turbulent eddies of different sizes. At high Reynolds numbers, a scale separation exists between the largest eddies and smallest eddies.

The largest eddies extract kinetic energy from the mean flow as the energy production. The length scale is comparable to the flow dimensions. These processes are highly anisotropic and mostly are not influenced by viscosity. Most transport and mixing happen in this range.

The smallest eddies have universal characters independent of the flow geometry and conditions. Those eddies in this range usually receive energy from the larger eddies and dissipate their energy into heat through the fluid's molecular viscosity. These eddies are isotropic with length scales as described by Kolmogorov scales. It is assumed that the small scale eddies are determined by viscosity and dissipation.

The intermediate eddies are called Taylor length scale eddies with the length scales in the inertial subrange. Compared to the dissipation range, the turbulence in this region is also isotropic but the eddies in this region are independent of both the largest eddies and the smallest eddies in the dissipation range. It is assumed that the eddies in this region can be characterized by the turbulent dissipation ε and the wave number κ (or eddy size l). Through dimensional analysis you obtain

$$E = C_k \kappa^{-5/3} \varepsilon^{2/3} \quad (63)$$

where the Kolmogorov constant C_k = 1.5.

If the flow is fully turbulent flow at a high Reynolds number, the energy spectra should exhibit a -5/3 decay in the inertia region. This is called Kolmogorov spectrum law or the -5/3 law.

Richardson (1922) introduced the energy cascade concept, "Big whorls have little whorls that feed on their velocity; And little whorls have lesser and so on to viscosity."

The largest eddies with integral length scale are unstable and break up, transferring kinetic energy to smaller eddies. A similar break-up process with these smaller eddies transfer their energy to subsequent smaller eddies. These processes continue until the eddy size is reduced to the smallest size and the eddy motion is stable. This process is known as the energy cascade, as shown in Figure 32.

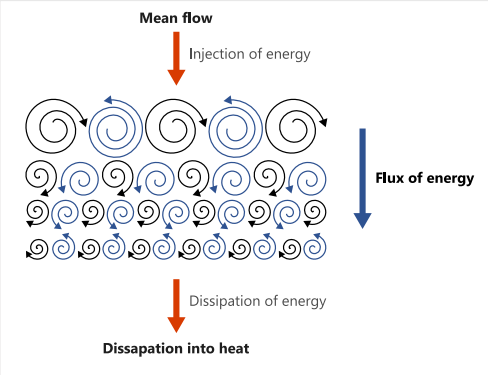

Figure 32: Energy Cascade

The image above illustrates a typical energy spectrum (E) of turbulent eddies in wave number space (κ). Since the turbulent flow has a wide range of eddies with different length scales, it is convenient to utilize the energy spectrum of the velocity field for the classification of eddies into three representative length scales, the integral length scale, the Taylor microscale and the Kolmogorov length scale.

The integral length scale is the largest eddy size of the energy spectrum. These are the most energetic and highly anisotropic eddies that produce energy via the interaction with the mean flow. Eddies in the integral range (A) are very sensitive to flow conditions and their sizes are close to the characteristic length of the flow (for example hydraulic diameter). Its spectrum is defined as $E \propto v^2 l$. The integral length scale is $l = k^{3/2}/\varepsilon$ and corresponding time scales of $t = k/\varepsilon$ and velocity scale $v = \sqrt{k}$.

The Taylor microscale is an intermediate eddy size of the energy spectrum between the largest eddy and the smallest eddy where the flow is inviscid. In this inertial subrange (B), the kinetic energy is transferred from large turbulent eddies to the small eddies in what is defined as the energy cascade. The occurrence of the energy cascade is related to the process of the vortex stretching. The vortex stretching causes the rotational rate of the turbulent eddies to increase and the radius of their cross sections to decrease. The energy spectrum of the inertial subrange is obtained through dimensional

analysis and shows that the energy spectrum is proportional to the product of the wave number and the dissipation rate $E \propto \kappa^{-5/3}\varepsilon^{2/3}$.

The Kolmogorov scale is the smallest eddy size and is in the dissipative range (C) of the energy spectrum. Turbulent eddies in the dissipative range are isotropic because the diffusive actions of strong viscosity smear out anisotropic characteristics of the larger eddies. In this region the kinetic energy received from larger eddies is dissipated into heat. The length scale of this region is assumed be a function of the kinematic viscosity (ν) and the turbulent dissipation rate per unit mass (ε). Using dimensional analysis you obtain

- The Kolmogorov length scale $\eta = \left(\frac{\nu^3}{\varepsilon}\right)^{1/4}$
- The Kolmogorov time scale $\tau_\eta = \left(\frac{\nu}{\varepsilon}\right)^{1/2}$
- The Kolmogorov velocity scale $v_\eta = (\nu\varepsilon)^{1/4}$
- The energy spectrum $E \propto \upsilon^{5/4}\varepsilon^{1/4}$.

The ratio of the integral length scale to the Kolmogorov length scale $l/\eta \sim \left(\frac{\rho v l}{\mu}\right)^{3/4} = \mathrm{Re}^{3/4}$.

Corresponding time scale and velocity scale ratios are, respectively, given as $t/\tau = \sqrt{\mathrm{Re}}$ and $v/v_\eta \sim \mathrm{Re}^{1/4}$.

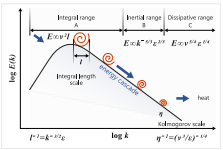

Figure 33: Schematic Representation of Turbulence Energy Spectrum

Considering these scale ratios, you can see larger scale separation between the integral length scale and the Kolmogorov length scale with an increase of the turbulent Reynolds number. This suggests that the Kolmogorov length scale is much smaller than the integral length scale for high turbulent Reynolds number.

References

Bradshaw, P., 1971, "An Introduction to Turbulence and Its Measurement," Pergamon Press, Oxford, England.

Hinze, J. O., 1975, "Turbulence," 2nd Edition, McGraw-Hill, New York, USA.

Launder, B.E., 1991, "An Introduction to the Modeling of Turbulence,' VKI Lecture Series 1991-02.

Pope, S. B., 2000, "Turbulent Flows," University Press, Cambridge, England.

Richardson, L. F., 1922, "Weather Prediction by Numerical Process," University Press, Cambridge, USA.

Saric, W.S., 1994, "Görtler Vortices," Annual Review of Fluid Mechanics, Vol. 26, pp. 379-409.

Tennekes, H. and Lumley, J.L., 1972, "A First Course in Turbulence," The MIT Press, Cambridge, USA.

van Dyke, M., 1982, "An Album of Fluid Motion," Stanford University, California, USA.

White, F.M., 1991, "Viscous Fluid Flow," McGraw-Hill, New York, USA.

Modeling of Turbulence

This section covers the numerical modeling of turbulence by various turbulence models, near wall modeling and inlet turbulence parameters specified for turbulence models.

Although turbulence has been researched for centuries it continues to pose some of the most difficult and fundamental problems in physics because it is a complex, nonlinear phenomenon.

It has the following characteristics:

- Three dimensional and time dependent
- Irregular and chaotic in nature
- Non repetitive
- Contains a vast range of length and time scales
- Has a length scale reduction with increasing Reynolds number
- Is sensitive to boundary and initial conditions

Considering these turbulence characteristics, resolving the turbulent quantities directly by means of Direct Numerical Simulation (DNS) is impractical due to the limitations of currently available computational resources. For this reason, the preferred approach is not to resolve turbulence but to model it with consideration of the following observations:

- Statistical averages of quantities in turbulent flows are reproducible.
- Engineering problems are concerned with the mean flow motion, not the instantaneous motion.

  Given these justifications, turbulence models are developed to account for the effects of eddies on the mean flow field in order to make Computational Fluid Dynamics (CFD) plausible on industrial scale engineering problems.

  In this section representative turbulent flow cases are provided to explain why turbulent flow simulations could be challenging. Resource requirements for DNS are examined in order to justify the need of turbulence modeling. After a brief comparison of resource requirements for various turbulence models the Reynolds-averaged Navier-Stokes equations (RANS) are introduced and turbulence models are presented to close the RANS equations. The focus then shifts to Large Eddy Simulation (LES).

  Overall, this discussion is primarily aimed at motivating the need for turbulence models when investigating high Reynolds number turbulent flow applications and to introduce commonly available turbulence models to new users.

Challenges in Simulating Turbulent Flows

In order to set the context for the modeling of turbulent flow it is essential to understand why turbulent flow simulations are challenging.

First, examine the turbulence characteristic non-repetition. Figure 34 shows two snapshots of smoke plumes from a burning incense stick. Both instantaneous plumes show the chaotic, continuously evolving movement of the smoke. Due to the sensitivity of the smoke plumes to surrounding conditions (temperature, density and cross flow velocity), the pattern of their movement never repeats. Thus, prediction on such instantaneous turbulent smoke evolutions is understood to be quite challenging.

Figure 34: Snapshots of Smoke Plumes

The Navier-Stokes Equations

The Navier-Stokes (NS) equations are the set of equations that govern the motion of a fluid.

These equations consist of the mass conservation equation and the momentum conservation equations for incompressible flows. The NS equations govern the behavior of a viscous fluid by balancing the forces with Newton's second law and assuming that the stress in the fluid is the sum of a diffusing viscous term and a pressure term. In the case of a Newtonian fluid, the instantaneous continuity equation is defined as

$$\frac{\partial \rho}{\partial t} + \frac{\partial \left(\rho u_j\right)}{\partial x_j} = 0 \tag{64}$$

where ρ is the fluid density and u_j is the velocity tensor.

The incompressible momentum equation is given by

$$\frac{\partial \left(\rho u_i\right)}{\partial t} + \frac{\partial \left(\rho u_i u_j\right)}{\partial x_j} = -\frac{\partial \left(p\delta_{ij}\right)}{\partial x_j} + \frac{\partial \tau_{ij}}{\partial x_j} \tag{65}$$

where ρ is the pressure, τ_{ij} is the viscous stress tensor and δ_{ij} is the Kronecker delta.

$$\delta_{ij} = \begin{cases} 0 & if \quad i \neq j, \\ 1 & if \quad i = j. \end{cases} \tag{66}$$

The left-hand side of the equation describes advection, which includes two terms, the acceleration term and convective term. The right hand side of the equation represents the summation of pressure and the shear-stress divergence terms. The convective term is non linear due to an acceleration associated with the change in velocity as a function of position. This term can be disregarded in one-dimensional flow and Stokes flow, or creeping flow.

For Newtonian fluid the viscous shear stress is assumed to be proportional to the shear strain rate, following Stokes Law. Thus, viscous stresses can be given by

$$\tau_{ij} = \mu\left(\frac{\partial u_i}{\partial x_j} + \frac{\partial u_j}{\partial x_i}\right) - \frac{1}{3}\frac{\partial u_k}{\partial x_k}\delta_{ij} \tag{67}$$

where μ is the molecular (dynamic) viscosity of the fluid.

Now, you have a full set of the Navier-Stokes equations to govern fluid flows. The next step is how to solve these equations. There are two approaches available: analytical approaches and numerical approaches. Since most flows involve convective accelerations, it is difficult to obtain the analytical solutions of the Navier-Stokes equations due to the non-linearity associated with the convective term and coupled nature of the equations. Although analytical solutions do exist for some simple flow cases with certain approximations, they are mostly limited to laminar flows. These are Couette flow and Hangen-Poiseuille flow. The former is a laminar flow between two parallel plates, one of which is moving relative to the others, and the latter is a laminar flow in a long cylindrical pipe of constant cross section. Therefore, a complete description of a turbulent flow can only be obtained by numerically solving the Navier-Stokes equations (Moin and Mahesh, 1998). These are divided into a numerical approach resolving turbulent flows by Direct Numerical Simulation (DNS) and numerical approaches not resolving turbulence but modeling it.

Direct Numerical Simulation

Direct Numerical Simulation (DNS) solves the time dependent Navier-Stokes equations, resolving from the largest length scale of a computational domain size to the smallest length scale of turbulence eddy (Kolmogorov length scale).

Considering a vast range of length scales within the computational domain, you can rightly claim that huge computer resource would be required for DNS. Examining the computer resource requirements for DNS will support this claim.

For a computational square box domain, the number of grid points (n) in one direction depends on the grid spacing ΔL.

$$n = \frac{L}{\Delta L} \tag{68}$$

In order to resolve the Kolmogorov length scale (n), the grid spacing ΔL and the Kolmogorov length scale should have the same order of magnitude.

$$n \sim \frac{L}{\eta} \tag{69}$$

Since the Kolmogorov length scale is a function of the fluid kinematic viscosity (ν) and the turbulent dissipation rate ((ε) $\eta = \left(\frac{\nu^3}{\varepsilon}\right)^{1/4}$), the number of grid points in one direction can be estimated from

$$n \sim L\frac{\varepsilon^{1/4}}{\nu^{3/4}} \tag{70}$$

Utilizing $\varepsilon \sim \frac{U^3}{L}$ the equation for the grid size can be rewritten as

$$n \sim \left(\frac{UL}{\nu}\right)^{3/4} \sim \mathrm{Re}^{3/4} \tag{71}$$

where U is the characteristic velocity.

For three-dimensional flows, the total grid size for DNS can be computed as

$$N = n^3 \sim \mathrm{Re}^{9/4} \tag{72}$$

For a flat plate, turbulent flow occurs when the Re > 500,000 (Schlichting and Gersten, 2000). The above relation shows the estimation of six trillion nodes, which easily exceeds the capacity of even the most advanced high performance computers.

In addition to the demanding grid size requirements of DNS, the computing time step size (Δt) should be small enough to resolve the Kolmogorov time scales. Since the Kolmogorov time scale depends on the Kolmogorov length scale and the characteristic velocity (U), the time step size can be approximated as

$$\Delta t \sim \frac{\eta}{U} \tag{73}$$

Given this, the number of time steps (n_t) can be estimated from the total duration of the simulation (T) and the time step size (Δt)

$$\Delta N_t = \frac{T}{\Delta t} \sim \frac{T}{\eta / U} \tag{74}$$

Utilizing $\eta = \mathrm{Re}^{-3/4} L$ the equation of the number of the time steps can be estimated as

$$N_t \sim \frac{T}{L/U}\mathrm{Re}^{3/4} \propto \mathrm{Re}^{3/4} \tag{75}$$

Finally, the number of floating point operations needed to perform DNS can be computed from the multiplication of total grid size (N) and the number of the time steps

$$N_f = N N_t \propto \mathrm{Re}^3 \tag{76}$$

Therefore, the computational cost for DNS is very expensive, confirming that DNS is not feasible for high Reynolds Number turbulent flows.

In addition, high-order (third-order or higher) numerical schemes are commonly used in order to reduce the numerical dissipation and to keep the problem size tractable. These include spectral methods or spectral element methods. Although these methods are very efficient in resolving the small scales of turbulence, they require that the computational domain be relatively simple. The direct result is that these high-order schemes have little flexibility in dealing with complex industrial geometries because of the structured (blocked) mesh approach. Finally, DNS requires special treatments for realistic initial and boundary conditions

Considering these observations it can be concluded that DNS attempting to resolve all turbulent length and time scales is restricted to the low Reynolds number range and is impractical for industrial flows due to huge computing resource requirements. Most DNS applications are served as benchmark databases for tuning turbulence models and have been used for fundamental turbulent flow studies, including homogeneous turbulent flows with mean strain, free shear layers, fully developed channel flows, jets and so on.

Turbulence Modeling

Three-dimensional industrial scale problems are concerned with the time averaged (mean) flow, not the instantaneous motion. The preferred approach is to model turbulence using simplifying approximations, and not resolve it.

Turbulence modeling is a procedure to solve a modified set of the Navier-Stokes equations by means of developing a mathematical model of the turbulent flow that represents the time-averaged characteristics of the flow. Turbulence modeling is used to compute the impact of eddies on the mean flow field. This approach is based on the assumption that the turbulent eddy motion is “universal” and can be related to the large-scale average motion.

Over the course of the past few decades, turbulence models of various complexities have been developed. Depending on the simplifications made to the Navier-Stokes equations, the turbulence models can be classified as shown below.

Large Eddy Simulation (LES)

LES solves the filtered Navier-Stokes equations to resolve eddies down to the inertial range and it uses subgrid models to account for the influence of eddies in the dissipative range. The computing requirement is substantially less than that of DNS but is still not practical for many industrial applications containing wall bounded flows.

Common types include:

- Smagorinsky model
- Germano dynamic model

Hybrid

Hybrid simulations are the bridge between LES and RANS by utilizing RANS for attached boundary layers and LES for separated flow regions. In general, hybrid simulations need spatial filtering processes to determine the local sub grid turbulent viscosity. Compared to LES and DNS, hybrid simulations are much more tractable since the numerical requirement is less severe than the other two approaches.

Common types include:

- Detached Eddy Simulation (DES)
- Delayed DES (DDES)
- Improved DDES (IDDES)
- Scale Adaptive Simulation (SAS)

- Wall Modeled LES (WMES)
- Zonal LES

Reynolds-averaged Navier-Stokes (RANS)

RANS simulations solve directly for the time averaged flow and model the effects of turbulent eddies on the mean flow. This method is the most computationally efficient CFD approach. Since most engineering problems are concerned with the time-averaged properties of the flow, this approach is used most frequently in the industry. The Reynolds averaging procedure introduces additional unknowns into the Navier Stokes equations, and it is thus necessary to develop additional turbulence model equations to close the set. These additional model equations can be categorized into turbulence models that use the Boussinesq assumption and turbulence models that do not use the Boussinesq assumption. The turbulence models with the Boussinesq assumption have two steps to compute Reynolds stresses for the RANS equations. First, turbulence models are needed for the computations of the eddy viscosity, second, the eddy viscosity is used for the estimation of the Reynolds stress with the Boussinesq assumption. The turbulence models without the Boussinesq assumption, for example, Reynolds stress models or nonlinear eddy viscosity models, determine the Reynolds (turbulent) stresses explicitly by solving an equation for each stress component.

Common types include:

- Seven equation models
- Reynolds stress model (RSM)
- One, two and three equation models + Boussinesq
- v2f, zeta-f
- k-ε, k-ω, SST
- Spalart-Allmaras (SA)

Figure 35 shows turbulence models and their corresponding energy spectrum ranges for modeling. For example, RANS models rely on their transport equations to model the entire wave number range, while LES needs a subgrid model to model behaviors of eddies in the dissipative range, but explicitly resolves the large eddies. The hybrid RANS/LES approach needs a model to cover the inertial range and the dissipative range.

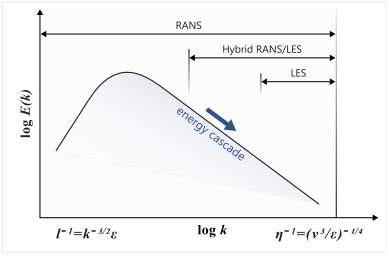

Figure 35: Turbulent Energy Spectrum Modeled by Various Turbulent Flow Simulation Approaches

As expected, computing requirements for these models differ since their models cover a different turbulent spectrum for the range of wave numbers. Spalart (2000) summarized resource requirements for each model, as shown below. Strictly speaking, DNS is not a turbulence model since it is resolving all scales of motion, however, it is included for comparison purposes. Grid numbers and time steps were estimated for a clean wing (Spalart, 2000). Grid numbers and time steps increase from RANS to DNS.

Table 4: CFD Methods (Spalart, 2000)

CFD methods	Reynolds Number Dependence	Empiricism	Grid	Time steps
DNS	strong	none	10^{16}	$10^{7.7}$
LES	weak	weak	$10^{11.5}$	$10^{6.7}$
DES (hybrid)	weak	strong	10^{8}	10^{4}
RANS	weak	strong	10^{7}	10^{3}

Reynolds-Averaged Navier-Stokes (RANS) Simulations

For incompressible turbulent flow the instantaneous velocity field can be decomposed into a time averaged velocity and its corresponding fluctuation.

This is commonly called the Reynolds' decomposition, which is shown in Figure 36.

$$u_i = \overline{u_i} + u_i' \tag{77}$$

where

- u_i: instantaneous velocity,

- $\overline{u_i} = \frac{1}{\Delta t}\int_t^{t+\Delta t} u_i dt$: time averaged velocity over Δt,
- u_i' velocity fluctuation.

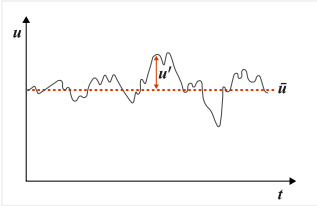

Figure 36: Turbulent Velocity Signals as a Function of Time

Similarly, instantaneous pressure can be decomposed into the time averaged and fluctuation terms.

$$p = \overline{p} + p' \tag{78}$$

where p is the instantaneous pressure.

Once this concept is substituted into the instantaneous Navier-Stokes equations and then time averaging is performed the RANS equations are obtained. The following equations are, respectively, the Reynolds-averaged continuity and Reynolds-averaged momentum equations:

$$\frac{\partial \rho}{\partial t} + \frac{\partial\left(\rho \overline{u}_j\right)}{\partial x_j} = 0 \tag{79}$$

$$\frac{\partial\left(\rho \overline{u}_i\right)}{\partial t} + \frac{\partial\left(\rho \overline{u}_i \overline{u}_j\right)}{\partial x_j} = -\frac{\partial\left(\overline{p}\delta_{ij}\right)}{\partial x_j} + 2\mu\frac{\partial \overline{S_{ij}}}{\partial x_j} + \frac{\partial \tau_{ij}^R}{\partial x_j} \tag{80}$$

where

- $\overline{S_{ij}} = \frac{1}{2}\left(\frac{\partial \overline{u_i}}{\partial x_j} + \frac{\partial \overline{u_j}}{\partial x_i}\right)$ is the mean strain rate tensor,
- $\tau_{ij}^R = -\rho\overline{u_i' u_j'}$ is the Reynolds stress tensor.

It is noted that the momentum equation has an unsteady term (the first term in the left hand side of the momentum equation). Wegner et al. (2004) argued that the RANS equations with the time term (unsteady RANS) can be applied to simulate unsteady flows when a time scale (T2) for large scale motions is larger than a time averaging period for RANS (T1) (see Figure 37). It is worth mentioning that RANS time averaging period (T1) should be considerably larger than the largest turbulence (integral) time scale, as URANS can only give a time averaged mean value for the velocity field, not solving turbulence. Thus, a representative URANS solution is demonstrated by the smoothed red line in the image below. Whereas the blue line represents the velocity profile with instantaneous fluctuations.

Steady RANS can be obtained by removing the time term when there is no large scale unsteadiness observed in turbulent flow.

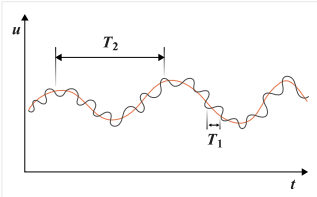

Figure 37: Time Scales for T2 for Large Unsteady Oscillation vs T1 for Turbulent Time Scale

Although Reynolds-averaging eliminates a need to compute the instantaneous flow field, it introduces a new unknown term in comparison to the Navier-Stokes equations. This unknown term is referred to as the Reynolds stress tensor, which represents an added stress due to the turbulent motions. This term arises from the decomposition of the convective term using the Reynolds decomposition. Since your goal is to eliminate any dependence on the instantaneous flow field in these simplified equations, this term should be modeled in terms of the mean flow. This challenge is known as the closure problem of turbulence.

One method that is available for computing the Reynolds Stresses that appear in the RANS equations is to use the Boussinesq approximation. This approach assumes a linear relationship between the turbulent Reynolds stresses and the mean rate of strain tensor:

$$\tau_{ij}^R = -\rho\overline{u_i'u_j'} = \mu_t\left[\frac{\partial\overline{u_i}}{\partial x_j}+\frac{\partial\overline{u_j}}{\partial x_i}-\frac{2}{3}\frac{\partial\overline{u_k}}{\partial x_k}\delta_{ij}\right]-\frac{2}{3}\rho k\delta_{ij} \quad (81)$$

where

- μ_t: the eddy viscosity,
- $k=\frac{1}{2}\overline{u_i'u_j'}$: the turbulent kinetic energy per unit mass,
- δ_{ij}: the Kronecker delta.

Since $\frac{\partial\overline{u_k}}{\partial x_k}$ = 0 for incompressible flow the isotropic eddy viscosity becomes

$$\tau_{ij}^R = \mu_t\left[\frac{\partial\overline{u_i}}{\partial x_j}+\frac{\partial\overline{u_j}}{\partial x_i}\right]-\frac{2}{3}\rho k\delta_{ij} \quad (82)$$

The only unknown in this equation is the eddy viscosity, which must be determined by the turbulence model. There are hundreds of available turbulence models that have been developed to provide this eddy viscosity. Some common Boussinesq models include

- Mixing length model
- Spalart-Allmaras model
- $k-\varepsilon$ model, RNG (Renormalized Group) $k-\varepsilon$model, Realizable $k-\varepsilon$ model
- $k-\omega$ model, SST (Shear Stress Transport) model
- $v2f$ model, zeta-f model

This approach is valid for many turbulent flows, for example, boundary layer, channel flow, round jets, turbulent shear flow and mixing layer, but not for all, for example, impinging flow and swirling flow. Under these circumstances, a model that is capable of predicting anisotropic Reynolds stresses is more appropriate. This can include a full Reynolds stress model (RSM), which determines the turbulent stresses by solving a transport equation for each stress component, or an eddy viscosity model that uses a non linear stress strain relationship to compute each Reynolds stress component separately. Although the improvement in accuracy achieved from this type of modeling is appealing, the introduction of anisotropic stresses is often accompanied by increased compute cost and a decrease in robustness.

The following section provides a review of some commonly used RANS models, ranging from algebraic models (zero equation models) up to the seven equation Reynolds Stress Model.

General Form of Turbulence Models

The general formation of turbulence models can be written as

$$\underbrace{\frac{\partial(\rho\phi)}{\partial t}}_{\text{Unsteady term}} + \underbrace{\frac{\partial\left(\rho\bar{u}_j\phi\right)}{\partial x_j}}_{\text{Convection term}} = \underbrace{\frac{\partial}{\partial x_j}\left[\left(\mu+\frac{\mu_t}{\sigma}\right)\frac{\partial\phi}{\partial x_j}\right]}_{\text{Diffusion term}} + \underbrace{P_\phi}_{\text{Production term}} + \underbrace{D_\phi}_{\text{Dissipation term}} \tag{83}$$

where ϕ is a turbulence model variable, μ_t is the eddy viscosity, μ is the material viscosity and σ is a constant.

The left-hand side of the equation describes advection, which includes two terms, the acceleration term and convective term. The right-hand side of the equation represents the summation of the diffusion, production and dissipation terms. The unsteady term represents the time dependence of turbulence model variables, while the convective term accounts for the rate of change of variables due to convection by the mean flow. The diffusion term on the right side of the equation describes the transport of turbulent variables due to the summation of material viscosity and eddy viscosity. The production term indicates the production rate of turbulent variables from the mean flow gradient, while the dissipation term represents the dissipation rate of turbulent variables due to viscous stresses.

Zero-Equation Eddy Viscosity Models

Mixing-Length Model

The Prandtl mixing-length model for Reynolds-averaged Navier-Stokes (RANS) is based on the assumption that turbulent eddies can be expressed in terms of a product of a velocity scale and a length scale. It has the advantages of fast computation and relatively accurate prediction for simple two-dimensional flows.

However, there exists a limitation in predicting turbulent flows where the turbulent length scale varies (for example, separation or circulation). Currently, the applications of mixing-length models are hardly adopted in commercial CFD codes, but are usually employed to describe near wall behaviors such as wall boundary treatments for more complex turbulence models.

Kinematic Eddy Viscosity

The kinematic eddy viscosity for the mixing-length model is computed using the following relationship

$$\nu_t = l_m^2 \left| \frac{\partial \overline{u}}{\partial y} \right| \tag{84}$$

where l_m is the mixing-length and $\frac{\partial \overline{u}}{\partial y}$ is the mean velocity gradient.

One Equation Eddy Viscosity Models

One equation Reynolds-averaged Navier-Stokes (RANS) models solve a single scalar transport equation to compute the eddy viscosity.

Common one equation models include the Spalart-Allmaras (SA) model and the Nut-92 model. The SA model is discussed in this manual due to its application in general purpose CFD codes and its popularity for the simulation of external flows and internal flows. The details of the Nut-92 model can be found in Shur et al. (1995).

Spalart-Allmaras (SA) Model

The SA model uses a transport equation to solve for a modified kinematic eddy viscosity, $\hat{\upsilon}$, as a function of the kinematic eddy viscosity (ν_t) (Spalart and Allmaras, 1992).

In this model, a length scale (d) in a dissipation term of the modified kinematic eddy viscosity transport equation is specified to determine the dissipation rate. This model has an advantage of having economic solutions for attached flows and moderately separated flows, but it is not recommended for massively separated flows, free shear flows and decaying turbulence.

Transport Equations

$$\frac{\partial(\rho\hat{\upsilon})}{\partial t} + \frac{\partial(\rho\hat{\upsilon}\overline{u_j})}{\partial x_j} = \frac{1}{\sigma}\left(\frac{\partial}{\partial x_j}\left[(\mu+\rho\hat{\upsilon})\frac{\partial\hat{\upsilon}}{\partial x_j}\right] + \rho C_{b2}\frac{\partial\hat{\upsilon}}{\partial x_j}\frac{\partial\hat{\upsilon}}{\partial x_j}\right) + P + D \tag{85}$$

where σ and C_{b2} are constants and μ is the fluid dynamic viscosity. P and D are the production term and destruction term of the modified turbulent viscosity, respectively.

Production of $\hat{\upsilon}$

$$P = \rho C_{b1} \hat{S} \hat{\upsilon} \tag{86}$$

where

- $\hat{S} = \sqrt{2\Omega_{ij}\Omega_{ij}} + \frac{\hat{\upsilon}}{\kappa^2 d^2} f_{v2}$,
- $\Omega_{ij} = \frac{1}{2}\left(\frac{\partial \overline{u_i}}{\partial x_j} - \frac{\partial \overline{u_j}}{\partial x_i}\right)$ is the rotation tensor,
- $f_{v2} = 1 - \frac{\chi}{1+\chi f_{v1}}$,

- d is the distance from the nearest wall,
- κ is the Von Kármán constant,
- C_{b1} is a constant.

Destruction of $\hat{\upsilon}$

$$D = -\rho C_{w1} f_w \left(\frac{\hat{\upsilon}}{d}\right)^2 \tag{87}$$

where

- $f_w = g\left(\frac{1+C_{w3}^6}{g^6+C_{w3}^6}\right)^{1/6}$
- $f_{t2} = C_{t3} exp\left(-C_{t4}\chi^2\right)$
- $g = r + C_{w2}\left(r^6 - r\right)$
- $r = \frac{\hat{\upsilon}}{\hat{S}\kappa^2 d^2}$
- C_{w1} is a constant.

Modeling of Turbulent Viscosity μ_t

The kinematic eddy viscosity for the Spalart-Allmaras model is computed using the following relationship

$$\mu_t = \rho\hat{\upsilon} f_{v1} \tag{88}$$

where

- $f_{v1} = \frac{\chi^3}{\chi^3 + C_{v1}^3}$ is the viscous damping function.
- $\chi = \frac{\hat{\upsilon}}{\nu}$.

Model Coefficients

$C_{w1} = \frac{C_{b1}}{\kappa^2} + \frac{1+C_{b1}}{\sigma^2}$, $C_{w2} = 0.3$, $C_{w3} = 2.0$, $C_{b1} = 0.1355$, $C_{b2} = 0.622$, $C_{v1} = 7.1$ $\sigma = \frac{2}{3}$, $\kappa = 0.41$.

Spalart-Allmaras (SA) Model with Rotation/Curvature Correction

The effects of system rotation and streamline curvature are present in turbomachinery components. Some examples include axial turbines, radial turbines, axial fans, compressors and centrifugal impellors.

This is where most linear eddy viscosity models fail. In order to incorporate the rotational and curvature effects for the SA model, Shur et al. (2000) introduced a version with the modified production term of the transport equation by multiplying the rotation function f_{r1}.

Modified Production of $\hat{\upsilon}$

$$P = \rho f_{r1} C_{b1} \hat{S} \hat{\upsilon} \tag{89}$$

where

- $f_{r1} = (1 + C_{r1}) \frac{2r^*}{1 + r^*} (1 - C_{r3} \ tan^{-1}[C_{r2} \hat{r}]) - C_{r1}$
- $r^* = \frac{S}{\hat{\omega}}$
- $S = \sqrt{2 S_{ij} S_{ij}}$ is the strain rate magnitude.
- $S_{ij} = \frac{1}{2}\left(\frac{\partial \overline{u_i}}{\partial x_j} + \frac{\partial \overline{u_j}}{\partial x_i}\right)$ is the strain rate tensor.
- $\hat{\omega} = \sqrt{2 \hat{\omega}_{ij} \hat{\omega}_{ij}}$ is the modified vorticity magnitude.
- $\hat{\omega}_{ij} = \frac{1}{2}\left(\left[\frac{\partial \overline{u_i}}{\partial x_j} - \frac{\partial \overline{u_j}}{\partial x_i}\right] + 2\varepsilon_{mjl}\Omega'_m\right)$ is the rotation tensor.
- $\hat{r} = \frac{2\omega_{ik} S_{jk}}{D^4}\left(\frac{\partial S_{ij}}{\partial t} + \overline{u_{ij}} \frac{\partial S_{ij}}{\partial x_j} + [\varepsilon_{imn} S_{jn} + \varepsilon_{jmn} S_{in}]\Omega'_m\right)$
- $D = \sqrt{\frac{1}{2}(S^2 + \hat{\omega}^2)}$
- Ω' is the rotation rate.

Model Coefficients

C_{r1} =1.0, C_{r2} =12.0, C_{r3} =1.0

Two Equation Eddy Viscosity Models

Two equation turbulence models are perhaps the most commonly used in industrial flow applications.

Although there are many two equation models available, some of the more popular ones include:

- $k - \varepsilon$ model, Renormalized Group (RNG) $k - \varepsilon$ model, Realizable $k - \varepsilon$ model,
- $k - \omega$ model, Shear Stress Transport (SST) model.

Standard k-ε Model

Launder and Spalding (1974) proposed the standard k-ε turbulence model utilizing the relationships described below.

The model has been shown to be relatively accurate for high Reynolds number flows in which the turbulence behavior is close to homogeneous, and the turbulence production is nearly balanced by dissipation. Nevertheless, its performance deteriorates when predicting boundary layers under adverse pressure gradients (Bradshaw, 1997). It also has difficulty in predicting the viscous sublayer. To resolve this issue, it is suggested that a correction be made to reproduce the law of the wall for incompressible flat-plate boundary layers (Wilcox, 2000). For low Reynolds number flows, the difference between the turbulent kinetic energy production and the dissipation rates may depart from their equilibrium value

of zero, thus, ad-hoc adjustments of empirical parameters are inevitable. Furthermore, the standard k-ε turbulence model does not perform well in shear layers and jets, where the turbulent kinetic energy is not balanced with the dissipation rates (Versteeg and Malalasekera, 2007). Finally, this model is not recommended for high swirling/curvature flows, diverging passage flows as well as flows with a body force under the influence of a rotating reference frame.

Transport Equations

Turbulent Kinetic Energy k

$$\frac{\partial(\rho k)}{\partial t}+\frac{\partial(\rho\overline{u_j}k)}{\partial x_j} =\frac{\partial}{\partial x_j}\left[\left(\mu+\frac{\mu_t}{\sigma_k}\right)\frac{\partial k}{\partial x_j}\right]+P_k+D_k \tag{90}$$

Turbulent Dissipation Rate ε

$$\frac{\partial(\rho\varepsilon)}{\partial t}+\frac{\partial(\rho\overline{u_j}\varepsilon)}{\partial x_j} =\frac{\partial}{\partial x_j}\left[\left(\mu+\frac{\mu_t}{\sigma_\varepsilon}\right)\frac{\partial \varepsilon}{\partial x_j}\right]+P_\varepsilon+D_\varepsilon \tag{91}$$

Production Modeling

Turbulent Kinetic Energy k

$$P_k=\mu_t S^2 \tag{92}$$

where

- $S=\sqrt{2S_{ij}S_{ij}}$ is the strain rate magnitude.
- μ_t is dynamic eddy viscosity.

Turbulent Dissipation Rate ε

$$P_\varepsilon=C_{\varepsilon 1}\frac{\varepsilon}{k}\mu_t S^2=C_{\varepsilon 1}\frac{\varepsilon}{k}P_k \tag{93}$$

Dissipation Modeling

Turbulent Kinetic Energy k

$$D_k=-\rho\varepsilon \tag{94}$$

Turbulent Dissipation Rate ε

$$D_\varepsilon=-C_{\varepsilon 2}\rho\frac{\varepsilon^2}{k} \tag{95}$$

Modeling of Turbulent Viscosity μ_t

$$\mu_t=C_\mu\frac{k^2}{\varepsilon} \tag{96}$$

Model Coefficients

$C_{\varepsilon 1}$ =1.44, $C_{\varepsilon 2}$ =1.92, C_μ =0.09, σ_k =1.0, σ_ε =1.3.

Renormalization Group (RNG) k-ε Model

The RNG k-ε turbulence model (Yakhot and Orszag, 1986) deduces the behavior of large scale eddies from that of the smaller ones by utilizing the scale similarity properties that are inherent in the energy cascade (Bradshaw, 1997).

This model employs a modified coefficient in the dissipation rate equation to account for the interaction between the turbulent dissipation and mean shear. It results in better prediction of flows containing high streamline curvature, flows over a backward facing step (Yakhot et al, 1992), and flows in an expansion duct than the standard k-ε turbulence model. However, its performance worsens when predicting flows in a contraction duct (Hanjalic, 2004).

Transport Equations

Turbulent Kinetic Energy k

$$\frac{\partial(\rho k)}{\partial t}+\frac{\partial(\rho\overline{u_j}k)}{\partial x_j} =\frac{\partial}{\partial x_j}\left[\left(\mu+\frac{\mu_t}{\sigma_k}\right)\frac{\partial k}{\partial x_j}\right]+P_k+D_k \tag{97}$$

Turbulent Dissipation Rate ε

$$\frac{\partial(\rho\varepsilon)}{\partial t}+\frac{\partial(\rho\overline{u_j}\varepsilon)}{\partial x_j} =\frac{\partial}{\partial x_j}\left[\left(\mu+\frac{\mu_t}{\sigma_\varepsilon}\right)\frac{\partial \varepsilon}{\partial x_j}\right]+P_\varepsilon+D_\varepsilon \tag{98}$$

Production Modeling

Turbulent Kinetic Energy k

$$P_k=\mu_t S^2 \tag{99}$$

Turbulent Dissipation Rate ε

$$P_\varepsilon=C_{\varepsilon 1}\frac{\varepsilon}{k}\mu_t S^2=C_{\varepsilon 1}\frac{\varepsilon}{k}P_k \tag{100}$$

Dissipation Modeling

Turbulent Kinetic Energy k

$$D_k=-\rho\varepsilon \tag{101}$$

Turbulent Dissipation Rate ε

$$D_\varepsilon=-C'_{\varepsilon 2}\rho\frac{\varepsilon^2}{k} \tag{102}$$

Modeling of Turbulent Viscosity μ_t

$$\mu_t=C_\mu\frac{k^2}{\varepsilon} \tag{103}$$

Model Coefficients

$C_{\varepsilon 1}$ =1.44, $C_{\varepsilon 2}$ =1.92, C_μ =0.09, σ_k =1.0, σ_ε =1.3, $C'_{\varepsilon 2} = \widetilde{C_{\varepsilon 2}} + \frac{C_\mu \lambda^3 (1-\lambda/\lambda_0)}{1+\beta\lambda^3}$, $\widetilde{C_{\varepsilon 2}}$ = 1.68, C_μ = 0.085, $\lambda = \frac{k}{\varepsilon} S$, λ_0 = 4.38, β = 0.012, σ_k = 0.72, σ_ε = 0.72.

Realizable k-ε Model

The standard k-ε turbulence model and RNG k-ε turbulence model do not satisfy mathematical constraints on the Reynolds stresses for the consistency with physics of turbulence.

These constraints include the positivity of normal stresses ($\overline{u'_\alpha u'_\alpha} \geq 0$) and Schwarz's inequality ($\overline{u'_\alpha u'_\alpha} \quad \overline{u'_\beta u'_\beta} \geq \overline{u'_\alpha u'_\beta} \quad \overline{u'_\alpha u'_\beta}$). The realizable k-ε model proposed by Shih et al. (1995) employs a formulation of turbulent viscosity with a variation of C_μ to satisfy these constraints. This is why this model is referred to as realizable. The second improvement made with the realizable model is to have a source term in the dissipation rate transport equation, which is derived from the transport equation of the mean square vorticity fluctuation. Compared to the standard k-ε turbulence model, it performs better when simulating planar jet flows, round jet flows and flows under adverse pressure gradients. Although the realizable model has significant performance improvement over the standard model, it has a problem in predicting impinging flow, swirling flow and secondary flows in a square duct since this model is based on the Boussinesq assumption. In addition, this model needs additional functions to simulate the near wall effects.

Transport Equations

Turbulent Kinetic Energy k

$$\frac{\partial(\rho k)}{\partial t} + \frac{\partial(\rho \overline{u_j} k)}{\partial x_j} = \frac{\partial}{\partial x_j}\left[\left(\mu + \frac{\mu_t}{\sigma_k}\right)\frac{\partial k}{\partial x_j}\right] + P_k + D_k \tag{104}$$

Turbulent Dissipation Rate ε

$$\frac{\partial(\rho \varepsilon)}{\partial t} + \frac{\partial(\rho \overline{u_j} \varepsilon)}{\partial x_j} = \frac{\partial}{\partial x_j}\left[\left(\mu + \frac{\mu_t}{\sigma_\varepsilon}\right)\frac{\partial \varepsilon}{\partial x_j}\right] + P_\varepsilon + D_\varepsilon + \rho C_1 S \varepsilon \tag{105}$$

Production Modeling

Turbulent Kinetic Energy k

$$P_k = \mu_t S^2 \tag{106}$$

Turbulent Dissipation Rate ε

$$P_\varepsilon = C_{\varepsilon 1} \frac{\varepsilon}{k} P_k \tag{107}$$

Dissipation Modeling

Turbulent Kinetic Energy k

$$D_k = -\rho\varepsilon \tag{108}$$

Turbulent Dissipation Rate ε

$$D_\varepsilon = -\rho C_{\varepsilon 2}\frac{\varepsilon^2}{k+\sqrt{v\varepsilon}} \tag{109}$$

Modeling of Turbulent Viscosity μ_t

$$\mu_t = C_\mu \frac{k^2}{\varepsilon} \tag{110}$$

Model Coefficients

$C_{\varepsilon 1}$ = 1.44, $C_{\varepsilon 2}$ = 1.9, σ_k = 1.0, σ_ε = 1.22.

where $U^* = \sqrt{S_{ij}S_{ij} + \widetilde{\Omega_{ij}}\widetilde{\Omega_{ij}}}$, $\widetilde{\Omega_{ij}} = \Omega_{ij} - 2\varepsilon_{ijk}\omega_k$, $\Omega_{ij} = \overline{\Omega_{ij}} - 2\varepsilon_{ijk}\omega_k$, $A_0 = 4.04$, $A_s = \sqrt{6}\ \ cos\phi$,

$\phi = \frac{1}{3}cos^{-1}\left(\sqrt{6}\ \ W\right), W = \frac{S_{ij}S_{jk}S_{kj}}{\sqrt{S_{ij}S_{ij}}}$,

$C_1 = max\left[0.43, \frac{\eta}{\eta+5}\right]$

where $\eta = S\frac{k}{\varepsilon}$, $S = \sqrt{2S_{ij}S_{ij}}$ is the strain rate magnitude.

Wilcox k-ω Model

Since all three k-ε turbulence models cannot be integrated all the way to walls, wall damping wall functions must be employed to provide correct near wall behavior. It is also known that the standard k-ε turbulence model fails to predict the flow separation under adverse pressure gradients.

Wilcox proposed a turbulence model similar to the standard k-ε turbulence model but replaced the dissipation rate (ε) equation with the eddy frequency (ω) equation (Wilcox, 2006; Wilcox, 2008). The eddy frequency (ω) is often referred to the specific dissipation rate and is defined as $\omega = \varepsilon / k$. The Wilcox k-ω turbulence model has an advantage over the k-ε turbulence model as the k-ω model does not require any wall functions for the calculation of the velocity distribution near walls. As a result, the k-ω turbulence model has better performance for flows with adverse pressure gradient when compared to the k-ε turbulence models. However, the k-ω model exhibits a strong sensitivity to the freestream boundary condition (Wilcox, 2006) for external flow applications.

Transport Equations

Turbulent Kinetic Energy k

$$\frac{\partial(\rho k)}{\partial t} + \frac{\partial\left(\rho\overline{u_j}k\right)}{\partial x_j} = \frac{\partial}{\partial x_j}\left[\left(\mu + \sigma_k\mu_t\right)\frac{\partial k}{\partial x_j}\right] + P_k + D_k \tag{111}$$

Eddy Frequency (Specific Dissipation Rate) ω

$$\frac{\partial(\rho k)}{\partial t}+\frac{\partial(\rho\overline{u_j}k)}{\partial x_j} = \frac{\partial}{\partial x_j}\left[(\mu+\sigma_k\mu_t)\frac{\partial k}{\partial x_j}\right]+P_k+D_k \quad (112)$$

Production Modeling

Turbulent Kinetic Energy k

$$P_k=\mu_t S^2 \quad (113)$$

Eddy Frequency ω

$$P_\omega=\frac{\gamma\omega}{k}\mu_t S^2 \quad (114)$$

where $\gamma=\frac{\beta_0}{\beta^*}-\frac{\sigma_\omega\kappa^2}{\sqrt{\beta^*}}$, $\beta=\beta_0 f_\beta$, $f_\beta=\frac{1+85\chi_\omega}{1+100\chi_\omega}$, $\chi_\omega=\left|\frac{\Omega_{ij}\Omega_{jk}\hat{S}_{ki}}{(\beta^*\omega)^3}\right|$, $\hat{S}_{ki}=S_{ki}-\frac{1}{2}\frac{\partial\overline{u_m}}{\partial x_m}\delta_{ki}$, $S_{ij}=\frac{1}{2}\left(\frac{\partial\overline{u_i}}{\partial x_j}+\frac{\partial\overline{u_j}}{\partial x_i}\right)$, $\Omega_{ij}=\frac{1}{2}\left(\frac{\partial\overline{u_i}}{\partial x_j}-\frac{\partial\overline{u_j}}{\partial x_i}\right)$

Dissipation Modeling

Turbulent Kinetic Energy (k)

$$D_k=-\rho\beta^* k\omega \quad (115)$$

Eddy Frequency (ω)

$$D_\omega=-\rho\beta\omega^2 \quad (116)$$

Modeling of Turbulent Viscosity μ_t

$$\mu_t=\frac{k}{\acute{\omega}} \quad (117)$$

where $\acute{\omega}=max\left[\omega, C_{lim}\sqrt{\frac{2\bar{S}_{ij}\bar{S}_{ij}}{\beta^*}}\right]$, $\bar{S}_{ij}=S_{ij}-\frac{1}{3}\frac{\partial\overline{u_k}}{\partial x_k}\delta_{ij}$, $C_{lim}=\frac{7}{8}$,

Model Coefficients

σ_k = 0.6, σ_ω = 0.5, β^* = 0.09, β_0 = 0.0708, κ = 0.4, $\sigma_d=\begin{cases}0.0 & for \ \frac{\partial k}{\partial x_j}\frac{\partial\omega}{\partial x_j}\le 0\\ \frac{1}{8} & for \ \frac{\partial k}{\partial x_j}\frac{\partial\omega}{\partial x_j}>0\end{cases}$.

Menter Shear Stress Transport (SST) k-ω Model

Menter (1994) suggested the SST model to overcome the freestream value sensitivity of the standard k-ω turbulence model by transforming the k-ε model into the k-ω model in the near-wall region, and by utilizing the k-ε model in the turbulent region far from the wall.

The SST model employs a modified source term in the eddy frequency equation. Among the different SST versions, the SST 2003 model (Menter, 2003) will be focused on in this section as it has been shown to be more accurate when predicting flows near stagnation zones by introducing a production limiter to constrain the kinetic energy production. This version also employs the strain rate magnitude in the definition of eddy viscosity rather than the vorticity magnitude employed in the standard SST model (1994). When compared to the k-ε model, the SST 2003 model achieves better accuracy for attached boundary layers and flow separation. The SST 2003 model also overcomes the freestream sensitivity of the k-ω turbulence model. However, this model shares a similar range of weakness with the k-ε equation models for the predictions of flows with strong streamline curvature and/or rotation, as well as flows under extra strains and body forces.

Transport Equations

Turbulent Kinetic Energy k

$$\frac{\partial(\rho k)}{\partial t}+\frac{\partial(\rho\overline{u_j}k)}{\partial x_j} =\frac{\partial}{\partial x_j}\left[(\mu+\sigma_k\mu_t)\frac{\partial k}{\partial x_j}\right]+\tilde{P}_k+D_k \tag{118}$$

Eddy Frequency (Specific Dissipation Rate) ω

$$\frac{\partial(\rho\omega)}{\partial t}+\frac{\partial(\rho\overline{u_j}\omega)}{\partial x_j} =\frac{\partial}{\partial x_j}\left[(\mu+\sigma_\omega\mu_t)\frac{\partial \omega}{\partial x_j}\right]+P_\omega+D_\omega+2(1-F_1)\frac{\rho\ \sigma_{\omega 2}}{\omega}\frac{\partial k}{\partial x_j}\frac{\partial \omega}{\partial x_j} \tag{119}$$

where

- The blending function $F_1=tanh\left\{\left(min\left[max\frac{\sqrt{k}}{\beta^*\omega d},\frac{500\upsilon}{d^2\omega},\frac{4\rho\sigma_{\omega 2}k}{CD_{k\omega}d^2}\right]\right)^4\right\}$,
- $F_1\begin{cases}0 & :activation\ \ of\ \ k-\varepsilon\ \ model\ \ for\ \ turbulent\ \ core\ \ flows\\ 1 & :activaition\ \ of\ \ k-\omega\ \ for\ \ flows\ \ near\ \ walls\end{cases}$
- $CD_{k\omega}=max\left(2\rho\sigma_{\omega 2}\frac{1}{\omega}\frac{\partial k}{\partial x_i}\frac{\partial \omega}{\partial x_i},\quad 10^{-10}\right)$,
- d is the distance to the nearest wall.

Production Modeling

Turbulent Kinetic Energy k

$$\tilde{P}_k=\min(P_k,\quad 10\rho\beta^*k\omega) \tag{120}$$

where

- Production $P_k=\mu_t S^2$

- Strain rate magnitude $S = \sqrt{2S_{ij}S_{ij}}$
- Strain rate tensor $S_{ij} = \frac{1}{2}\left(\frac{\partial \overline{u_i}}{\partial x_j} + \frac{\partial \overline{u_j}}{\partial x_i}\right)$
- Constant β^*

Eddy Frequency (ω)

$$P_\omega = \alpha \rho S^2 \tag{121}$$

where

- Blending function for specifying constants $\alpha = \alpha_1 F_1 + \alpha_2(1 - F_1)$
- $\alpha_1 = \frac{5}{9}$ for the inner layer
- α_2 = 0.44 for the outer layer.

Dissipation Modeling

Turbulent Kinetic Energy k

$$D_k = -\rho\beta^* k\omega \tag{122}$$

Eddy Frequency ω

$$D_\omega = -\rho\beta\omega^2 \tag{123}$$

Modeling of Turbulent Viscosity μ_t

$$\mu_t = \frac{\rho \quad a_1 \quad k}{\max(a_1\omega, \quad S \quad F_2)} \tag{124}$$

where

- The second blending function $F_2 = tanh\left(max\left(2\frac{\sqrt{k}}{\beta^*\omega \quad d}, \quad \frac{500v}{d^2\omega}\right)\right)^2$,
- Fluid kinematic viscosity v,
- Constant β^*.

Model Coefficients

β^* = 0.09.

Following constants for SST are computed by a blending function $\phi = \phi_1 F_1 + \phi_2(1 - F_1)$: $\sigma_{\omega 1} = 0.5$, $\sigma_{\omega 2} = 0.856$, $\sigma_{k1} = 0.85$, $\sigma_{k2} = 1.00$, $\beta_1 = \frac{3}{40}$, $\beta_2 = 0.0828$.

Shear Stress Transport (SST) Model with Rotation/Curvature Correction

Since the SST model relies on the Boussineq approximation, it also has poor performance for the prediction of flows with streamline curvature and system rotation because the Reynolds stress tensor is aligned to the mean strain rate tensor.

In order to remedy this problem, the rotation curvature correction for the SST 2003 model modifies the production terms in both the kinetic energy equation and eddy frequency equation (Smirnov and Menter, 2009). The corrected model yields better performance over the SST base model when predicting flows with strong streamline curvature and rotating flows caused by strong swirl or geometric constraints.

Production Modeling

Turbulent Kinetic Energy k

$$\tilde{P}_k = \min\left(f_{r1}P_k, \quad 10 f_{r1}\rho\beta^* k\omega\right) \tag{125}$$

where

- $f_{r1} = max\left(min\left[f_{rotation}, \quad 1.25\right], \quad 0.0\right)$
- $f_{rotation} = \left(1+C_{r1}\right)\frac{2r^*}{1+r^*}\left(1-C_{r3} \quad tan^{-1}\left[C_{r2}\hat{r}\right]\right) - C_{r1}$
- $\hat{r} = \frac{2\Omega_{ij}\mathrm{S}_{ij}}{\sqrt{\Omega_{ij}\Omega_{ij}}\,D}\left(\frac{D\mathrm{S}_{ij}}{Dt} + \left[\varepsilon_{imn}\mathrm{S}_{jn} + \varepsilon_{jmn}\mathrm{S}_{in}\right]\Omega_m^{rot}\right)$
- $\Omega_{ij} = \frac{1}{2}\left[\left(\frac{\partial\overline{u_i}}{\partial x_j} - \frac{\partial\overline{u_j}}{\partial x_i}\right) + 2\varepsilon_{mji}\Omega_m^{rot}\right]$
- $\mathrm{S}_{ij} = \frac{1}{2}\left(\frac{\partial\overline{u_i}}{\partial x_j} + \frac{\partial\overline{u_j}}{\partial x_i}\right)$
- $D = \sqrt{max\left(S^2, \quad 0.09\omega^2\right)}$
- $r^* = \frac{S}{W}$
- $S = \sqrt{2S_{ij}S_{ij}}$
- $W = \sqrt{2W_{ij}W_{ij}}$

Eddy Frequency ω

$$P_\omega = f_{r1}\alpha\rho S^2 \tag{126}$$

Model Coefficients

β^* = 0.09, C_{r1} = 1.0, C_{r2} = 2.0, C_{r3} = 1.0.

Three-Equation Eddy Viscosity Models

v2-f Model

In order to account for the near wall turbulence anisotropy and non local pressure strain effects, Durbin (1995) introduced a velocity scale v2 and the elliptic relaxation function f to the standard k-ε turbulence model.

The velocity scale v2 represents the velocity fluctuation normal to the streamline and represents a proper scaling of the turbulence damping near the wall, while the elliptic relaxation function f is used to model the anisotropic wall effects. Compared to the k-ε turbulence models, the v2-f model produces more accurate predictions of wall-bounded flows dominated by separation but suffers from numerical stability issues.

Transport Equations

Turbulent Kinetic Energy k

$$\frac{\partial(\rho k)}{\partial t}+\frac{\partial(\rho\overline{u_j}k)}{\partial x_j} = \frac{\partial}{\partial x_j}\left[\left(\mu+\frac{\mu_t}{\sigma_k}\right)\frac{\partial k}{\partial x_j}\right]+P_k+D_k \tag{127}$$

Turbulent Dissipation Rate ε

$$\frac{\partial(\rho\varepsilon)}{\partial t}+\frac{\partial(\rho\overline{u_j}\varepsilon)}{\partial x_j} = \frac{\partial}{\partial x_j}\left[\left(\mu+\frac{\mu_t}{\sigma_\varepsilon}\right)\frac{\partial \varepsilon}{\partial x_j}\right]+P_\varepsilon+D_\varepsilon \tag{128}$$

Velocity Scale v^2

$$\frac{\partial(\rho\overline{v^2})}{\partial t}+\frac{\partial(\rho\overline{u_j}\overline{v^2})}{\partial x_j} = \frac{\partial}{\partial x_j}\left[\left(\mu+\frac{\mu_t}{\sigma_{v2}}\right)\frac{\partial \overline{v^2}}{\partial x_j}\right]+P_{v2}+D_{v2} \tag{129}$$

Elliptic Relation for the relaxation function f

$$L^2\frac{\partial^2 f}{\partial x_j^2}-f = \frac{(C_1-1)}{T}\left(\frac{v^2}{k}-\frac{2}{3}\right)-C_2\frac{P_k}{\varepsilon}$$

where

- $L=C_L\ max\left(\frac{k^{3/2}}{\varepsilon}, C_\eta\left[\frac{v^3}{\varepsilon}\right]^{1/4}\right)$: the length scale,
- $T=max\left(\frac{k}{\varepsilon}, C_T\sqrt{\left[\frac{v}{\varepsilon}\right]}\right)$: the time scale.

Production Modeling

Turbulent Kinetic Energy k

$$P_k=\mu_t S^2 \tag{130}$$

Turbulent Dissipation Rate ε

$$P_\varepsilon = C_{\varepsilon 1}\frac{\varepsilon}{k}\mu_t S^2 = C_{\varepsilon 1}\frac{\varepsilon}{k}P_k \tag{131}$$

Velocity Scale v^2

$$P_{v2} = \rho k f \tag{132}$$

Dissipation Modeling

Turbulent Kinetic Energy k

$$D_k = -\rho\varepsilon \tag{133}$$

Turbulent Dissipation Rate ε

$$D_\varepsilon = -C_{\varepsilon 2}\rho\frac{\varepsilon^2}{k} \tag{134}$$

Velocity Scale v^2

$$D_{v2} = -\rho\varepsilon\frac{\overline{v^2}}{k} \tag{135}$$

Modeling of Turbulent Viscosity μ_t

$$\mu_t = \rho C_\mu \overline{v^2} T \tag{136}$$

Model Coefficients

$C_{\varepsilon 1}$ = 1.44, $C_{\varepsilon 2}$ = 1.92, C_μ = 0.22, σ_k = 1.0, σ_ε = 1.3. C_1 = 1.4, C_2 = 0.45, C_T = 6.0, C_L = 0.25, C_η = 85, σ_{v2} = 1.0.

Zeta-F Model

The base model of the zeta-f model is the v2f model described by Durbin (1995).

However, by introducing a normalizing velocity scale, the numerical stability issues found in the v2f model have been improved (Hanjalic et al., 2004; Laurence et al., 2004; Popovac and Hanjalic, 2007).

Transport Equations

Turbulent Kinetic Energy k

$$\frac{\partial(\rho k)}{\partial t} + \frac{\partial(\rho\overline{u_j}k)}{\partial x_j} = \frac{\partial}{\partial x_j}\left[\left(\mu + \frac{\mu_t}{\sigma_k}\right)\frac{\partial k}{\partial x_j}\right] + P_k + D_k \tag{137}$$

Turbulent Dissipation Rate ε

$$\frac{\partial(\rho\varepsilon)}{\partial t} + \frac{\partial(\rho\overline{u_j}\varepsilon)}{\partial x_j} = \frac{\partial}{\partial x_j}\left[\left(\mu + \frac{\mu_t}{\sigma_\varepsilon}\right)\frac{\partial \varepsilon}{\partial x_j}\right] + P_\varepsilon + D_\varepsilon \tag{138}$$

Normalized Velocity Scale $\varsigma = \frac{\overline{v^2}}{k}$

$$\frac{\partial(\rho\varsigma)}{\partial t}+\frac{\partial(\rho\overline{u_j}\varsigma)}{\partial x_j} = \frac{\partial}{\partial x_j}\left[\left(\mu+\frac{\mu_t}{\sigma_\varsigma}\right)\frac{\partial\varsigma}{\partial x_j}\right]+P_\varsigma+D_\varsigma \quad (139)$$

Elliptic Relation for the Relaxation Function f

$$L^2\frac{\partial^2 f}{\partial x_j^2}-f = \frac{1}{T}\left(C_1+C'_2\frac{P_k}{\varepsilon}-1\right)\left(\varsigma-\frac{2}{3}\right) \quad (140)$$

where $L=C_L \ max\left(min\left[\frac{k^{3/2}}{\varepsilon},\frac{\sqrt{k}}{\sqrt{6}\,C_\mu|S|\varsigma}\right],C_\eta\left[\frac{\nu^3}{\varepsilon}\right]^{1/4}\right)$: the length scale, $T=max\left(min\left[\frac{k}{\varepsilon},\frac{0.6}{\sqrt{6}\,C_\mu|S|\varsigma}\right],C_T\sqrt{\left[\frac{\nu}{\varepsilon}\right]}\right)$: the time scale.

Production Modeling

Turbulent Kinetic Energy k

$$P_k=\mu_t S^2 \quad (141)$$

Turbulent Dissipation Rate ε

$$P_\varepsilon=C_{\varepsilon1}\frac{\varepsilon}{k}\mu_t S^2=C_{\varepsilon1}\frac{\varepsilon}{k}P_k \quad (142)$$

Velocity Scale ς

$$P_\varsigma=\rho f$$

Dissipation Modeling

Turbulent Kinetic Energy k

$$D_k=-\rho\varepsilon \quad (143)$$

Turbulent Dissipation Rate ε

$$D_\varepsilon=-C_{\varepsilon2}\rho\frac{\varepsilon^2}{k} \quad (144)$$

Velocity Scale ς

$$D_\zeta=-\rho\frac{\zeta}{k}P_k \quad (145)$$

Modeling of Turbulent Viscosity μ_t

$$\mu_t=\rho C_\mu\varsigma kT \quad (146)$$

Model Coefficients

$C_{\varepsilon1}$ = 1.44, $C_{\varepsilon2}$ = 1.92, C_μ = 0.22, σ_k = 1.0, σ_ε = 1.3. C_1 = 1.4, C'_2 = 0.65, C_T = 6.0, C_L = 0.36, C_η = 85, σ_ζ = 1.2.

Reynolds Stress Models

The Reynolds stress model (RSM) determines the turbulent stresses by solving a transport equation for each stress component.

The RSM accounts for the effects of flow history and streamline curvature, as well as system rotation and stratification (Wilcox, 2000). Reynolds stress models are known to give superior results over one and two equation models when dealing with flows with streamline curvature, flows with sudden change in strain rate, and flows with secondary motions, all at the cost of an increased computing time (Bradshaw, 1997). There are many types of Reynolds stress models, the two most common being the RSM based on the dissipation rate (ε) and the RSM based on the eddy frequency (ω). In this section the dissipation rate (ε) model is discussed.

Transport Equations

Reynolds Stresses $\overline{u'_i u'_j}$

$$\frac{\partial\left(\rho\,\overline{u'_i u'_j}\right)}{\partial t}+\frac{\partial\left(\rho\overline{u_k}\,\overline{u'_i u'_j}\right)}{\partial x_k} = P_R+D_R+\Pi_{ij}+D_{RM}+D_{RT} \tag{147}$$

Turbulent Dissipation Rate ε

$$\frac{\partial(\rho\varepsilon)}{\partial t}+\frac{\partial\left(\rho\overline{u_j}\varepsilon\right)}{\partial x_j} = \frac{\partial}{\partial x_j}\left[\left(\mu+\frac{\mu_t}{\sigma_\varepsilon}\right)\frac{\partial\varepsilon}{\partial x_j}\right]+P_\varepsilon+D_\varepsilon \tag{148}$$

Production Modeling

Reynolds Stresses $\overline{u'_i u'_j}$

$$P_R = -\rho\left(\overline{u'_i u'_k}\frac{\partial\overline{u_j}}{\partial x_k}+\overline{u'_j u'_k}\frac{\partial\overline{u_i}}{\partial x_k}\right) \tag{149}$$

Turbulent Dissipation Rate ε

$$P_\varepsilon = C_{\varepsilon 1}\frac{\varepsilon}{k}\mu_t S^2 = C_{\varepsilon 1}\frac{\varepsilon}{k}P_k \tag{150}$$

Dissipation Modeling

Reynolds Stresses $\overline{u'_i u'_j}$

$$D_R = -2\mu\left(\frac{\partial\overline{u_i}}{\partial x_k}\frac{\partial\overline{u_j}}{\partial x_k}\right) \tag{151}$$

Turbulent Dissipation Rate ε

$$D_\varepsilon = -C_{\varepsilon 2}\rho\frac{\varepsilon^2}{k} \tag{152}$$

Molecular Diffusion Modeling

Reynolds Stresses $\overline{u'_i u'_j}$

$$D_{RM} = \mu \frac{\partial}{\partial x_k}\left(\frac{\partial \overline{u'_i u'_j}}{\partial x_k}\right) \tag{153}$$

Turbulent Diffusion Modeling

Reynolds Stresses $\overline{u'_i u'_j}$

$$D_{RT} = \frac{\mu_t}{\rho \sigma_k}\frac{\partial}{\partial x_k}\left(\frac{\partial \overline{u'_i u'_j}}{\partial x_k}\right) \tag{154}$$

Pressure-Strain Modeling

Reynolds Stresses $\overline{u'_i u'_j}$

$$\Pi_{ij} = \Pi_{ij,s} + \Pi_{ij,f} + \Pi_{ij,w} \tag{155}$$

where $\Pi_{ij,s} = -C_1 \frac{\rho\varepsilon}{k}\left(\overline{u'_i u'_j} - \frac{2}{3}k\delta_{ij}\right)$,

$\Pi_{ij,f} = \Pi_{ij,f1} + \Pi_{ij,f2}, \Pi_{ij,f1} = -C_2\left(-\rho\left(\overline{u'_i u'_k}\frac{\partial \overline{u_j}}{\partial x_k} + \overline{u'_j u'_k}\frac{\partial \overline{u_i}}{\partial x_k}\right) - \frac{\partial}{\partial x_k}\left(\rho \overline{u_k}\,\overline{u'_i u'_j}\right)\right)$,

$\Pi_{ij,f2} = -\frac{1}{3}\delta_{ij}\left(-\rho\left(\overline{u'_k u'_k}\frac{\partial \overline{u_k}}{\partial x_k} + \overline{u'_k u'_k}\frac{\partial \overline{u_k}}{\partial x_k}\right) - \frac{\partial}{\partial x_k}\left(\rho \overline{u_k}\,\overline{u'_k u'_k}\right)\right)$, $\Pi_{ij,w} = \Pi_{ij,w1} + \Pi_{ij,w2}$,

$\Pi_{ij,w1} = C_3 \frac{\varepsilon_{nc}}{k_{nc}}\left(\overline{u'_k u'_m}\eta_k\eta_m\delta_{ij} - \frac{3}{2}\overline{u'_i u'_k}\eta_j\eta_k - \frac{3}{2}\overline{u'_j u'_k}\eta_i\eta_k\right)\frac{k^{3/2}}{C_w \varepsilon \chi}$,

$\Pi_{ij,w2} = C_4\left(\Pi_{km,f}\eta_k\eta_m\delta_{ij} - \frac{3}{2}\Pi_{ik,f}\eta_j\eta_k - \frac{3}{2}\Pi_{jk,f}\eta_i\eta_k\right)\frac{k^{3/2}}{C_w \varepsilon \chi}$

where η_k is the x_k component of the unit normal to the wall and χ is the normal distance from the wall.

Modeling of Turbulent Viscosity μ_t

$$\mu_t = \rho C_\mu \frac{k^2}{\varepsilon} \tag{156}$$

Model Coefficients

$C_{\varepsilon 1}$ = 1.44, $C_{\varepsilon 2}$ = 1.92, C_μ = 0.09, σ_k = 1.0, σ_ε = 1.0, C_1 = 1.8, C_2 = 0.6, C_3 = 0.5, C_4 = 0.3, $C_w = \frac{C_{\mu 3/4}}{\kappa}$

Turbulent Transition Models

All of the previously described models are incapable of predicting boundary layer transition. To include the effects of transition additional equations are necessary.

Transitional flows can be found in many industrial application cases including gas turbine blades, airplane wings and wind turbines. It is known that conventional turbulence models over predict the wall shear stress for transitional flows. Thus, transition models can be used to improve the accuracy of CFD solutions when flows encounter turbulent transition of the boundary layer.

γ-Reθ Model

Langtry and Menter (2009) proposed one of the most commonly used transition models in industrial CFD applications. The $\gamma - Re_\theta$ model is a correlation based intermittency model that predicts natural, bypass and separation induced transition mechanisms.

The $\gamma - Re_\theta$ model is coupled with the Shear Stress Transport (SST) turbulence model and requires two additional transport equations for the turbulence intermittency (γ) and transition momentum thickness Reynolds number (Re_θ). The turbulence intermittency is a measure of the flow regime and is defined as $\gamma = \frac{t_{\text{turbulent}}}{t_{\text{laminar}} + t_{\text{turbulent}}}$ where $t_{\text{turbulent}}$ represents the time that the flow is turbulent at a given location, while t_{laminar} represents the time that the flow is laminar.

For example, while the intermittency value is zero, the flow is considered to be laminar. A value of one is for fully turbulent flow. The transition momentum thickness Reynolds number is responsible for capturing the non local effects of turbulence intensity and is defined as $Re_\theta = \frac{\rho \bar{u}\ \theta}{\mu}$ where the momentum thickness is $\theta = \int_0^\delta \frac{u}{\bar{u}}\left(1 - \frac{u}{\bar{u}}\right) dy.$

To couple with the SST model, Langtry and Menter (2009) modified the production term and dissipation term of the turbulent kinetic energy to account for the changes in the flow intermittency.

Transport Equations

Turbulent Kinetic Energy k

$$\frac{\partial(\rho k)}{\partial t} + \frac{\partial\left(\rho \overline{u_j} k\right)}{\partial x_j} = \frac{\partial}{\partial x_j}\left[\left(\mu + \sigma_k \mu_t\right)\frac{\partial k}{\partial x_j}\right] + \tilde{P}_k + D_k \tag{157}$$

Eddy Frequency (Specific Dissipation Rate) ω

$$\frac{\partial(\rho\omega)}{\partial t} + \frac{\partial\left(\rho \overline{u_j}\omega\right)}{\partial x_j} = \frac{\partial}{\partial x_j}\left[\left(\mu + \sigma_\omega \mu_t\right)\frac{\partial \omega}{\partial x_j}\right] + P_\omega + D_\omega + 2\left(1 - F_1\right)\frac{\rho\ \sigma_{\omega 2}}{\omega}\frac{\partial k}{\partial x_j}\frac{\partial \omega}{\partial x_j} \tag{158}$$

Turbulent Intermittency γ

$$\frac{\partial(\rho\gamma)}{\partial t} + \frac{\partial\left(\rho \overline{u_j}\gamma\right)}{\partial x_j} = \frac{\partial}{\partial x_j}\left[\left(\mu + \frac{\mu_t}{\sigma_f}\right)\frac{\partial \gamma}{\partial x_j}\right] + P_\gamma + D_\gamma \tag{159}$$

Transition Momentum Thickness Reynolds Number Re_θ

$$\frac{\partial\left(\rho\ \mathrm{Re}_\theta\right)}{\partial t} + \frac{\partial\left(\rho \overline{u_j}\mathrm{Re}_\theta\right)}{\partial x_j} = \frac{\partial}{\partial x_j}\left[\sigma_f\left(\mu + \mu_t\right)\frac{\partial \mathrm{Re}_\theta}{\partial x_j}\right] + P_\theta \tag{160}$$

Production Modeling

Turbulent Kinetic Energy k

$$\tilde{P}_k = \gamma_{eff} \min\left(P_k, \quad 10\rho\beta^* k\omega\right)\frac{\partial \overline{u}_i}{\partial x_j} \tag{161}$$

where

- Production $P_k = \mu_t S^2$
- Strain rate magnitude $S = \sqrt{2\mathrm{S}_{ij}\mathrm{S}_{ij}}$
- Strain rate tensor $\mathrm{S}_{ij} = \frac{1}{2}\left(\frac{\partial \overline{u}_i}{\partial x_j} + \frac{\partial \overline{u}_j}{\partial x_i}\right)$
- Constant β^*

Turbulent Dissipation Rate ε

$$P_\varepsilon = \alpha\rho S^2 \tag{162}$$

where

- Blending function for specifying constants $\alpha = \alpha_1 F_1 + \alpha_2\left(1 - F_1\right)$
- $\alpha_1 = \frac{5}{9}$ for the inner layer
- α_2 = 0.44 for the outer layer.

Turbulent Intermittency γ

$$P_\gamma = F_{length} C_{a1} \quad S \quad \sqrt{\left(\gamma F_{onset}\right)}\left(1 - \gamma C C_{e1}\right) \tag{163}$$

where $F_{onset} = max\left(min\left(max\left[\frac{Re_v}{2.193 \quad Re_{\theta 0}}, \left(\frac{Re_v}{2.193 \quad Re_{\theta 0}}\right)^4\right], 2\right) - max\left(1 - \left(\frac{R_T}{2.5}\right)^3, 0\right)\right)$ $Re_v = \frac{Sd^2}{\nu}$, $R_T = \frac{k\nu}{\omega}$

Transition Momentum Thickness Reynolds Number Re_θ

$$P_\theta = C_{\theta t}\frac{1}{t}\left(\mathrm{Re}_\theta - \overline{\mathrm{Re}_\theta}\right)\left(1 - F_\theta\right) \tag{164}$$

where $F_\theta = \min\left(\max\left[F_{wake} e^{-\left(\frac{d}{\delta}\right)^4}, \quad 1 - \left(\frac{\gamma - 1/C_{e2}}{1 - 1/C_{e2}}\right)^2\right], 1\right)$, $F_{wake} = e^{-\left(\frac{Re_\omega}{1E+5}\right)^2}$, $Re_\omega = \frac{\omega d^2}{\nu}$, $\delta = \frac{50\Omega d}{\overline{u}}\delta_{BL}$,

$\delta_{BL} = 7.5\theta_{BL}$, $\theta_{BL} = \frac{\overline{Re_\theta}\nu}{\overline{u}}$

Dissipation Modeling

Turbulent Kinetic Energy k

$$D_k = -\min\left(\max\left[\gamma_{eff}, \quad 0.1\right], 1.0\right)\rho\beta^* k\omega \tag{165}$$

Turbulent Dissipation Rate ω

$$D_\omega = -\rho\beta\omega^2 \tag{166}$$

Turbulent Intermittency γ

$$D_\gamma = -C_{a2}F_{\text{turbulent}}\Omega\gamma\left(C_{e2}\gamma - 1\right) \tag{167}$$

where $F_{\text{turbulent}} = e^{\left(-\frac{R_T}{4}\right)^4}$

Modeling of Turbulent Viscosity μ_t

$$\mu_t = \frac{\rho \;\; a_1 \;\; k}{\max\left(a_1\omega, \;\; S \;\; F_2\right)} \tag{168}$$

where

- The second blending function $F_2 = tanh\left(max\left(2\frac{\sqrt{k}}{\beta^*\omega \;\; d}, \;\; \frac{500v}{d^2\omega}\right)\right)^2$,
- Fluid kinematic viscosity v,
- Constant β^*.

Correlations

$$Re_\theta = \left(1173.51 - 589.428 \;\; Tu + \;\; \frac{0.2196}{Tu^2}\right)F\left(\lambda_\theta\right) \tag{169}$$

$$Re_{\theta t} = \begin{cases} \left(1173.51 - 589.428 \;\; Tu + \;\; \frac{0.2196}{Tu^2}\right)F\left(\lambda_\theta\right) & for \quad Tu \le 1.3 \\ 331.5\left(Tu - 0.5658\right)^{-0.671} \;\; F\left(\lambda_\theta\right), & for \quad Tu > 1.3 \end{cases} \tag{170}$$

$$F\left(\lambda_\theta\right) \begin{cases} 1 - \left(-12.986\lambda_\theta - 123.66\lambda_{\theta 2} - 405.689\lambda_{\theta 3}\right) \;\; e^{-\left(\frac{Tu}{1.5}\right)^5} & for \quad \lambda_\theta \le 0 \\ 1 + 0.275\left(1 - e^{-35\lambda_\theta}\right)^{-0.671} \;\; e^{-\left(\frac{Tu}{1.5}\right)}, & for \quad \lambda_\theta > 0 \end{cases} \tag{171}$$

where $\lambda_\theta = \frac{\theta^2}{v}\frac{d\bar{u}}{ds}$ is the pressure gradient.

Model Coefficients

β^* = 0.09.

The following constants for SST are computed by a blending function $\phi = \phi_1 F_1 + \phi_2\left(1 - F_1\right)$: $\sigma_{\omega 1}$ = 0.5, $\sigma_{\omega 2}$ = 0.856, σ_{k1} = 0.85, σ_{k2} = 1.00, $\beta_1 = \frac{3}{40}$, β_2 = 0.0828. C_{e1} = 1.0, C_{e2} = 50, C_{a1} = 2.0, C_{a2} = 0.06, $C_{\theta 1}$ = 1.0, $C_{\theta 2}$ = 2.0, σ_f = 1.0.

Large Eddy Simulation (LES)

LES is often regarded as an impractical tool for industrial CFD applications as it requires large computational resources.

LES is associated with the severe requirements of small mesh size and time step size so that the turbulent length scale and time scale in the inertial range is properly resolved. These simulations also have an issue with resolving flows close to walls where energetic vortical structures become very small with the increase of Reynolds number. However, there are cases where LES provides significant benefits, including combustion chemical reaction problems and acoustic problems.

Filtered Navier-Stokes Equations

While Reynolds-averaged Navier-Stokes (RANS) resolves the mean flow and requires a turbulence model to account for the effect of turbulence on the mean flow, Large Eddy Simulation (LES) computes both the mean flow and the large energy containing eddies.

A subgrid model is used to capture the effects of small scale turbulent structures. The spatial filtering process is used to filter out the turbulent structures from the instantaneous flow field which are smaller than a given filter size. This filtering process is based on the decomposition of instantaneous variables (velocity, pressure) into filtered (resolved) and sub filter (unresolved or residual) variables. Here, velocity is used as an example.

$$u_i = \overline{u_i} + u''_i \tag{172}$$

where

- u_i: instantaneous velocity,
- $\overline{u_i}$: filtered velocity,
- u''_i: sub filtered (unresolved) velocity.

The filtered velocity field is obtained from a low pass filtering operation due to a weighted filter G, defined as $\overline{u_i} = \iiint G(x, x', \Delta) u_i(x', t) dx'_1 dx'_2 dx'_3$.

The weighted filter includes

- $G(x, x') = \frac{1}{\pi}\left(\frac{\sin\left(\frac{\pi(x-x')}{\Delta}\right)^2}{(x-x')}\right)$: a cut-off filter,
- $G(x, x') = \sqrt{\frac{6}{\pi\Delta^2}}\, exp\left(\frac{-6(x-x')^2}{\Delta^2}\right)$: a Gaussian filter,
- $G(x, x') = \begin{cases} \frac{1}{\Delta} & \forall \quad |x-x'| \le \frac{1}{2}\Delta \\ 0 & \forall \quad |x-x'| > \frac{1}{2}\Delta \end{cases}$: a top-hat filter,

where $\Delta = \sqrt[3]{\Delta x \Delta y \Delta z}$ is a cutoff width, representing a spatial averaging over a grid element. Among those, a top-hat filter (or similar one) is a popular choice for commercial CFD codes where unstructured meshes are usually adopted.

Although the LES decomposition method resembles the Reynolds method, they have an important difference due to the following. $\widetilde{(\overline{u_i})} \neq \overline{u_i}$, $\widetilde{u''_i} \neq 0$

Once this concept is substituted into the instantaneous Navier-Stokes equations, and then the spatial-averaging (or filtering) is made, the filtered Navier-Stokes equations are obtained. The filtered Navier-Stokes equations include the equations for the filtered continuity and filtered momentum equations, which are given below.

$$\frac{\partial(\rho\overline{u_i})}{\partial x_i} = 0 \tag{173}$$

$$\frac{\partial(\rho\overline{u_i})}{\partial t} + \frac{\partial(\rho\overline{u_i u_j})}{\partial x_j} = -\frac{\partial(\overline{p}\delta_{ij})}{\partial x_j} + 2\mu\frac{\partial\overline{S_{ij}}}{\partial x_j} \tag{174}$$

where

- $\overline{u_i u_j} = \widetilde{(\overline{u_i u_j})} + \widetilde{(u''_i \overline{u_j})} + \widetilde{(\overline{u_i} u''_j)} + \widetilde{(u''_i u''_j)}$ is due to the decomposition of the nonlinear convective term in the momentum equation.
- $\overline{S_{ij}} = \frac{1}{2}\left(\frac{\partial\overline{u_i}}{\partial x_j} + \frac{\partial\overline{u_j}}{\partial x_i}\right)$ is the filtered strain rate tensor.

The filtered momentum equation is rearranged as

$$\frac{\partial(\rho\overline{u_i})}{\partial t} + \frac{\partial(\rho\widetilde{\overline{u_i}\overline{u_j}})}{\partial x_j} = -\frac{\partial\overline{p}}{\partial x_j} + 2\mu\frac{\partial\overline{S_{ij}}}{\partial x_j} + \frac{\partial\tau^*_{ij}}{\partial x_j} \tag{175}$$

where

- $\tau^*_{ij} = -\rho(C_{ij} + R_{ij})$ is a double decomposition stress tensor.
- $C_{ij} = \widetilde{(u''_i \overline{u_j})} + \widetilde{(\overline{u_i} u''_j)}$ is the cross stress tensor, representing the interactions between large and small turbulence eddies.
- $R_{ij} = \widetilde{(u''_i u''_j)}$ is the Reynolds subgrid stress tensor.

Since $\widetilde{(\overline{u_i}\overline{u_j})}$ in the convection term of the filtered momentum equation needs a secondary filtering process, it is rewritten as shown below (Leonard, 1974),

$$\widetilde{(\overline{u_i}\overline{u_j})} = L_{ij} + \overline{u_i}\overline{u_j} \tag{176}$$

where $L_{ij} = \widetilde{(\overline{u_i}\overline{u_j})} - \overline{u_i}\overline{u_j}$ is the Leonard stress tensor, representing interactions among large turbulent eddies.

Utilizing the decomposition process shown above, the filtered momentum equations can be rewritten as

$$\frac{\partial(\rho\overline{u_i})}{\partial t} + \frac{\partial(\rho\overline{u_i}\overline{u_j})}{\partial x_j} = -\frac{\partial\overline{p}}{\partial x_j} + 2\mu\frac{\partial\overline{S_{ij}}}{\partial x_j} + \frac{\partial\tau'_{ij}}{\partial x_j} \tag{177}$$

where

- $\widetilde{S_{ij}} = \frac{1}{2}\left(\frac{\partial \widetilde{u_i}}{\partial x_j} + \frac{\partial \widetilde{u_j}}{\partial x_i}\right)$ is the filtered strain rate tensor,
- $\tau'_{ij} = -\rho\left(C_{ij} + R_{ij} + L_{ij}\right) = \rho\widetilde{u_i u_j} - \rho\widetilde{u_i}\widetilde{u_j}$ is the subgrid stress tensor.

Similar to RANS, the subgrid stress tensor is an unknown and must be computed by a subgrid model. However, the subgrid stress tensor differs from the Reynolds stress tensor. The table below summarizes the differences between time averaging for RANS and spatial averaging for LES. Common subgrid scale (SGS) models available to solve the filtered Navier-Stokes equations include:

- Smagorinsky-Lilly SGS model
- Germano Dynamic Smagorinsky-Lilly model
- Wall-Adapting Local Eddy-Viscosity (WALE)

Table 5: Time-Averaging (RANS) vs. Spatial-Averaging (LES)

	RANS	**LES**
Double averaging	$\overline{(\overline{u_i})} = \overline{u_i}$	$\widetilde{(\widetilde{u_i})} \neq \widetilde{u_i}$
Turbulence averaging	$\overline{u'_i} = 0$	$\widetilde{u''_i} \neq 0$
Averaging (or filtering) of convective term of Navier Stokes	$\overline{u_i u_j} = \left(\overline{\overline{u_i}\,\overline{u_j}}\right) + \left(\overline{u'_i \overline{u_j}}\right) + \left(\overline{\overline{u_i} u'_j}\right) + \overline{u'_i u'_j}$	$\widetilde{u_i u_j} = \left(\widetilde{\widetilde{u_i}\,\widetilde{u_j}}\right) + \left(\widetilde{u''_i \widetilde{u_j}}\right) + \left(\widetilde{\widetilde{u_i} u''_j}\right) + \left(\widetilde{u''_i u''_j}\right)$
Turbulent stress	$\tau^R_{ij} = -\rho\overline{u'_i u'_j}$	$\tau'_{ij} = \rho\widetilde{u_i u_j} - \rho\widetilde{u_i}\widetilde{u_j}$

Smagorinsky-Lilly Subgrid Scale Model

The Smagorinsky-Lilly SGS model is based on the Prandtl's mixing length model and assumes that a kinematic SGS viscosity can be expressed in terms of the length scale and the strain rate magnitude of the resolved flow.

$$\tau'_{ij} = \rho\widetilde{u_i u_j} - \rho\widetilde{u_i}\widetilde{u_j} = -2\mu_s\widetilde{S_{ij}} \tag{178}$$

where

- $\mu_s = \rho\left(C_S\Delta\right)^2\sqrt{2\widetilde{S_{ij}}\widetilde{S_{ij}}}$ is the subgrid turbulent viscosity,
- Model constant 0.17 < C_s < 0.21 (Lilly, 1996)
- $\widetilde{S_{ij}} = \frac{1}{2}\left(\frac{\partial \widetilde{u_i}}{\partial x_j} + \frac{\partial \widetilde{u_j}}{\partial x_i}\right)$ is the filtered (resolved) strain rate tensor

A major drawback of this model is that the model constant (C_s) does not vary in space and time. Furthermore, this model has no correct wall behavior and it is too dissipative for laminar turbulent transition cases. These limitations led to the development of a dynamic model for which the model constant is allowed to vary depending on the grid resolution and flow regime.

Dynamic Subgrid Scale Model

Recognizing C_s variations in space and time, Germano et al. (1991) proposed the dynamic model to compute the value of C_s rather than specifying it explicitly.

It is implemented by utilizing two filters: a cutoff filter Δ and a test (coarse) cutoff filter $\tilde{\Delta}$.

The subgrid stress tensor τ'_{ij} with the cutoff filter (Δ) is: $\tau'_{ij} = \rho\widetilde{u_i u_j} - \rho\tilde{u}_i\tilde{u}_j = -2\rho(C_S\Delta)^2|\widetilde{S}|\widetilde{S_{ij}}$. Where $|\widetilde{S}| = \sqrt{2\widetilde{S_{ij}}\widetilde{S_{ij}}}$ is the strain rate magnitude.

Figure 38 shows a resolved turbulence region utilizing Large Eddy Simulation (LES) and a modeled region assuming the subgrid tensor τ'_{ij}.

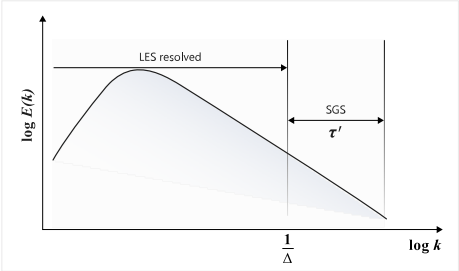

Figure 38: Energy Spectrum for LES Using the Cutoff Filter Width (Δ)

The test subgrid stress tensor T_{ij} with the coarse filter ($\tilde{\Delta}$) can be written as

$$T_{ij} = \rho\widetilde{\tilde{u}_i\tilde{u}_j} - \rho\tilde{\tilde{u}}_i\tilde{\tilde{u}}_j = -2\rho(C_S\tilde{\Delta})^2|\widetilde{\tilde{S}}|\widetilde{\tilde{S}_{ij}} \quad (179)$$

where

- $|\widetilde{\tilde{S}}| = \sqrt{2\widetilde{\tilde{S}_{ij}}\widetilde{\tilde{S}_{ij}}}$ is the coarse filtered strain rate magnitude.
- $\widehat{\tilde{S}_{ij}} = \frac{1}{2}\left(\frac{\partial\widehat{\tilde{u}}_i}{\partial x_j} + \frac{\partial\widehat{\tilde{u}}_j}{\partial x_i}\right)$ is the filtered strain rate tensor, using the coarse cutoff filter.

Figure 39 shows a resolved LES region and a corresponding subgrid modelled region (T) when the coarse filter is employed.

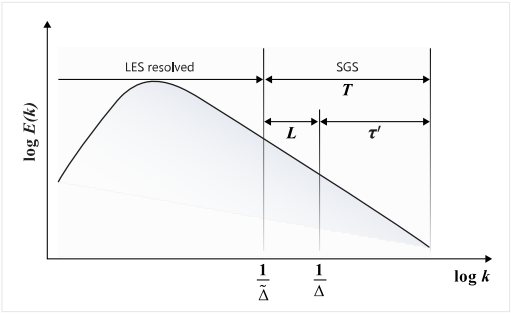

Figure 39: Energy Spectrum for LES Using the Test Cutoff Filter Width ($\tilde{\Delta}$)

Because of the coarse filtering, the test (coarse) subgrid stress tensor T_{ij} should be a summation of the coarse filtered subgrid stress tensor $\widetilde{\tau_{ij}}$ and the Leonard stress tensor L_{ij}.

$$L_{ij} = T_{ij} - \widetilde{\tau_{ij}} = \quad \rho\widetilde{u_i u_j} - \rho\tilde{u}_i\tilde{u}_j - \rho\widetilde{u_i}\widetilde{u_j} + \rho\widetilde{u_i}\widetilde{u_j} = \rho\widetilde{u_i}\widetilde{u_j} - \rho\tilde{u}_i\tilde{u}_j \tag{180}$$

where

- $\widetilde{\tau_{ij}}$ is the subgrid tensor for the cutoff filter (or grid filtered), then test filtered.

$$\widetilde{\tau_{ij}} = \rho\widetilde{u_i u_j} - \rho\widetilde{u_i}\widetilde{u_j} = -2\rho\left(C_S\Delta\right)^2\widetilde{|S|S_{ij}} \tag{181}$$

- L_{ij} is the Leonard subgrid stress tensor, representing the contribution to the subgrid stresses by turbulence length scales smaller than the test filter but larger than the cutoff filter.

The Leonard subgrid stress tensor can be arranged as

$$L_{ij} = -2\rho\left(C_S\hat{\Delta}\right)^2\widetilde{|S|S_{ij}} + 2\rho\left(C_S\Delta\right)^2\widetilde{|S|S_{ij}} = 2\rho C_S{}^2\Delta^2\left(\widetilde{|S|S_{ij}} - \alpha^2\widetilde{|S|S_{ij}}\right) \tag{182}$$

where $\alpha = \hat{\Delta}/\Delta$.

The Leonard subgrid stress tensor can be rewritten as

$$L_{ij} = 2\rho C_S{}^2\Delta^2\left(\widetilde{|S|S_{ij}} - \alpha^2\widetilde{|S|S_{ij}}\right) = C_S{}^2 M_{ij} \tag{183}$$

where $M_{ij} = 2\rho\Delta^2\left(\widetilde{|S|S_{ij}} - \alpha^2\widetilde{|S|S_{ij}}\right)$.

Since the above equation is overdetermined a minimum least square error method is used to determine the coefficient C_s.

$$C_s{}^2 = \frac{L_{ij}M_{ij}}{M_{ij}M_{ij}} \tag{184}$$

In order to avoid numerical instabilities associated with the above equation, as the numerator could become negative, averaging of the error in the minimization is employed.

$$C_{s2} = \frac{L_{ij}M_{ij}}{M_{ij}M_{ij}} \tag{185}$$

Hybrid Simulations

In recent years, hybrid methods have increasingly been employed for the simulation of unsteady turbulent flows.

These models form a bridge between Large Eddy Simulation (LES) and Reynolds-averaged Navier-Stokes (RANS) by utilizing RANS for attached boundary layer calculations and LES for the separated regions. In general, hybrid simulations need spatial filtering processes to determine the local sub grid turbulent viscosity. Compared to LES and Direct Numerical Simulation (DNS), hybrid simulations are extremely robust since the numerical requirement is less severe than the two other approaches. Hybrid simulations include Detached Eddy Simulation (DES), Delayed Detached Eddy Simulation (DDES) and Improved Delayed Detached Eddy Simulation (IDDES).

Detached Eddy Simulations

Detached Eddy Simulation (DES) uses one of the one or two equation Reynolds-averaged Navier-Stokes (RANS) turbulence models to define the turbulence length scale or distance from the wall. The distance is then used to determine the region for which the RANS or Large Eddy Simulation (LES) models will be used.

DES using the Spalart-Allmaras (SA) model employs a modified distance function to replace the distance (d) in the SA model's dissipation term (Spalart et al., 1997).

$$\tilde{d} = \min\left(d, \quad C_{DES}\Delta\right) \tag{186}$$

where d is the distance to the closest wall, C_{DES} is a constant and Δ is a metric of the local element size, often chosen as the largest grid spacing in all three directions ($\Delta = \max\left[\Delta x, \Delta y, \Delta z\right]$).

The SA model is activated in a boundary layer region where d < Δ, while a Smagorinsky-like LES model is used in regions where Δ < d. Similarly, Strelets (2001) adopted the SST model as the baseline model for DES, which computes a turbulence length scale and compares it with a grid length size for a switch between LES and RANS. However, both approaches need careful determinations of local grid sizes because these grid sizes act as the switch for the activation of LES and RANS.

Delayed Detached Eddy Simulations

Delayed Detached Eddy Simulation is an improved version of DES that avoids the undesired activation of Large Eddy Simulation (LES) in boundary layer regions when the maximum grid size is less than the distance to the closest wall (Δ < d).

In this model (Spalart et al., 2006), the length scale is redefined as:

$$\tilde{d} = d - f_d \max(0, d - C_{DES}\Delta) \tag{187}$$

where $f_d = 1 - tanh((8h)^3)$, $h = \frac{\tilde{\nu}}{\sqrt{\bar{u}_{ij}\bar{u}_{ij}}\kappa^2 d^2}$, $\kappa = 0.41$.

Improved Delayed Detached Eddy Simulations (DDES)

Shur et al. (2008) proposed an improved DDES to ensure that most of the turbulence is resolved when the model is operating as a wall modeled Large Eddy Simulation (LES).

This is achieved by introducing a blending function of length scales defined as:

$$\tilde{d} = \widetilde{f_d}(1 + f_e)d + (1 - \widetilde{f_d})C_{DES}\Delta \tag{188}$$

where

- $\widetilde{f_d} = \max([1 - f_d], f_b)$,
- $f_b = \min(2 \quad e^{-9\alpha^2}, \quad 1.0)$,
- $\alpha = 0.25 - \frac{d}{\Delta}$,
- $f_e = \max([f_{e1} - 1], \quad 1.0) f_{e2}$,
- $f_{e1} = \begin{cases} 2 \quad e^{-11.09\alpha^2}\frac{\Delta}{d}, & if \quad \alpha \geq 0 \\ 2 \quad e^{-9\alpha^2}\frac{\Delta}{d}, & if \quad \alpha < 0 \end{cases}$,
- $f_{e2} = 1.0 - \max(\tanh((C_t^2 h_t)^3), \quad \tanh((C_l^2 h_l)^{10}))$,
- $h_t = \frac{\nu_t}{\sqrt{\bar{u}_{ij}\bar{u}_{ij}}\kappa^2 d^2}$,
- $h_l = \frac{\nu}{\sqrt{\bar{u}_{ij}\bar{u}_{ij}}\kappa^2 d^2}$.

Near-Wall Modeling

For internal wall bounded flows, proper mesh resolution is required in order to calculate the steep gradients of the velocity components, turbulent kinetic energy, dissipation, as well as the temperature.

Furthermore, the first grid locations from the wall and the stretching ratio between subsequent points are also determinant factors that affect solution accuracy. Since boundary layer thickness is reduced as the Reynolds number increases, the computational cost increases for higher Reynolds number flows due to the dense grid requirements near the walls. Additionally, it is hard to determine the first grid locations for complex three dimensional industrial problems without adequate testing and simulation.

For high Reynolds number flows, it is numerically efficient if flows within boundary layers are modeled rather than resolved down to the wall. This suggests that a coarse mesh is used at the expense of numerical accuracy when compared to fully wall resolved approaches.

Wall Function

Figure 40 shows velocity profiles over a flat plate under the zero pressure gradient.

Velocity profile and wall distances are scaled by the friction velocity ($u_\tau = \sqrt{\frac{\tau_w}{\rho}}$ where τ_w is the wall shear stress and ρ is the fluid density). This is referred to as the log-law velocity profile. As shown in Figure 40, the velocity profiles are divided into three distinguished regions, the viscous sublayer, the buffer layer and the logarithmic layer.

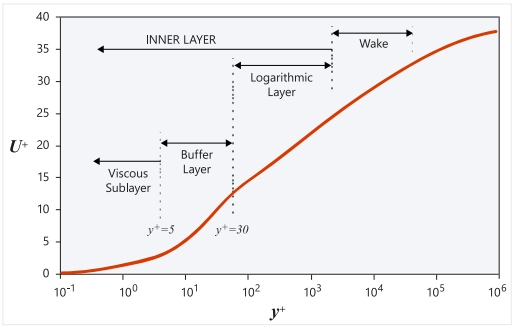

Figure 40: Log-law Velocity Profile

The wall function utilizes the universality of the log-law velocity profile to obtain the wall shear stress. This wall function approach allows the reduction of mesh requirement near the wall as the first mesh location is placed outside the viscous sublayer.

Overall, the log-law based wall model is economical and reasonably accurate in most flow conditions, especially for high Reynolds number flows. However, it tends to display poor performance in situations with low Reynolds number flows, strong body forces (rotational effect, buoyancy effect), and massively separated flows with adverse pressure gradients.

Velocity Profile in the Viscous Sublayer (y+ < 5)

In the viscous sublayer, the normalized velocity profile (U^+) has a linear relationship with the normalized wall distance.

$$U^+ = y^+ \tag{189}$$

where $U^+ = \frac{\overline{u}}{u_\tau}$ is the velocity ($\overline{u}$) parallel to the wall, normalized by the friction velocity. The friction velocity is defined as $u_\tau = \sqrt{\frac{\tau_w}{\rho}}$, τ_w is the wall shear stress and ρ is the fluid density. $y^+ = \frac{\rho u_\tau y}{\mu}$ is the

normalized wall distance (or wall unit). The distance from the wall is y and μ is the fluid dynamic viscosity.

Velocity Profile in the Logarithmic Layer (30 < y+ < 500)

In the logarithmic layer the velocity profile can be given by a logarithmic function

$$U^+ = \frac{1}{\kappa}\log(y^+) + B \tag{190}$$

where κ= 0.4 is the Von Kármán constant and B = 5.5 is a constant.

The wall shear stress can be estimated from the above equation via the iterative solution procedure.

Velocity Profile in the Buffer Layer (5 < y+ < 30)

Since two equations mentioned before are not valid in the buffer layer a special function is needed to bridge the viscous sublayer and the logarithmic layer. Details are not covered here.

Kinematic Eddy Viscosity

The kinematic eddy viscosity can be obtained as $v_t = \kappa y u_\tau$.

Two Layer Wall Model

The two equation turbulence models based on eddy frequency (ω) and the Spalart-Allmaras (SA) model do not require special wall treatments to solve the boundary layer as these models are valid through the viscous sub layer.

However, the two equation turbulence models based on turbulence dissipation rate (ε) need additional functions to simulate the near wall effects. The two layer wall model is one of them. In the two layer model, turbulent kinetic energy is determined from the turbulent kinetic energy transport equation, while dissipation rate is resolved with a one equation turbulence model (Wolfstein, 1969) in the near wall, viscous-affected regions where $Re_y = \frac{\rho y\sqrt{k}}{\mu} < 200$.

$$\varepsilon = \frac{k^{3/2}}{l_\varepsilon} \tag{191}$$

where

- $l_\varepsilon = C_l y\left(1 - \exp\left[-\frac{Re_y}{A_\varepsilon}\right]\right)$,
- $C_l = \kappa C_\mu^{-3/4}$,
- κ is the Von Kármán constant,
- A_ε = 5.08 (Chen and Patel, 1988).

The eddy viscosity can be written as

$$v_t = C_\mu l_\mu \sqrt{k} \tag{192}$$

where

- $l_\mu = C_l y\left(1 - \exp\left[-\frac{Re_y}{A_\mu}\right]\right)$,
- A_μ = 70.

Inlet Turbulence Parameters

CFD simulations require specification of turbulence variables at inlet boundaries.

When measured turbulence data is available you can explicitly specify turbulence variables. For example, eddy viscosity for the Spalart-Allmaras (SA) model, turbulent kinetic energy and eddy frequency/dissipation rate for k-ε and k-ω based models. When measured data is not available, there are estimations for the turbulence values that are based on the turbulence intensity and turbulence length scale or eddy viscosity ratio.

Turbulence Intensity

The turbulence intensity (I) is defined as the ratio of the root-mean-square of the turbulent velocity fluctuations (u') and the mean velocity ($\overline{u}$):

$$I \equiv \frac{u'}{\overline{u}} \tag{193}$$

where $u' = \sqrt{\frac{\left(\overline{u'_x}^2 + \overline{u'_y}^2 + \overline{u'_z}^2\right)}{3}} = \sqrt{\frac{2k}{3}}$ and $\overline{u} = \sqrt{\left(\overline{u}_x^2 + \overline{u}_y^2 + \overline{u}_z^2\right)}$.

For fully developed internal flows the turbulence intensity can be estimated as

$$I = 0.16 \quad Re_h^{-1/8} \tag{194}$$

where $Re_h = \frac{\rho \overline{u} D_h}{\mu}$ is the Reynolds number and D_h is a hydraulic diameter.

The following turbulence intensity values can be assumed

- 5 percent < I < 20 percent for rotating machineries, for example, turbines and compressors.
- 1 percent < I < 5 percent for internal flows.
- I~0.05 percent for external flows.

Turbulence Length Scale

The turbulence length scale represents the characteristic size of the turbulent eddies within a flow field. This parameter is often used to characterize the nature of the turbulence and appears in some form in nearly every turbulence model. RANS turbulence models have different definitions of the turbulence length scale based on the turbulence model and the type of application.

Estimated turbulence length scales based on the flow conditions:

- $l = 0.038 D_h$ for fully developed internal flows.
- $l = 0.22\delta$ for developing flows.

where $\delta \approx 0.382\frac{x}{Re_x^{1/5}}$ is the turbulent boundary layer thickness over a flat plate and $Re_x = \frac{\rho \bar{u} x}{\mu}$ is the Reynolds number and x is the distance from the start of the boundary layer.

Eddy Viscosity Ratio

The eddy viscosity ratio (v_r) is the ratio between the eddy viscosity (v_t) and fluid kinematic viscosity (v). The eddy viscosity ratio is set between 1 and 10 for internal flows, while it should be between 0.2 and 1.3 for external flows.

Inlet Turbulence Specification for the SA Model

The SA model has three options to estimate the turbulence variable at the inlet.

- Option 1: Eddy viscosity v_t
- Option 2: Turbulence intensity I and length scale l. For the eddy viscosity, $v_t = \sqrt{\frac{3}{2}}\,\bar{u}\quad I\quad l$.
- Option 3: Viscosity ratio $\quad v_r$. For the eddy viscosity, $v_t = v\quad v_r$

Inlet Turbulence Specification for the k-ε Models

- Option 1: Kinetic energy k and dissipation rate ε
- Option 2: Turbulence intensity I and length scale l. For the kinetic energy, $k = \frac{3}{2}(\bar{u}I)^2$. For the dissipation rate, $\varepsilon = C_\mu \frac{k^{3/2}}{l}$, where C_μ = 0.09.
- Option 3: Turbulence intensity I and viscosity ratio $\quad v_r$. For the kinetic energy, $k = \frac{3}{2}(\bar{u}I)^2$. For the dissipation rate, $\varepsilon = \frac{C_\mu \quad k^2}{v \quad v_r}$.

Inlet Turbulence Specification for the k-ω Models

- Option 1: Kinetic energy k and eddy frequency ω
- Option 2: Turbulence intensity I and length scale l. For the kinetic energy, $k = \frac{3}{2}(\bar{u}I)^2$. For the eddy frequency, $\omega = \frac{\sqrt{k}}{l \quad C_{\mu 1/4}}$.
- Option 3: Turbulence intensity I and viscosity ratio $\quad v_r$. For the kinetic energy, $k = \frac{3}{2}(\bar{u}I)^2$. For the dissipation rate, $\omega = \frac{k}{v \quad v_r}$.

Summary

During the past decades turbulence models of various complexities have been developed. Turbulence models that employ the most assumptions are typically the least demanding from a CPU cost standpoint.

As the number of assumptions associated with the model decreases, the cost and accuracy of the model typically increases. Since no universal turbulence model exists, CFD users need to choose the best turbulence model specific to their application. The most cost effective approach is typically steady Reynolds-averaged Navier-Stokes (RANS). When the flow is naturally unsteady and exhibits oscillations in the quantities of interest, URANS may be employed to improve the accuracy of solutions and gain a better understanding of how much the flow field fluctuates as a function time. For applications when the flow transitions from laminar to turbulent as a function of space, a dedicated transition model is required in order to accurately predict the near wall behavior. When the application demands additional knowledge of the turbulent fluctuations for separated, reattaching or impinging flow fields, hybrid simulations (Detached Eddy Simulation (DES), Delayed Detached Eddy Simulation (DDES)) may be employed. Although the modeling assumption is still made within the boundary layer, the tradeoff between accuracy and computational efficiency is often worthwhile compared to Large Eddy Simulation (LES) or Direct Numerical Simulation (DNS). Finally, when the application requires detailed information about nearfield fluctuations, or for combustion and acoustic applications, LES should be considered.

Based on the information presented it is up to you to understand the complexity of your simulation and make an appropriate decision on which turbulence model to use. Generally, it is recommended to start with a simple turbulence model since a majority of industrial problems can be well defined with a steady state assumption. Even if the application is inherently unsteady, this is still a good place to start as a significant amount of information can be garnered from running RANS. If the initial RANS fails to provide the level of accuracy required for the specific application you will need to consider the use of a hybrid model or LES. Often times the flow regime exhibits sensitivities to the selection of the turbulence model, specifically RANS vs. Hybrid/LES. In any case, the selection of the turbulence model should be verified against previous simulation or validated with experimental/analytical data for the flow in question.

Numerical Approximation Techniques

This section on numerical approximation techniques covers topics, which describe the numerical modeling of the fluid flow equations on a computational domain, such as spatial discretization using finite difference, finite element and finite volume techniques, temporal discretization and solution methods.

Overview

The governing equations, that is, the Navier – Stokes equations in continuum mechanics are a set of coupled non–linear partial differential equations derived from the conservation laws for mass, momentum and energy.

For a numerical solution of a mathematical continuum model, the focus is to devise efficient, robust, and reliable algorithms for the solution of the partial differential equations. To do this the partial differential equations are converted to a discrete system of algebraic equation using a discretization procedure. In case of a CFD simulation, the discretization of the governing equations, that is, the derivation of equivalent algebraic relations should accurately represent the equations and the physics modeled.

There are a number of discretization techniques that have been developed to solve different kinds of problems in CFD. These methods can be broadly classified into two categories:

- Mesh based methods – These methods require division of the problem domain into a grid or mesh over which the governing equations are discretized. The points are positioned according to a topological connectivity which ensures the compatibility of the numerical technique used. Examples of these methods include Finite Difference (FD), Finite Volume (FV) and Finite Element (FE) methods.
- Mesh free methods – These methods use a collection of nodes in the domain which do not have any apparent connectivity. These methods are particularly important in simulations where the nodes are created or destroyed, simulations where the deformations are so large that the connectivity might introduce distortion and in cases where the domain possesses discontinuities or singularities. A few examples of these methods are: Smoothed Particle Hydrodynamics (SPH), Finite Pointset Method (FPM), Meshless Local Petrov Galerkin (MLPG) and Lattice Boltzman methods.

Of the methods discussed above, mesh based methods are more popular and are among the most widely used in CFD codes. The following sections describe the mesh based discretization methods (FD, FV and FE) and the time discretization techniques used to solve the partial differential equations governing a fluid flow.

Finite Difference Method (FDM)

This section describes the formulation and methodology of finite difference method to solve the governing equations on a computational domain.

The finite difference method is the oldest method for the numerical solution of partial differential equations. It is also the easiest to formulate and program for problems which have a simple geometry.

When calculating derivatives finite difference replaces the infinitesimal limiting process with a finite quantity. The derivative of a function at point expressed as:

$$\frac{\partial f}{\partial x} = \lim_{\Delta x \to 0} \frac{f(x+\Delta x) - f(x)}{\Delta x} \tag{195}$$

is replaced by:

$$\frac{\partial f}{\partial x} = \frac{f(x+\Delta x) - f(x)}{\Delta x} + O(\Delta x) \tag{196}$$

The preceding expression is commonly referred to as the forward difference approximation. This derivative can have more refined approximations using a number of approaches such as truncated Taylor series expansions and polynomial fitting.

The term $O(\Delta x)$ gives an indication of the magnitude of the error as a function of the mesh spacing and is therefore termed as the order of magnitude of the finite difference method. In the above formulation, the finite difference approximation employed is first-order accurate. A second-order approximation would have the order of magnitude expressed as $O(\Delta x^2)$. Most of the finite difference methods used in practice are second-order accurate. An example of a second-order method is the central difference approximation of the first derivative. It is expressed as:

$$\frac{\partial f}{\partial x} = \frac{f(x+\Delta x) - f(x-\Delta x)}{2\Delta x} + O(\Delta x^2) \tag{197}$$

The basic methodology in the simulation process using finite difference approach consists of the following steps.

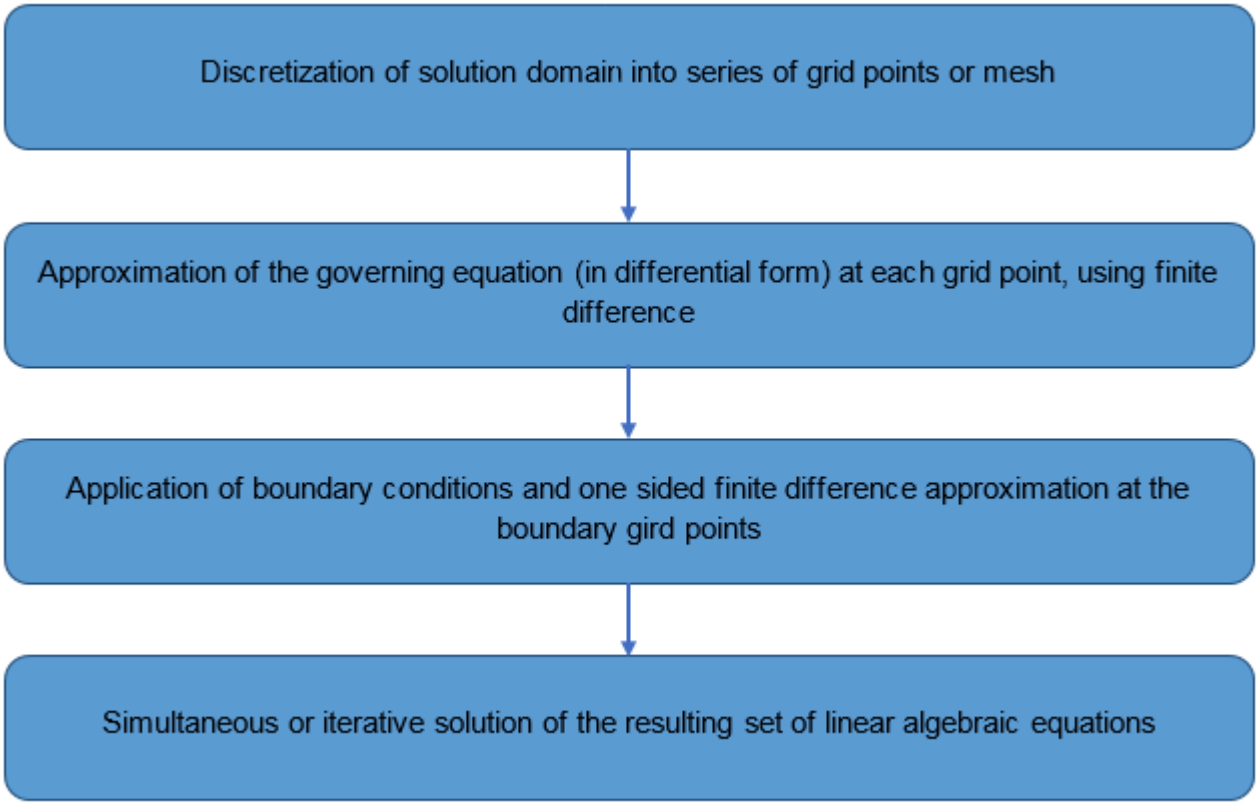

Figure 41: Basic Methodology in the Simulation Process Using Finite Difference Approach

The finite difference formulation generally employs a structured grid. The most commonly used indices are i, j and k for the grid lines at $x = x_i$, $y = y_j$ and $z = z_k$, respectively. The function value at such a grid point is expressed as $f_{i,j,k} \equiv f_{ijk} \equiv f\left(x_i, y_j, \quad z_k\right)$.

Consider the one dimension advection-diffusion equation for a scalar quantity φ governed by

$$\frac{d(\rho u \varphi)}{dx} = \frac{d}{dx}\left(\epsilon \frac{d\varphi}{dx}\right) \tag{198}$$

where u is the specified velocity, ρ is the density of the fluid and ϵ is the diffusivity.

If the domain is defined by the boundary $x = 0$ and $x = L$ and the boundary conditions by $\varphi(0) = \varphi_0$ and $\varphi(L) = \varphi_L$, the domain can be discretised (non-uniformly) by a total of $N + 1$ grid points for the finite difference solution of the problem.

The diffusion term can be approximated using the central difference (both the inner and outer derivative) as:

$$\frac{d}{dx}\left(\epsilon\frac{d\varphi}{dx}\right)_i \approx \frac{\left(\epsilon\frac{d\varphi}{dx}\right)_{i+\frac{1}{2}} - \left(\epsilon\frac{d\varphi}{dx}\right)_{i-\frac{1}{2}}}{\frac{1}{2}\left(x_{i+1} - x_{i-1}\right)} \tag{199}$$

$$\frac{d}{dx}\left(\epsilon\frac{d\varphi}{dx}\right)_i \approx \frac{\left(\epsilon_{i+\frac{1}{2}}\frac{\varphi_{i+1}-\varphi_i}{x_{i+1}-x_i}\right) - \left(\epsilon_{i-\frac{1}{2}}\frac{\varphi_i-\varphi_{i-1}}{x_i-x_{i-1}}\right)}{\frac{1}{2}\left(x_{i+1} - x_{i-1}\right)} \tag{200}$$

The convection term can also be approximated using the central difference as:

$$\frac{d}{dx}\left(\rho u\varphi\right)_i \approx \frac{\left(\rho u\varphi\right)_{i+1} - \left(\rho u\varphi\right)_{i-1}}{x_{i+1} - x_{i-1}} \tag{201}$$

If the grid is uniform and the values of density, velocity and coefficient of diffusion are constant throughout the domain the above equations reduce to:

$$\rho u\frac{\varphi_{i+1} - \varphi_{i-1}}{2\Delta x} = \epsilon\frac{\varphi_{i+1} - 2\varphi_i + \varphi_{i-1}}{\Delta x^2} \tag{202}$$

The resulting set of linear algebraic equations can be solved to get the values of at the grid points.

Finite difference methods are advantageous for the numerical solution of partial differential equations because of their simplicity, efficiency and low computational cost. Their major drawback is their geometrical inflexibility, such as application on an unstructured grid or moving boundaries. Their formulation increases in complexity as the complexity of the domain increases.

The restrictions resulting from the above mentioned geometrical complexities can be alleviated by the use of methods such as grid transformation and immersed boundary techniques.

Finite Volume Method (FVM)

This section describes the formulation and methodology of finite volume method to solve the governing equations on a computational domain. It also describes the cell centered and face centered approaches used for finite volume formulation.

The finite volume formulation is based on the approximate solution of the integral form of the conservation equations. The problem domain is divided into a set of non overlapping control volumes referred to as finite volumes, where the variable of interest is usually taken at the centroid of the finite volume. The finite volume is also referred to as a cell or element.

The governing equations are integrated over each finite volume and interpolation profiles are assumed in order to describe the variation of the concerned variable of interest between the cell centroids. The resulting discretization equation expresses the conservation principle for the variable inside the finite volume.

The governing differential equations discussed in this manual each have a dependent variable that obeys a generalized conservation principle. If the dependent variable (scalar or vector) is denoted by φ, the generic differential equation is:

$$\underbrace{\frac{\partial(\rho\varphi)}{\partial t}}_{Transient\ term} + \underbrace{\nabla\cdot(\rho\vec{u}\varphi)}_{Convection\ term} = \underbrace{\nabla\cdot(\epsilon\nabla\varphi)}_{Diffusion\ term} + \underbrace{S_\varphi}_{Source\ term} \tag{203}$$

where

- ϵ is the diffusion coefficient.
- The transient term $\frac{\partial\rho\varphi}{\partial t}$ accounts for the rate of change of φ inside the control volume.
- The convection term $\nabla\cdot(\rho\vec{u}\varphi)$ accounts for the transport of φ due to the velocity field $\vec{u}$.
- The diffusion term $\nabla\cdot(\epsilon\nabla\varphi)$ accounts for the transport of φ due to its gradients.
- The source term S_φ accounts for any sources or sinks that affect the quantity φ.

When the above equation is integrated over a three dimensional control volume it yields

$$\int_{CV}\frac{\partial(\rho\varphi)}{\partial t}\ dV + \int_{CV}\nabla\cdot(\rho\vec{u}\varphi)\ dV = \int_{CV}\nabla\cdot(\epsilon\nabla\varphi)\ dV + \int_{CV}S_\varphi\ dV \tag{204}$$

The divergence terms (convection and diffusion) can be converted into surface integrals using Gauss divergence theorem and the above equation can be rewritten as

$$\frac{\partial}{\partial t}\int_{CV}\rho\varphi\ dV + \oint_S\hat{n}\cdot(\rho\vec{u}\varphi)\ dS = \oint_S\hat{n}\cdot(\epsilon\nabla\varphi)\ dS + \int_{CV}S_\varphi dV \tag{205}$$

where

- $\hat{n}$ is the unit vector normal to the surface dA
- S is the boundary of the control volume
- $\hat{n}\cdot(\rho\vec{u}\varphi)$ is the convective flux of φ across the boundary dS
- $\hat{n}\cdot(\epsilon\nabla\varphi)$ is the diffusive flux of φ across the boundary dS

The integral conservation in the scalar transport equation applies to each control volume as well as the complete solution domain thus satisfying the global conservation of quantities such as mass, momentum and energy. These quantities can be evaluated as fluxes at the surfaces of each control volume.

In order to obtain an algebraic (discretised) equation for each control volume the surface and volume integrals are approximated using quadrature formulae in terms of function values at the storage location. This may require values of variable at points other than the computational nodes of the control volume. Values at these locations are obtained using interpolation schemes.

The overall finite volume approach involves the following steps.

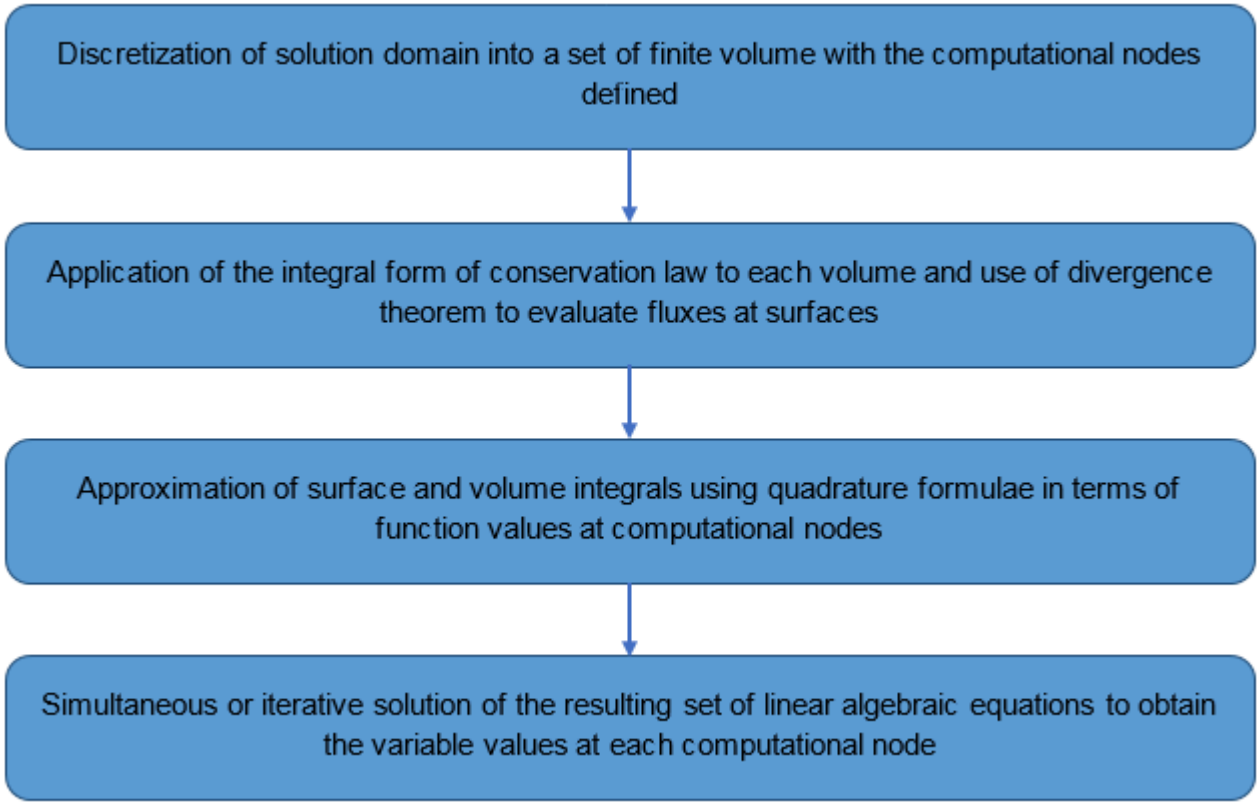

Figure 42: Finite Volume Approach

There are two common approaches to finite volume discretization.

- Cell centered approach: The domain is defined by a suitable grid of finite volumes and the computational nodes are assigned at the centroid of the control volumes.
- Face/Node centered approach: The domain is first defined by a set of nodes and control volumes are constructed around these nodes as cell centers such that the faces of the control volume lie between these nodes.

The cell centered approach and node centered approach have nearly the same accuracy and efficiency for most of the cases which use a structured grid.

To illustrate how the conservation equations in CFD can be discretised using finite volume method an example involving the steady transport of x-momentum in a uniform 2D rectangular grid can be considered:

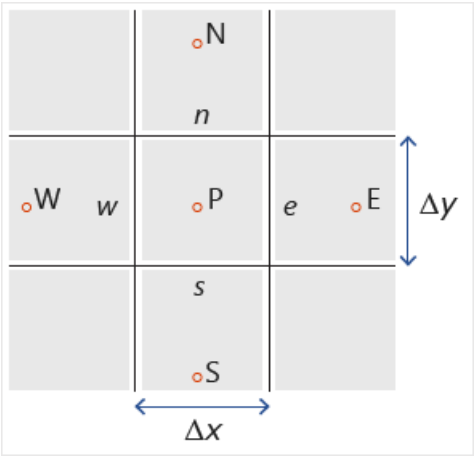

Figure 43: Finite Volume Stencil Around Point P

A cell centered approach is employed with the points P, W, E, N, S representing the cell centers and the notations n, e, s, w representing the faces of cell P. The notation N (n), E(e), S(s), W(w) represent the north, east, south and west directions, respectively.

The velocity u is stored at the nodes N, E, S, W and it is represented as u_N, u_E, u_S, u_W, respectively. The finite volume approximation starts by integrating the x-momentum equation over the control volume P.

$$\iint_V \left[\frac{\partial}{\partial x}(\rho u^2)+\frac{\partial}{\partial y}(\rho uv)\right]dx\ \ dy = -\iint_V \frac{\partial p}{\partial x}dx\ \ dy \tag{206}$$

$$+\iint_V \left[\frac{\partial}{\partial x}\left(\mu\frac{\partial u}{\partial x}\right)+\frac{\partial}{\partial y}\left(\mu\frac{\partial u}{\partial y}\right)\right]dx\ \ dy \tag{207}$$

This leads to:

$$\left[\int \rho u^2 dy\right]_w^e+\left[\int \rho uv dx\right]_s^n=\left[\int \mu\frac{\partial u}{\partial x}dy\right]_w^e+\left[\int \mu\frac{\partial u}{\partial y}dx\right]_s^n-\iint_V \frac{\partial p}{\partial x}dx\ \ dy \tag{208}$$

Evaluation of Source Terms

The source terms can be approximated by evaluating them at cell centers and multiplying them by the volume of the cell.

$$\iint_V \frac{\partial p}{\partial x}dx\ \ dy \approx \left(\frac{\partial p}{\partial x}\right)_P \Delta x\ \ \Delta y$$

In the example considered the pressure gradient at center of cell P can be evaluated by interpolating the pressure values from surrounding nodes. Other source terms can be evaluated similarly, interpolating where necessary to estimate the cell center values.

Evaluation of Diffusive Fluxes

The diffusive fluxes can be approximated as

$$\left[\int \mu\frac{\partial u}{\partial x}dy\right]_w^e+\left[\int \mu\frac{\partial u}{\partial y}dx\right]_s^n \approx \left[\mu\frac{\partial u}{\partial x}\Delta y\right]_w^e+\left[\mu\frac{\partial u}{\partial y}\Delta x\right]_s^n$$

The gradients of velocity at the cell faces (e, w, n, s) can be approximated using central difference comprising of the cell center values. This results in diffusive fluxes being represented as

$$\left[\int \mu \frac{\partial u}{\partial x} dy\right]_w^e + \left[\int \mu \frac{\partial u}{\partial y} dx\right]_s^n \approx (\mu \Delta y)_e \frac{u_E - u_P}{\Delta x} - (\mu \Delta y)_w \frac{u_P - u_W}{\Delta x}$$

$$- (\mu \Delta y)_n \frac{u_N - u_P}{\Delta y} - (\mu \Delta y)_s \frac{u_P - u_S}{\Delta y}$$

The discretised equation which is second-order accurate takes the form

$$a_e u_E + a_w u_W + a_n u_N + a_s u_S - a_p u_P$$

Evaluation of Convective Fluxes

The convective fluxes can be approximated as

$$\left[\int \rho u^2 dy\right]_w^e + \left[\int \rho uv dx\right]_s^n \approx \left[\rho u^2 \Delta y\right]_w^e + \left[\rho uv \Delta x\right]_s^n$$

The discretised equation takes the form

$$c_e u_e - c_w u_w + c_n u_n - c_s u_s$$

where c_e, c_w and so on are mass fluxes through the east, west, north and south faces.

The values of u at cell faces need to be obtained using appropriate interpolation schemes between the cell center values. A few examples of such schemes are linear interpolation (CDS), quadratic upwind interpolation (QUICK), total variation diminishing (TVD).

Finite Element Method (FEM)

The finite element approach is based on the discretization of the domain into a set of finite elements, which are usually triangles or quadrilaterals in a two dimensions and tetrahedral, hexahedra, pyramids or wedges in three dimensions, and using variational principles to solve the problem by minimizing an associated error function or residual.

The unknown variables are approximated over the domain using interpolation procedure in terms of nodal values and set of known functions called shape functions. This approximation is substituted into the governing (conservation) equations in their differential form and the resulting error (residual) is minimized in an average sense using a weighted residual approach.

The variational or weighted residual formulations transforms the governing equations into an integral form called the global weak form. The weak form when applied to each finite element results in a set of discrete equations in terms of the nodal unknown which can then be solved by a number of methods.

In this formulation the governing differential equation for a quantity φ is expressed as:

$$L(\varphi) = \frac{\partial \varphi}{\partial t} + \frac{\partial}{\partial x_j}\left(f_j - f_j^d\right) - s = 0 \tag{209}$$

where

- L is a differential operator with its associated initial and boundary conditions.
- $f_j = f\left(u_j, \varphi\right)$ is the convective flux vector.
- $f_j^d = f\left(\epsilon \frac{\partial \varphi}{\partial x_j}\right)$ is the diffusive flux vector.
- s is the contribution due to a source.

An approximate solution $\overline{\varphi}$ of the above equation is assumed, having the form:

$$\varphi(x) \approx \overline{\varphi}(x) = \sum_i N_i \varphi_i(x) \tag{210}$$

where

- N_i is the prescribed shape (interpolation) function.
- φ_i is the unknown value of the variable φ at a discrete spatial point i.

Finite element method requires transformation of the governing differential equation into an integral equation over the domain. This is accomplished through approaches such as weighted residual formulation and least squares formulation.

Overall, the finite element approach contains the following steps.

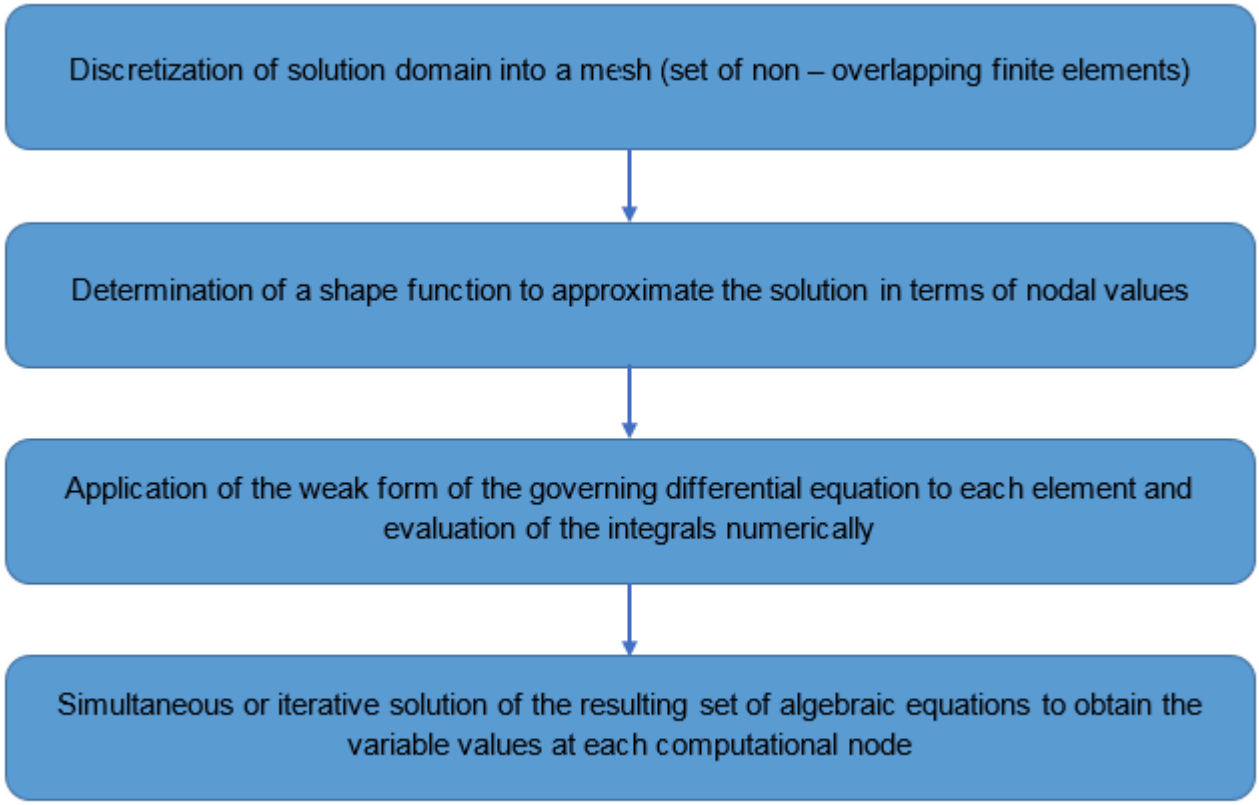

Figure 44: Finite Element Approach

A few of the approaches used to convert the differential equations into their weak integral forms are discussed below.

Weighted Residual Formulation

Substitution of the approximated form into the governing equations results in an error or residual function denoted by R and expressed as:

$$L(\overline{\varphi}) = R \tag{211}$$

In order to determine the nodal values φ_i, the inner product of the residual with a prescribed weighted function w_i is set to zero

$$\int_{\Omega} R w_i \; d\Omega \equiv \int_{\Omega} L(\overline{\varphi}) w_i \; d\Omega = 0 \tag{212}$$

The above equation is called the strong form of the weighted residual method. In many cases it is possible to perform integration by parts and obtain the weak form of the equation which contains lower order derivatives than the ones occurring in L and has reduced continuity requirement for the weighted function. The weak form is expressed as:

$$\int_{\Gamma} A(\overline{\varphi}) w_i \; d\Gamma + \int_{\Omega} B(\overline{\varphi}) C(w_i) \; d\Omega = 0 \tag{213}$$

where A, B and C are the differential operators with lower order derivatives than L and Ω represents the domain and Γ the boundary of the domain.

Different solution methods are obtained based on the choice of the weight function. Some of these approaches are:

- Point Collocation: $w_i(x) = \delta(x, x_i)$ where δ is the Dirac-Delta function. This is analogous to the finite difference approach.
- Subdomain Collocation: $w_i(x) = 1$ for the i^{th} subdomain (element) and zero elsewhere. This leads to a finite volume formulation.
- Galerkin method: $w_i(x) = N_i(x)$ where N is a shape function assumed over an element.
- Petrov Galerkin method: $w_i(x) \neq N_i(x)$. This represents a generalization of all methods except the Galerkin method.

Least Squares Formulation

The least square approach is based on minimizing the residual function in a least square sense. A least square function is constructed by taking the inner product of residual function with itself and defined as:

$$I(\overline{\varphi}) = L(\overline{\varphi})^2 \tag{214}$$

Using variational principles leads to a least square weak form written as:

$$\int_{\Omega} L(w_i) L(\overline{\varphi}) \; d\Omega = 0 \tag{215}$$

Galerkin Least Squares Formulation

Galerkin least square approach is an extension of the Galerkin weighted residual method and the least square approach. It uses stabilizing terms obtained by minimizing the residual of the governing equation. The use of variational principles on the resulting equations results in the following formulation:

$$\langle L(\varphi_i), w_i \rangle + S^{GLS} = \langle L(\varphi_i), w_i \rangle + \sum_k \langle L(\varphi_i), \tau_k L(w_i)_k \rangle = 0 \tag{216}$$

where

- $\langle L(\varphi_i), w_i \rangle$ represents the Galerkin approximation.
- S^{GLS} represents the least squares stabilization.
- $\langle , \rangle$ represents the inner dot product of the comma separated terms.
- τ_k represents the stabilization parameter.

Time Discretization

This section describes the various approaches used to discretize the governing equation in the temporal domain such as two step, multistep and multistage methods.

In order to determine a numerical solution of the governing differential equations the temporal domain must also be discretised apart from the spatial domain. The direction of influence of the time coordinate is only in the future. Therefore, all the solution methods for time dependent problems advance in time from a given initial data.

A vast majority of the methods used for temporal discretization are linear in nature. The time dependent variable is updated using a linear combination of the variable and its time derivatives. Linear approaches can be broadly categorized based on the number of steps, stages and derivatives used in the discretization.

Some of the widely used time discretization approaches are described below.

Generalized Two Step Methods

Two step methods involve function values at two instances in time, generally considering the current time step at which the solution is known and the next time step at which the solution has to be computed.

Consider a first-order ordinary differential equation for a dependent variable φ expressed as:

$$\frac{d\varphi}{dt} = f(t, \varphi) \tag{217}$$

with an initial condition $\varphi(t_0) = \varphi^0$.

A generalized scheme using a weighted average value for the approximation of the variable value at the n+1th time step is expressed as:

$$\varphi^{n+1} = \varphi^n + \Delta t\left[\theta f^{n+1} + (1-\theta) f^n\right] \tag{218}$$

where f^n represents the function value at the nth time step and θ represents the weight.

The nature and stability of the temporal discretization scheme depends on the choice of the weight $\theta = 0, \frac{1}{2}$ and 1 represent the forward Euler, Crank-Nicholson and the backward Euler schemes, respectively.

Multistep Methods

Multistep methods involve function values at more than two instances of time. These methods are generally derived by fitting a polynomial to the temporal derivative of the dependent variable, that is, $f(t, \varphi)$.

These methods include the Adams-Bashforth and Adams-Moutlton methods. The order of the method depends on the number of points in time at which the polynomial fitting it used. A third-order accurate Adams-Moulton method is expressed as:

$$\varphi^{n+1} = \varphi^n + \frac{\Delta t}{2}\left[5f^{n+1} + 8f^n - f^{n-1}\right] \tag{219}$$

These methods require initial data at many steps, hence they are not self starting.

Multistage Methods

Multistage methods involve computation of the function values multiple times at the same time step. They generally involve predictor and corrector steps to compute the values at the n+1th time step.

Numerical solution schemes are often referred to as being explicit or implicit. When a direct computation of the dependent variables can be made in terms of known quantities the computation is said to be explicit. When the dependent variables are defined by coupled set of equations, and either a matrix or iterative technique is needed to obtain the solution, the numerical method is said to be implicit.

Explicit methods are easy to program but are conditionally stable whereas implicit methods offer better stability but are computationally expensive. Predictor-Corrector methods offer a compromise between these choices. A variety of methods exist based on the choice of base method and the time instants used in the predictor and corrector steps.

The most popular methods in this category are the Runge-Kutta methods. A fourth-order Runge-Kutta method is constructed as follows:

- Explicit Euler Predictor: $\varphi_{*}^{n+\frac{1}{2}} = \varphi^{n} + \frac{\Delta t}{2} f^{n}$
- Implicit Euler Corrector: $\varphi_{**}^{n+\frac{1}{2}} = \varphi^{n} + \frac{\Delta t}{2} f_{*}^{n+\frac{1}{2}}$
- Mid-point rule Predictor: $\varphi_{*}^{n+1} = \varphi^{n} + \Delta t f_{**}^{n+\frac{1}{2}}$
- Simpsons rule Corrector: $\varphi^{n+1} = \varphi^{n} + \frac{\Delta t}{6}\left[f^{n} + 2f_{*}^{n+\frac{1}{2}} + 2f_{**}^{n+\frac{1}{2}} + f_{*}^{n+1}\right]$

Generalized-α Method

The generalized α method is an implicit method of time integration which achieves high frequency numerical dissipation while at the same time minimizing unwanted low frequency dissipation and offers unconditional stability for linear problems. It is a variant of the generalized two step theta scheme discussed above where the first temporal derivatives are evaluated as variables.

For a linear system defined by:

$$\dot{\varphi} = \frac{d\varphi}{dt} = \lambda\varphi \tag{220}$$

The generalized α method for integration from time step t_n to t_{n+1} is constructed as follows:

- $\dot{\varphi}_{n+\alpha_m} = \lambda\varphi_{n+\alpha_f}$
- $\varphi_{n+1} = \varphi_n + \Delta t\dot{\varphi}_n + \Delta t\gamma\left(\dot{\varphi}_{n+1} - \dot{\varphi}_n\right)$
- $\dot{\varphi}_{n+\alpha_m} = \dot{\varphi}_n + \alpha_m\left(\dot{\varphi}_{n+1} - \dot{\varphi}_n\right)$
- $\varphi_{n+\alpha_f} = \varphi_n + \alpha_n\left(\varphi_{n+1} - \varphi_n\right)$

where Δt is the time step size $\left(\Delta t = t_{n+1} - t_n\right)$ and $\alpha_m, \alpha_f, \gamma$ are free parameters.

The above four equations combine to yield the following system:

$$\emptyset_{n+1} = c\,\emptyset_n \tag{221}$$

where the solution vector $\emptyset_n$ at t_n is defined as $\emptyset_n = \left\{\varphi_n, \Delta t\dot{\varphi}_n\right\}^T$.

Direct Versus Iterative Solution Methods

This section describes the direct and iterative solution methods used to solve the linear system of equations obtained after spatial and temporal discretization of the governing equations.

Most of the methods of discretization discussed (FDM, FVM and FEM) yield a linear system of equations that need to be solved.

The resultant expression is of the form:

$$Ax = b \tag{222}$$

that is

$$\begin{bmatrix} a_{11} & a_{12} & \cdots & a_{1n} \\ a_{21} & a_{22} & & a_{2n} \\ \vdots & & \ddots & \vdots \\ a_{n1} & a_{n2} & \cdots & a_{nn} \end{bmatrix} \begin{bmatrix} x_1 \\ x_2 \\ \vdots \\ x_3 \end{bmatrix} = \begin{bmatrix} b_1 \\ b_2 \\ \vdots \\ b_3 \end{bmatrix} \tag{223}$$

where

- A is a matrix of known coefficients.
- b is a vector of given coefficients.
- x is a vector of unknowns such as density, velocity and temperature.

The methods used to solve the linear system of equations can be classified into two categories:

Direct Methods

Direct methods obtain an exact solution of the linear system of equations. These methods generally consist of elementary matrix operations to simplify the equations that will allow an exact computation. Some of these methods are:

- Cramer's Rule: The solution to $Ax = b$ is computed directly by $x = A^{-1}b$ and using Cramer's rule to compute the inverse of the coefficient matrix by calculating the co factor and adjoint of matrix A.
- LU Decomposition: This approach is based on the assumption that matrix A is composed of an upper triangular and a lower triangular matrix, that is $A = LU$. This results in $Ax = (LU)x = L(Ux) = Ly$ after which the systems $Ly = b$ and $Ux = y$ are solved separately.
- Gaussian Elimination: The given linear system of equations is converted to an augmented form given by $\begin{bmatrix} a_{11} & a_{12} & \cdots & a_{1n} \\ a_{21} & a_{22} & & a_{2n} \\ \vdots & & \ddots & \vdots \\ a_{n1} & a_{n2} & \cdots & a_{nn} \end{bmatrix} \begin{bmatrix} b_1 \\ b_2 \\ \vdots \\ b_3 \end{bmatrix} \begin{bmatrix} x_1 \\ x_2 \\ \vdots \\ x_3 \end{bmatrix}$ which is then converted to an upper triangular form

after elementary operations. The solution to the original system of equations is found by back substitution from the last row of the augmented matrix.

Direct methods work well for simple problems which generate lower order matrices but they are computationally expensive and inefficient for large sparse matrices. Moreover the coefficient matrix A depends on the properties of the fluid, such as viscosity or density which evolves as the solution is refined for the primary variables. Therefore it is not efficient to seek an exact solution to $Ax = b$ for every global iteration because the variables used to build A and b are evolving.

Iterative Methods

Iterative methods obtain an approximate solution of the linear system of equations that is based on iterations. An approximate solution of the primary variables is calculated which is then fed back into the primary equations to refine the variables. For large scale CFD problems it is more efficient to slightly improve over each variable at one turn and then cycle over to all the coupled variables in the subsequent iteration to reduce the error.

Iterative methods generate an approximate solution to the system that tends to converge to an exact solution. After m iterations the approximation is described as:

$$Ax^{(m)} = b - r^{(m)} \tag{224}$$

where $r^{(m)}$ is the residual after m iterations. The error in the approximation is defined as:

$$\epsilon^{(m)} = x - x^{(m)} \tag{225}$$

which results in the expression

$$A\epsilon^{(m)} = r^{(m)} \tag{226}$$

The purpose of the iterative methods is to drive this residual below the convergence criteria set.

The solution of the linear system of equations can be expressed as:

$$x^{(m+1)} = Cx^{(m)} + d \tag{227}$$

Based on the way that the solution at every iteration is updated, iterative methods can be classified into two types:

- Stationary Iterative Methods: The terms C and d are not dependent on the iteration count m. Some examples of these methods include Jacobi method, Gauss-Seidel method, Successive Overrelaxation method (SOR) and Symmetric Successive Overrelaxation method (SSOR).
- Non-Stationary Iterative Methods: The terms C and d are updated at every iteration. Some examples of these methods include Conjugate Gradient method (CG), Generalized Minimal Residual method (GMRES) and Conjugate Gradient Squared Method (CGS).

AcuSolve Solver Features (CFD Theory for AcuSolve)

This section on AcuSolve solver features covers the description of various solver features available in AcuSolve such as heat transfer, fluid structure interaction and turbulence modeling.

Commercial solvers for fluid flow analysis come in many forms. They use a collection of numerical methods and approximation approaches to solve the governing continuum equations discussed in this manual.

AcuSolve is a general purpose CFD flow solver that is used in a wide variety of applications and industries. The flow solver is architected for parallel execution on shared and distributed memory computer systems and provides fast and efficient transient and steady state solutions for standard unstructured element topologies.

AcuSolve is based on Galerkin Least Squares (GLS) finite element method. The GLS formulation provides second-order accuracy for spatial discretization of all variables and utilizes tightly controlled numerical diffusion operators to obtain stability and maintain accuracy. In addition to satisfying conservation laws globally, the formulation implemented in AcuSolve ensures local conservation for individual elements. Equal order nodal interpolation is used for all working variables, including pressure and turbulence equations. The semi discrete generalized alpha method is used to integrate the equations in time. This approach has been verified as being second-order accurate in time.

AcuSolve uses a time marching procedure to solve both steady state and transient simulations. In the case of steady state simulations, the inertia (mass) terms of the conservation equations are only included in the Galerkin part of the finite element weighted residual formulation. This inclusion adds stability to the nonlinear iterations. Other parts of the finite element formulation (such as the least-squares operator) do not include the inertia terms. This exclusion accelerates non linear convergence to steady state at the expense of time accuracy. The initial time step size is set to a significantly large value (1.0e+10).

For transient simulations the inertia terms are included in all the operators of the finite element formulation in order to preserve time accuracy.

The resultant system of equations is solved as a fully coupled pressure/velocity matrix system using a preconditioned iterative linear solver. The iterative solver yields robustness and rapid convergence on large unstructured meshes even when high aspect ratio and badly distorted elements are present.

AcuSolve consists of multiple features designed to tackle various flow physics such as temperature flow, solar radiation and rigid body dynamics.

Heat Transfer

AcuSolve supports various features for the modeling of the heat transfer phenomenon.

- Convective Heat Transfer: Heat transfer due to the motion of molecules within a fluid. This includes both natural and forced convection.
- Conjugate Heat Transfer: Heat transfer between solids and fluids.
- Radiation Heat Transfer: Heat transfer due to radiation between surfaces having high temperatures.

- Solar Radiation: Heat transfer due to incident solar radiation on a surface.
- Additional features: Thermal shells, viscous heating and compression heating.

AcuSolve Heat Transfer Methodology

AcuSolve uses an advective-diffusive equation governing the transport of enthalpy.

$$\rho\frac{\partial h}{\partial t}+(\rho\vec{u}\cdot\nabla)h \quad =\rho s \quad +\nabla\cdot q \tag{228}$$

This approach permits the conservation of energy with the Galerkin Least Squares formulation.The temperature is derived from the state equation specified for the flow.

There are two common approaches used for the solution of thermal problems in AcuSolve.

- Segregated approach: The enthalpy equation is solved separately from the flow equations. This approach can be further divided into two parts:
- Sequential solving: The enthalpy equation is solved in a sequential manner after solving the coupled flow equations using feed- forward of the velocity field into the enthalpy equation. This approach is appropriate for cases where the temperature field does not affect the flow field significantly. This can offer benefits in speed since the iterations on flow field are not carried along as part of the temperature equation. If the flow field has already converged sufficiently, additional iterations are wasted. This approach also enables “frozen flow” thermal simulations where the flow field is held constant, but different scenarios of the temperature field are investigated.
- Concurrent solving: The enthalpy equation is solved in a sequential manner after the flow equations but there is feedback of the temperature dependent variable from the enthalpy equation back to the flow equations during each iteration. This approach is appropriate for cases involving temperature dependent material properties.
- Coupled approach: The enthalpy equation is coupled into the global system and solved in conjunction with the flow equations. This approach is often times more stable for cases exhibiting a large degree of coupling between the temperature and flow fields, that is, buoyancy driven flows.

AcuSolve Enclosure Radiation Methodology

AcuSolve simulates the surface to surface radiation using a two step approach:

- View factor computation: In radiative heat transfer view factor is the proportion of radiation incident on one surface due to another surface. The view factors for each facet defining the radiation enclosure are computed using the hemicube algorithm and smoothed using least squares method as a pre-processing step. The view factors are not recomputed during the simulation.
- Heat flux addition: The radiative heat flux, based on view factors, computed using the Stefan-Boltzmann law and the total radiosity, based on Kirchoff's law, is added to the enthalpy transport equation during the solver run.

The enclosure radiation model is supported only on fluid mediums, that is, the fluid side of the fluid/solid surface.

View factor computation is an important point when dealing with moving mesh simulation. Since the view factors are not recomputed during the solver run the boundary elements forming the enclosure should not deform.

AcuSolve Solar Radiation Methodology

AcuSolve uses an ideal grey surface solar radiation model to calculate the solar heat flux. The fluxes are computed using a ray trace algorithm and five optical properties of the surface, specular transmissivity, diffuse transmissivity, specular reflectivity, diffuse reflectivity and absorbtivity. These properties are constrained by the relation:

$$\tau_s(\theta)+\tau_d(\theta)+\rho_s(\theta)+\rho_d(\theta)+\alpha(\theta)=1 \tag{229}$$

AcuSolve Thermal Shell Methodology

AcuSolve permits the definition of thermal shells as material medium to simulate heat transfer in thin solid mediums. This is particularly useful when the thickness of the component makes it inconvenient to use it as a solid medium. The shell medium supports only bricks and wedges.

AcuSolve can model shell layers of varying thickness and material properties. There are two mechanisms by which the heat transfer equation is solved in the thermal shell depending on the number of layers:

- Single Layer: The elements in a single layer shell are considered as full volume elements. The coordinates of the nodes on the opposite faces of the shell are offset by the thickness provided and the heat transport equations are used to determine the heat transfer within the shell. For this scenario the thermal shell includes all heat transfer effects that are present in a three dimensional volume element.
- Multiple Layer: The nodes on the opposite faces have the same coordinates but have different node numbers in order to support the temperature differences across the shell. A one dimensional heat equation, through the shell thickness at the element nodes, is derived by neglecting thermal inertia and conduction parallel to the surface. This means that the heat flux is the same in all the layers. If each layer material model has a constant conductivity then this simplified heat equation is solved exactly. If any of the conductivities is a function of temperature then a two-pass procedure is used to approximately solve the resulting nonlinear system. Once the temperatures are known at the corners of all the layers in each element they can be interpolated to the quadrature points in the usual manner.

Viscous and Compression Heating

AcuSolve can simulate heat transfer due to viscosity and compressibility of the fluid in case of highly viscous flows and variable density flow models. The terms corresponding to viscous and compression heating are added to the enthalpy transport equation:

$$\rho\frac{\partial h}{\partial t}+(\rho\vec{u}\cdot\nabla)h \quad =\rho s \quad +\nabla\cdot q+\tau:\nabla\vec{u}+\frac{Dp}{Dt} \tag{230}$$

where

- $\tau:\nabla\vec{u}$ is the viscous heating term
- $\frac{Dp}{Dt}$ is the material derivative of pressure which describes the compression heating

Fluid Structure Interaction (FSI)

One of the rich features of AcuSolve lies in its ability to simulate FSI problems.

AcuSolve simulates these problems using two different technologies:

Practical FSI (P-FSI)	In P-FSI simulations, AcuSolve and the structural code are run separately. The Eigen solution obtained from a structural solver is projected onto the CFD mesh and used as boundary conditions to displace the fluid mesh. The mass, stiffness and damping arrays are also transferred from the structural model to flexible body in the CFD model, completing the inputs necessary to compute the structural deformation. P-FSI is preferred for simulations that have linear structural response (linear material properties and small mesh deformations).
Direct Coupled FSI (DC-FSI)	For applications involving a nonlinear structural response, AcuSolve is coupled at run time to a structural solver using the DC-FSI approach. The codes are run in tandem and exchange forces and displacements at each time step. This technique captures all nonlinearities in the structural model and can exploit the full capabilities of the structural solver. The DC-FSI technology within AcuSolve performs all projection and interpolation between the structural and CFD meshes without the use of any middleware. The supported structural solvers for AcuSolve include OptiStruct, Abaqus and MD-Nastran.

Variable Property Support

AcuSolve provides an extensive set of features to model the different material properties of the fluid and the surrounding media.

The different material properties that can be modeled are discussed in the following sections.

Density

The density models can be specified for all types of media supported by AcuSolve (solid, fluid and shell). They are:

- Constant Density: A constant density for the media. This is generally used for incompressible flow simulations.
- Boussinesq Model: Use of the Boussinesq approximation, where the variation in density is assumed to be a linear function of temperature and the density variation is accounted only in the body force terms.
- Isentropic Model: The constant entropy gas model, where the variation in density is taken into account for all the terms in the momentum equations.
- Ideal Gas Model: The density is based on the ideal gas law. The variation in density is taken into account for all the terms in the momentum equations.

- Customized Models: Custom variable property functions for density can be specified using curve fit options (piecewise linear and cubic spline) as a function of single independent variable. User functions can be used to model more complex density models. In case of customized models the density variation is applicable to all the terms.

Viscosity

The molecular viscosity models used in the flow (momentum) equations, specified for the fluid medium are:

- Constant Viscosity: A constant viscosity for the fluid medium. This is the simplest case of a Newtonian model for calculation of the stress tensor.
- Ramped Viscosity: The viscosity is ramped down 1,000 times from the viscosity value specified at time step one to the viscosity value at time step ten, after which the value from time step ten is used.
- Non-Newtonian Models: Non-Newtonian viscosity models based on Power Law, Bingham model, Carreau-Yasuda model can be specified.
- Customized Models: Custom variable property functions for viscosity can be specified using curve fit options (piecewise linear and cubic spline) as a function of single independent variable. User functions can be used to model more complex viscosity models.

Porosity

AcuSolve uses the Darcy-Forchheimer porosity model for the flow (momentum) equations, specified for the fluid medium. The porosity model modifies the momentum equation as follows:

$$\frac{\rho}{\phi}\left[\frac{\partial \vec{u}}{\partial t}+(\rho\vec{u}\cdot\nabla)\vec{u}+R\vec{f}\right]=-\nabla p+\rho b+\nabla\cdot\tau \tag{231}$$

where

- $\vec{f}$ is the field vector contribution due to porous media, also referred to as porous media forces.
- R is the rotation tensor which rotates $\vec{f}$ to the global coordinate system.

The porous media forces are given by:

$$f_i=\left(\frac{C_{Darcy}\mu}{k_i}+\frac{C_{Forch}\rho}{\sqrt{k_i}}|u|\right)u_i \tag{232}$$

where

- C_{Darcy} and C_{Forch} are the Darcy and Forchheimer coefficients, respectively.
- k_i is the permeability in the principal direction i.

Viscoelasticity

AcuSolve supports simulations involving viscoelastic materials using the Upper Convected Maxwell Model and the Upper Convected Maxwell Log Model. The viscoelastic models used in the flow (momentum) equations, have various sub models to determine the rate of stress build up and rate of stress decay. These include:

- Oldroy-B Model: Stress build up and decay rate obtained by defining the relaxation time and polymer viscosity of the fluid.
- Giesekus Model: Stress build up and decay rate obtained by defining the mobility factor along with the relaxation time and polymer viscosity of the fluid.
- Phan-Thien-Tanner Model (PTT): Stress build up and decay rate obtained by defining the PTT extensibility factor and the diffential ratio along with the relaxation time and polymer viscosity of the fluid.
- Customized Models: Customized models based on a user function.

Additional Properties

AcuSolve also supports the modeling of several additional properties such as Surface Tension, Conductivity, Diffusivity, Contact Angle and Specific Heat of the fluid medium.

All of these material properties except Contact Angle can be specified using customized models based on curve fit options (piecewise linear and cubic spline) as a function of single independent variable or by using user functions.

The Conductivity can be additionally specified to be based on an Isotropic Prandtl number Model, ramped to a value or set as anisotropic using the customized models.

The Diffusivity can be additionally ramped to a value.

Contact Angle for free surfaces with surface tension can be set to a constant value or automatically computed from the boundary conditions.

Scalar Transport of Multiple Species

AcuSolve has the capability to track multiple species in a fluid flow by using the scalar transport equations for each of them individually.

The species transport equation is similar to the generalized governing equations for the fluid flow and it is expressed as:

$$\rho \frac{\partial \varphi_i}{\partial t} + (\rho \vec{u} \cdot \nabla)\varphi_i = \nabla \cdot \Psi_i + \rho\sigma_i \tag{233}$$

where

- φ_i represents the ith scalar species.
- Ψ_i is the diffusion flux vector for species φ_i.
- σ_i is the source per unit mass for species φ_i.

The diffusivity flux vector is expressed as:

$$\Psi = d\nabla\varphi \tag{234}$$

where d is the diffusivity for species φ. The diffusivity can be modeled as constant, ramped against time step or customized using variable property and user functions.

The material properties can be set to be functions of species concentration. This models a 'miscible' property relative to mixing of multiple fluids.

Turbulence Modeling

AcuSolve supports a variety of turbulence models for fluid flow simulations.

For steady state simulations the Reynolds-averaged Navier-Stokes equations are solved to arrive directly at the time averaged flow field. In case of transient simulations the governing equations are integrated in time to yield an accurate description of the flow field. There are also many different turbulence closure methods available for each type of simulation.

The various turbulence models used in AcuSolve are:

One Equation and Two Equation Models	Spalart-Allmaras (SA) turbulence model
	Shear Stress Transport (SST) turbulence model
	$k-\omega$ turbulence model
	$k-\varepsilon$ model
	RNG $k-\varepsilon$ model
	Realizable $k-\varepsilon$ model
Detached Eddy Simulation (DES) Models	SA – DES
	SST – DES
	Dynamic DES (DDES)
Large Eddy Simulation (LES) Models	Classical (Smaroginsky) model
	Dynamic subgrid LES model

Turbulent Boundary Layer Modeling

AcuSolve also offers three approaches for the simulation of turbulent boundary layer. These approaches involve setting the turbulence laws close to the wall and are described as follows:

Fully Resolved	This approach integrates equations directly to the wall and uses near wall damping functions to produce appropriate behavior.
Wall Function	This approach uses a wall model based on the standard Law of the Wall for turbulent boundary layers.
Running Average Wall Function	This approach enforces the Law of the Wall on the running average flow field.

The wall functions used in AcuSolve are valid through the viscous sublayer and the buffer layer and have the advantage of having no lower bound limit. The upper bound limit for $y+$ is 300.

AcuSolve Workflow

4

This chapter covers the following:

AcuSolve Workflow Introduction

This section gives a brief description of a general workflow of a typical CFD process. It describes in short the problem description, pre-processing, solving and post-processing aspects of a CFD workflow.

The entire workflow of a typical CFD analysis can be summarized as follows.

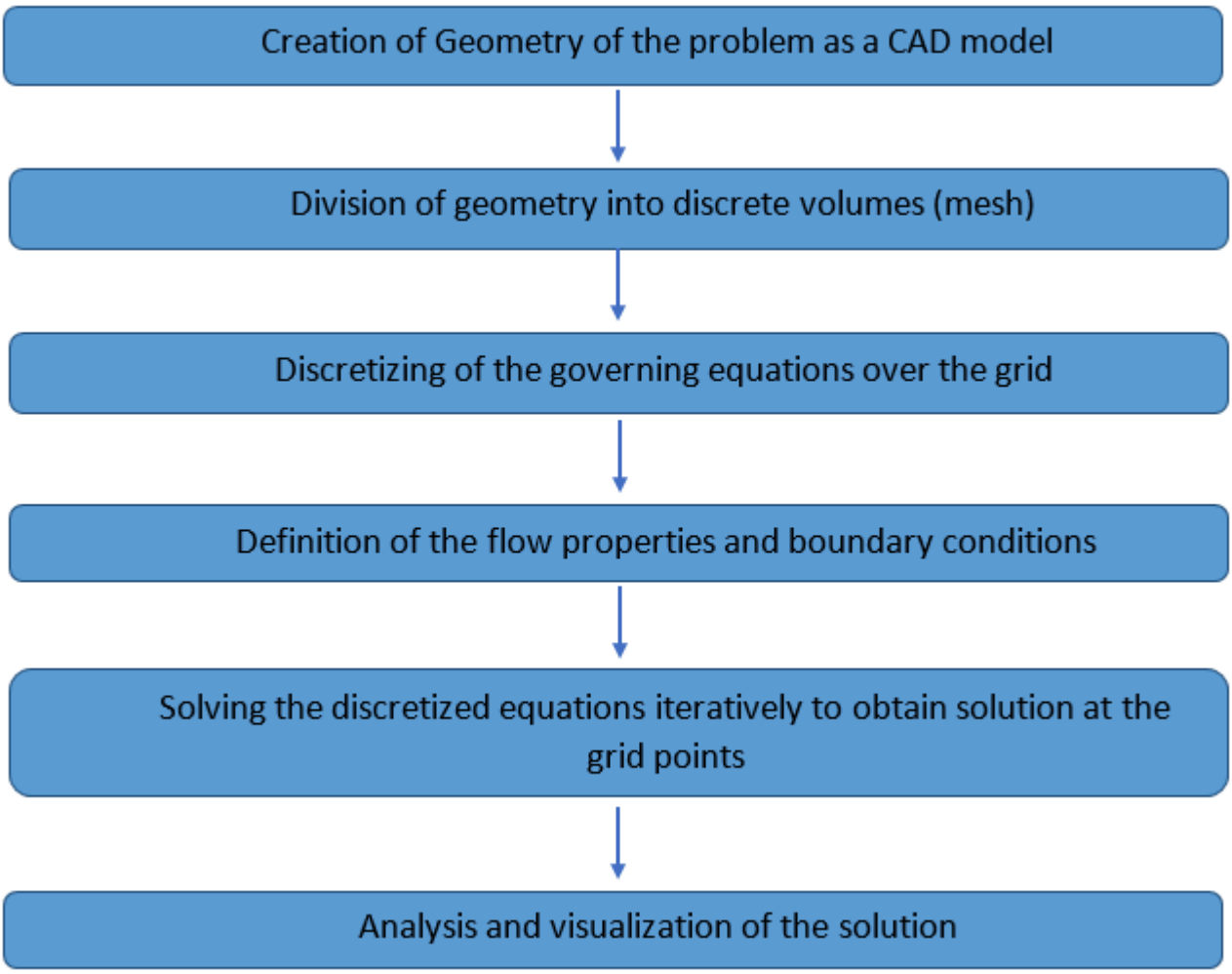

Figure 45: Basic Workflow

AcuSolve is a robust software that does all of the above steps of CFD and provides the accurate solution to the problem.

General Workflow

The accurate simulation of a flow field using CFD requires a number of steps to be taken. In order to set the problem up properly for simulation it is necessary to first understand the physics. Once the physics have been understood a model can be constructed. The following steps describe the set of steps that should be taken when performing a CFD simulation.

Problem Description

Though often neglected, this step is the foremost important aspect of a successful CFD simulation. Before attempting a CFD simulation a clear description of the problem is necessary. This step involves the following tasks.

- Identify the domain of interest: Though in principle domain of any size can be analysed with CFD simulation, it is often wise to choose the critical regions in which flow field is of importance and simulate the flow in that domain. Minimizing the size of the domain keeps the simulation costs low, but comes at the expense of introducing non physical behavior in the simulation by having boundaries too close to regions in the flow where the results are of interest. It is important to select boundaries where the flow character is known so that proper boundary conditions can be applied.
- Identify the nature of the flow: It is always helpful to make an educated guess on the nature of the flow, such as whether it is steady/transient, laminar/turbulent, thermal/non thermal. For example, while analysing a flow in a pipe that has low Reynolds number, say Re ~ 100, it is useful to perform a laminar analysis rather than doing an expensive turbulent flow analysis with a larger mesh count. In case of turbulent flows, it is advisable to choose turbulence model based on the physics present, while keeping in mind the areas where the flow will be critical.

Pre-Processing

This process involves geometry import, mesh generation and specifying the relevant physics equations to be solved. Pre-processing also involves defining the fluid properties, boundary conditions and body force parameters. AcuSolve uses HyperWorks CFD and SimLab for the pre-processing of the geometry and the mesh generation.

Solving

Solving is the critical part of a CFD simulation. The governing flow equations are discretized. All these algebraic equations are then solved for the unknown flow parameters. The final solution is the quantitative representation of these parameters at the mesh generated nodes. As a first step of solving, the AcuPrep module of AcuSolve checks for the compatibility of the information provided in the pre-processing step. The source of errors in AcuPrep could be because of insufficient inputs, syntax errors, and so on. After AcuPrep the actual solving of equations is performed.

Post-Processing

Having solved for the unknowns, the next step is the analysis of this huge data to obtain relevant insight. This data can be analysed either in the form of contour plots or tabular data to identify the critical portions of the flow field.

Guidelines for Quality CFD Modeling

5

This chapter covers the following:

Introduction to CFD Modeling Guidelines

The field of computational field dynamics (CFD) has seen tremendous advancement in recent decades, riding on the back of the phenomenal advances in computational science and power.

CFD evolved throughout the 20th century. In the pre-1950s, semi-analytical methods were developed to solve the complex problems that were still unsolved using analytical solution methods. During the same time period, numerical methods also advanced and became more mature with respect to numerical stability, speed and accuracy. Post 1950, with the availability of low cost computing power and advancement in computer science, researchers all over the world were able to develop complex CFD models and test them on a variety of applications, enabling the advancement of CFD at an accelerated scale. High-fidelity CFD solvers running on powerful computers today can accurately model complex fluid flows, solving the governing equations over billions of grid points, performing trillions of calculations at speeds unthinkable of a few years ago.

However, access to large amounts of computing power does not necessarily equate to high quality results from a CFD analysis. Modern CFD solvers are specialized and complex computer programs. The accuracy of the results provided by the solvers is subject to the accuracy of the inputs. It is necessary that a complete and correct set of inputs be provided to the solvers so that they can perform their task as correctly as possible. Some of the essential aspects of these inputs to be provided to the solvers are discussed in this section. You will be able to apply the basic yet important CFD analysis guidelines that are discussed to your own applications. Following these guidelines in most cases will ensure that the results obtained from the CFD analyses are reasonably accurate with only a small margin of error. However, it cannot be stressed enough that these guidelines should be treated as such, only guidelines, and not an authoritative set of instructions that will ensure correct analyses every time and for every application. You are both encouraged and solicited to apply sound engineering judgement to individual cases, as well as explore validation of your modeling methodology for each application of interest.

A CFD simulation involves solving of the complex Navier-Stokes equations, often coupled with other equations to determine distribution of flow, temperature and turbulence fields across a discretized simulation domain. The Navier-Stokes equations are highly nonlinear and are impossible to solve analytically with available methods. CFD solvers solve these equations numerically, often with a set of assumptions to simplify the solution and a set of parameters specific to the numerical method employed, to produce a stable solution. The numerical approach employed can vary from solver to solver. Also critical to the solution method is the set of constraints that you provide to the solver. This requires sound understanding of the problem definition and the objective of the simulation. At best, a CFD solver is a tool to simplify the task of solving the complex flow-field equations and must be applied carefully for the results to be a true and reliable representation of the actual physical processes. However, since even the best solver technique is based on a numerical approximation method, every CFD result has a degree of error and uncertainty introduced in it by these approximations.

Obtaining accurate results from a CFD simulation depends on many factors, such as how well you have modeled the conditions of interest and how well the CFD software has solved the equations necessary to model these conditions. In order to minimize the errors associated with a solution you must understand what these errors are. Some of these common error sources are listed below.

- Modeling error: This type of error occurs because of the difference between the true physical processes and the equations that are used to model the processes.

- Numerical or Discretization error: This type of error is induced because the model equations are not solved continuously but on a finite number of grid points in the domain.
- Iteration or Convergence error: This type of error is induced because the solution is iterated to a finite convergence level, which is not zero.
- Round-off error: This type of error is induced because the numbers are rounded off when stored in computer memory because of storage limitations.
- Input errors: These are the errors induced due to uncertainties in inputs, such as the choice of physical model pertinent to the application, boundary condition specification and inaccurate input.
- Code errors: These are the errors in the CFD solver code.

Ensuring accurate results requires extensive verification of the software and extensive validation of the modeling approach for the application of interest. Verification and validation are important to minimize the solver-side sources of error and uncertainty in the CFD analysis. Verification will ensure that the solver solves the equations correctly and validation tests the extent to which a chosen model accurately represents reality. Verification and validation are an important aspect of the CFD modeling process but will not be the focus of this discussion. Instead, this section focuses on general CFD quality assurance guidelines that you should follow to ensure that you can expect reasonable results from your analysis. The discussion is divided into several topic areas that represents an important aspect of modeling that addresses one of the error types discussed above. You need to be focused on these aspects, besides the user errors, to ensure high quality results. The following modeling aspects are discussed.

- Geometric sensitivity for geometric uncertainties
- Mesh sensitivity for discretization error
- Boundary condition sensitivity for errors in boundary conditions input
- Physical model sensitivity for modeling error
- Convergence tolerance sensitivity for convergence error

For many CFD applications the true solution to the equations is not always known. In the absence of an analytical solution, or high quality experimental data to compare against, it is difficult to judge the accuracy of a CFD simulation. However, you can still investigate the suitability of your modeling practices by performing sensitivity studies. This practice reveals aspects of your model that have a significant impact on your solution. Once these aspects are identified further work can be done to determine the most appropriate modeling practices for each of these aspects that will minimize the error associated with the individual aspects, ensuring good quality of results overall. It should be noted that performing a full suite of sensitivity studies to evaluate the solution is a costly and time consuming process. Since there are a number of aspects to be evaluated and all of them can impact the solution combining all of them in a single study is not advisable. It is best to study them one at a time. When performing a sensitivity study one aspect of the model that is being studied should alone be changed and everything else should be kept unchanged until a satisfactory solution is achieved. This process is then repeated for all of the aspects that you are interested in studying. In practice, many investigations are avoided and engineering judgment is used in its place. However, for applications where accuracy is of high importance a full set of sensitivity studies needs to be performed to ensure that modeling errors are minimized in the solution. It should be remembered that the sensitivity studies cannot take into account user and code errors and do not warrant that the solution achieved will be the true physical solution. The following discussion describes different sensitivity studies that are commonly performed when investigating the modeling practices to produce a quality solution.

As an exercise, and also to demonstrate to you the effect of the choices made for each of these aspects over the course of a sensitivity study, the discussion of the topics covered will be accompanied with the discussion of a simple but interesting case, the backward facing step case. For a detailed description of the case refer to the AcuSolve Validation manual in your AcuSolve installation directory. However, here you will not analyze the case with the objective of validating the model but with emphasis on educating you about guidelines for setting up the model correctly and identifying the appropriate modeling choices to make. A brief discussion of the case is as follows.

The problem consists of a fluid flowing in a channel with a sharp expansion. The step in the channel causes the flow to detach at the step and reattach some distance downstream of the step. The detached flow also causes recirculation in the region between the step and the reattachment point. The fluid properties are close to that of air. The Reynolds number at the inlet is 36,000, which is based on the step height. The flow is turbulent and you will pursue a steady state solution. The objective of the analysis is the accurate representation of the recirculation zone and determination of the reattachment point. The image below shows the schematic geometry of the case setup.

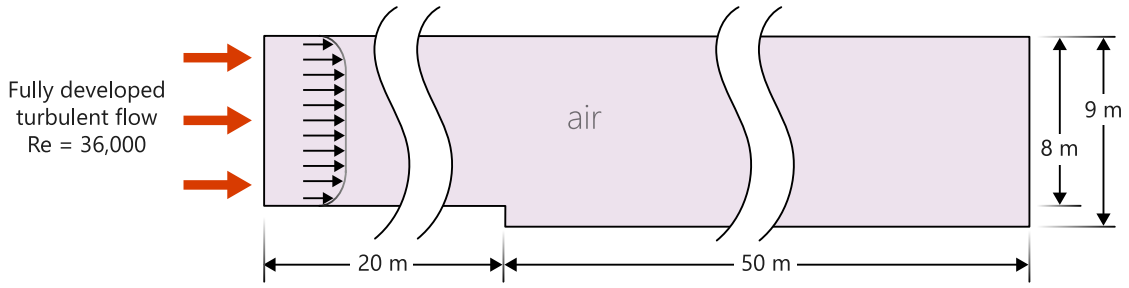

Figure 46: Schematic Geometry of the Backward Facing Step Case

This situation roughly mimics the behavior of flow exiting from a flow channel into a plenum of a plate type heat exchanger. An engineer is interested in placing a pressure tap along the lower wall to measure the total pressure drop through the system. In order to avoid spurious measurements from the pressure tap it is necessary to place the tap downstream of the recirculation region. Therefore, the location of the reattachment point must be known.

Geometric Sensitivity

This section discusses and illustrates the effects of the geometrical representation of the problem, and the discretization of the geometry on your CFD solution.

CFD simulation involves the creation of a discrete mathematical model of an object, assembly, region in space, and so on. In order to obtain accurate results from the CFD analysis, analysts must ensure that they are using an appropriate representation of the geometry that they are trying to simulate. When simulating flow involving complex geometric features, it is necessary to evaluate the degree to which the discretized representation of the geometry matches the actual component of interest. For example, it is common practice to remove small features such as small bolt holes and fasteners when simulating complex assemblies. These features may or may not have a significant impact on the results of the simulation. Analysts need to determine the appropriate level of detail required to achieve an accurate representation of the flow field. This often times requires a geometry sensitivity study to determine.

Another aspect of proper geometry modeling is how well the mesh matches the geometry. For curved geometries, it is necessary to have sufficient element density to resolve the curvature smoothly and provide an appropriate reproduction of the shapes. In addition to the mesh density, it is also necessary to ensure that the underlying CAD model provided appropriate resolution of the geometry. When constructing meshes from discrete CAD models you must pay particular attention to this to ensure that the discrete model is an appropriate representation of the true geometry.

The third geometric modeling aspect is the extent of the domain used for analysis. When modeling external flows, it is necessary to model a sufficiently large domain that minimizes the impact of the numerical constraints applied to the model. For example, when trying to simulate an airfoil in an infinite medium it is necessary to size the domain large enough so that the surrounding region is not constraining the flow around the airfoil in an unrealistic manner. Similarly, for internal flows, the boundaries of the domain should be located far away from the location of any phenomena of interest in the domain to minimize any interference in the results due to the presence of the boundaries.

A final aspect of the geometric modeling applies to the problems that have a rotating component within the domain. Examples of such flows are the flows in pumps and turbomachines where fluid interacts with a rotating part, adding swirl to the flow. The common approach while modeling such cases is splitting the domain into a rotating part which immediately surrounds the rotating component (rotor), and the static part that makes up the rest of the domain. While modeling such cases, it is very important to understand the sensitivity of the location of the interface which will separate the static and the rotating part. An interface located either too close or too far from the rotor reduces the accuracy of the solution. For an accurate solution it is advisable to test the sensitivity of the solution to the location of this interface. Unfortunately, there are no set guidelines to determine this, as the optimum location is a function of the dimensions of the domain and the rotor, the relative velocity between the fluid and the rotor, and so on.

The Backward Facing Step Case

A look at the schematic of the backward facing step case indicates that the outlet boundary of the domain has been modeled at a distance of 50 times the step height downstream from the step location. It is desired that the extent of the recirculation zone and the subsequent reattachment of the flow downstream of the step are not affected by the proximity to the boundary.

The extent to which the boundaries should be distanced from the region of interest should be evaluated on a case by case basis. It can be argued that using a distance of 50 times the step height is a very conservative estimate for the backward facing step (BFS) problem, which may be considered a relatively simple problem. Using such a conservative value is not always feasible especially as geometries and models become complex. The modeling aim should be to minimize the interference of boundaries on the results. Unless there is a constraint on the model that prevents shifting the boundaries sufficiently far from the region of interest, or you are interested in studying the effect of boundaries on the model, this practice should be followed.

Mesh Sensitivity

This section illustrates the various effects that mesh refinement, mesh quality and topology have on your CFD solution.

Mesh Refinement

The role of a CFD solver is to approximate the solution to a coupled set of partial differential equations.

This typically entails solving for the pressure, velocity and turbulence fields within a given domain. These fields can be both spatially and temporally varying. To obtain a solution to the governing equations, the simulation domain is discretized into small, finite regions, referred to as elements or cells, that are made up of faces that are connected by nodes or vertices. The solver then solves the governing equations over each of these finite regions to approximate the solution over the whole domain. In the case of a finite element solver, the solution is obtained and stored at the nodal locations. In other words, the solution is permitted to vary at the locations of the nodes in finite element solvers. The solution between the nodal locations is assumed to vary linearly, in most cases. With this in mind, it is clear that the mesh resolution thus must be sufficient so that all variations in the flow are sufficiently captured by an assumed linear profile between the locations where the solution is stored. Mesh resolution is a measure of the distance between two consecutive measurement points in the mesh.

A consistent numerical analysis will provide a result which approaches the actual result as the mesh resolution approaches zero. In this case the elements become infinitesimally small and the mesh behaves almost like a continuous representation of the domain. Thus, the discretized equations will approach the solution of the actual equations. One significant issue in numerical computations is what level of mesh resolution is appropriate. This is a function of the flow conditions, type of analysis, geometry and other variables. An insufficiently resolved mesh that has nodes far apart will not capture the gradients well enough when assuming linear variations between nodes and will lead to a less accurate numerical solution. An unnecessarily finely resolved mesh will lead to higher solution costs without any gain in accuracy. You are often left to start with a coarse mesh resolution and then conduct a series of mesh refinements to assess the effect of mesh resolution. This is known as a mesh refinement study. Strategic mesh refinement will call for you running a solution on the coarse mesh, studying the results and identifying the areas that require enhanced resolution to improve the solution. The refinement process should be continued until the results do not change with further refinement. Such a solution may be referred to as the grid converged solution.

CFD practitioners must recognize the distinction between a numerical result which approaches an asymptotic numerical value and one which approaches the true solution. It is hoped that as the mesh is refined and resolution improves the computed solution will not change much and approach an asymptotic grid converged value, that is, the true numerical solution. However, there still may be error between this asymptotic value and the true physical solution to the equations. This behavior is shown in the image below.

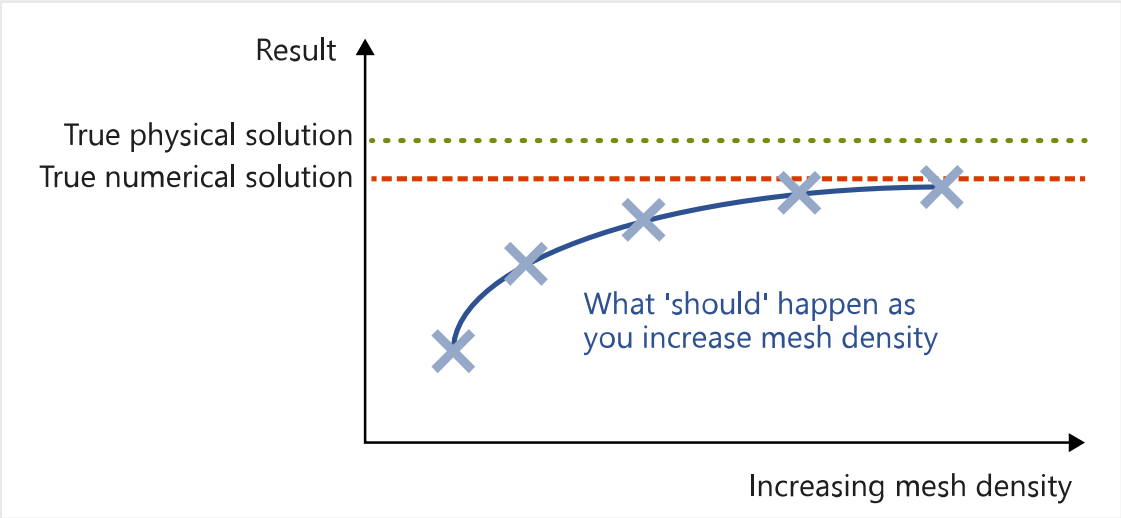

Figure 47: Effect of Increasing Mesh Density on Accuracy of the CFD Solution

Mesh Quality and Topology

Another possible sensitivity associated with the mesh used for a CFD analysis applies to the quality and type of elements that are used.

Each CFD solver has its own guidelines for what types of elements behave best from a stability, accuracy and convergence stand point. In addition to this, there are generally guidelines about the quality of each type of element that is suitable for use within the solver. Many finite volume solvers cite the aspect ratio of the elements, element skewness, orthogonality of the element faces and the element growth factor as critical metrics for determining their suitability for use. For this reason, it is sometimes recommended by code vendors that you use hexahedra elements for finite volume codes. Finite element solvers typically do not have this same constraint and will often recommend the use of tetrahedral

elements. You should consider the needs of your solver when constructing a mesh to determine the most suitable discretization for your application.

The Backward Facing Step Case

The following example uses the backward step facing case. Consider a simulation of this flow using a CFD solver. Assume that you are creating a very coarse mesh on the geometry and then you are running a simulation. The CFD solver produces a solution to the Reynolds-averaged Navier-Stokes (RANS) equations on this discretization that results in a seemingly realistic flow field. The flow is characterized by the large separation zone downstream of the step and the recovering boundary layer after reattachment. Representative results for such a simulation are shown in the image below.

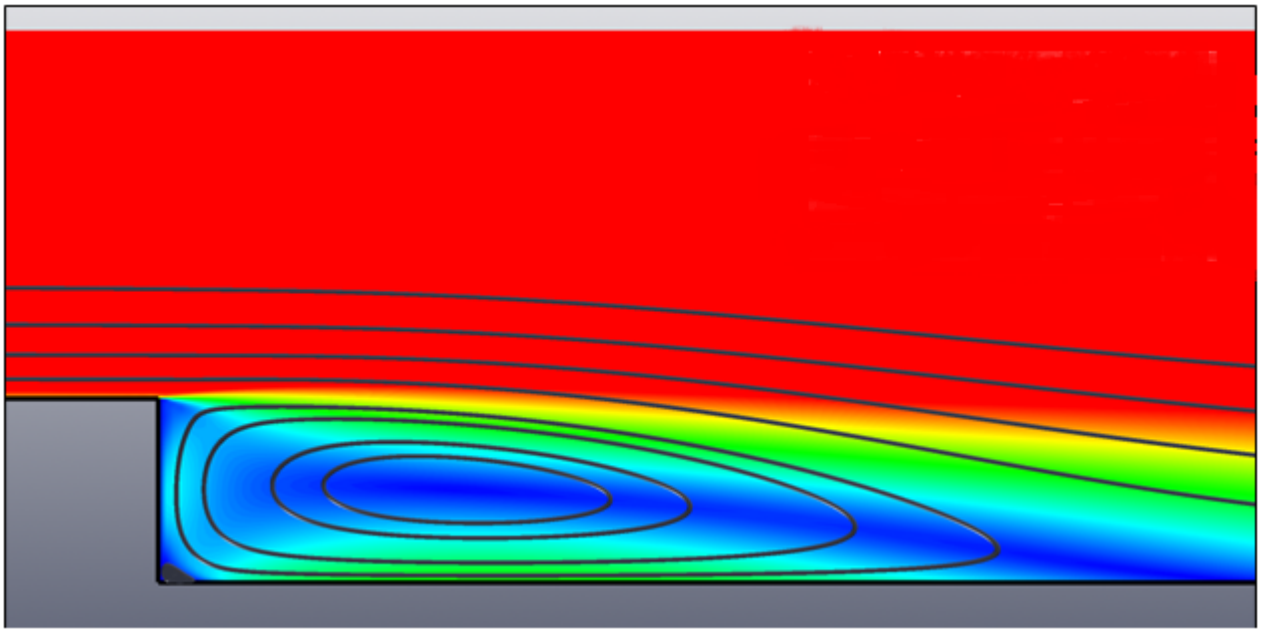

Figure 48: Streamlines Showing Separation Zone in Backward Facing Step Model

However, if there are insufficient points in the mesh to provide a good estimate of the gradients between the solution points the solver will not be able to resolve the flow features properly. Using this example, the shear layer that develops in the separation zone is under resolved and this leads to a poor representation of the reattachment point. In order to improve the solution it is necessary to refine the mesh in the locations of high velocity gradients. By doing this, the solver is better able to represent the local variations in the solution leading to a better approximation of the true solution to the governing equations. The image below shows five different meshes created for the backward facing step problem. Each mesh is progressively refined with respect to the previous mesh to illustrate the areas of refinement that must be paid careful attention to for this particular application.

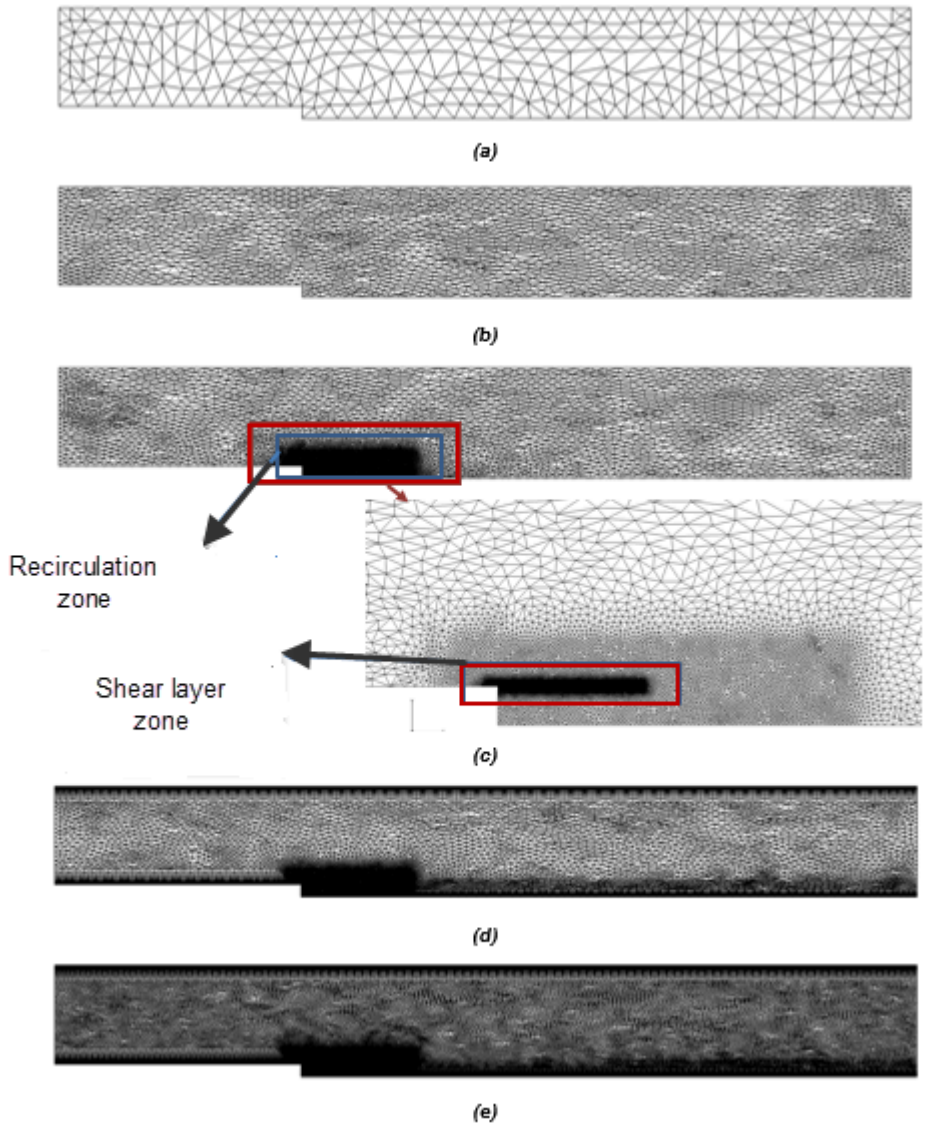

(a) Mesh 1; (b) Mesh 2; (c) Mesh 3; (d) Mesh 4; (e) Mesh5

Figure 49: Five Meshes Used in Backward Facing Step Mesh Sensitivity Study

The figure below shows the velocity profiles obtained from the solutions of each of the meshes using a consistent solver setup. Images (a) to (d) each correspond to the solution from mesh one through four, respectively. It is easy to see how the solution improves with each refinement in the mesh. A detailed discussion of these figures is covered in the mesh refinement process below.

Figures a-d each correspond to mesh one through four, respectively.

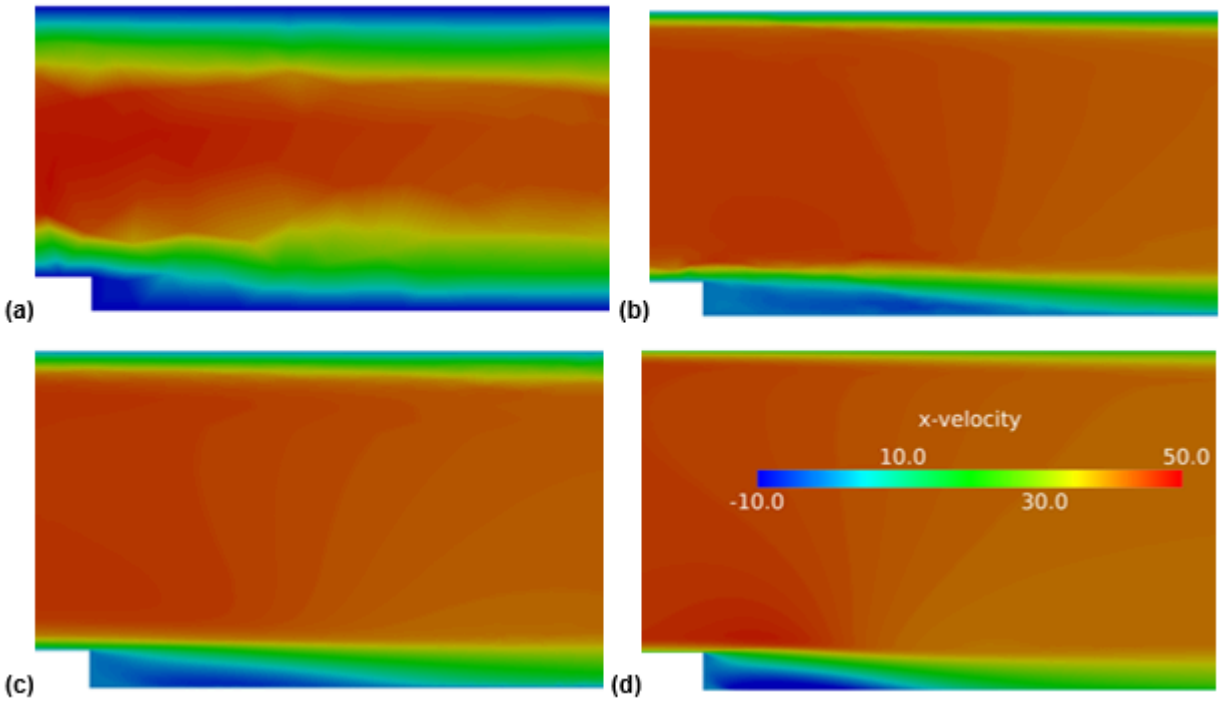

(a) Mesh 1; (b) Mesh 2; (c) Mesh 3; (d) Mesh 4

Figure 50: Velocity Profiles Downstream of the Step Depicting Mesh Sensitivity for the Backward Facing Step Case

The refinement process is briefly discussed below.

Mesh 1-image (a)

This is the first mesh created for this case. As mentioned earlier, you begin with a coarser mesh which is systematically refined to achieve a mesh suitable for the application.

Global absolute element size of 2m for each element is used for this mesh.

A look at the solution from Mesh 1 (image 5a) reveals thick boundary layers near the top and bottom walls and core flow velocity gradients in the vertical direction.

The reattachment location could not be obtained from this solution and the flow appears to never have made contact with the lower wall downstream of the step.

Mesh 2-image (b)

The previous solution had a poor representation of the core flow and boundary layers, indicating a mesh resolution insufficient to capture the gradients present.

It is advised to use the anisotropic mesh size setting for this case. This means that you will specify a different mesh setting for the horizontal and vertical direction for efficiency. Using anisotropic mesh sizing allows you to efficiently refine the mesh by targeting the specific direction where gradients are stronger. The mesh

displayed in image 4(b) is generated using the following global mesh size specification.

Mesh Size Type	Absolute Anisotropic
Element size in horizontal direction (x)	2 m
Element size in vertical direction (y)	0.4 m

This will give about five times more elements in vertical direction.

This solution (image 5b) shows much better resolution of the velocity field, but the shear layer and the recirculation zone are not properly represented in the solution as irregularities can be seen in the velocity profiles in these locations.

The reattachment point for this mesh is observed to be at a distance of 8.44 m downstream of the step.

Mesh 3 – image (c)

The shear layer zone and the recirculation zone must be properly resolved for proper representation.

Mesh can be refined in these zones using localized mesh refinement zones. The suggested mesh zones for this refinement are shown in the image. The mesh sizes used for these zones are as follows:

- Recirculation zone mesh size is 0.1 m.
- Shear layer zone mesh size is 0.01 m.

After refinement the shear layer and the recirculation zone are much better represented, as shown in image (c).

The reattachment point for this mesh is observed to be at a distance of 7.42 m downstream of the step.

Mesh 4-image (d)

Without proper resolution at the boundary it is difficult to visualize where exactly the recirculation zone ends and the flow reattaches to the lower wall. In this step boundary layers are added near the walls to remedy that.

The following settings are used for creating the boundary layers.

Wall Lower Downstream, Wall Lower Upstream, Wall Upper	**Wall - Step**
Mesh Type: Absolute Anisotropic	Mesh Type: Absolute
X, Y element size: 2 m, 0.4 m	Element size: 0.1 m
Boundary layer type: Full control	Boundary layer: No
Resolve type: Number of layers	
First element height: 0.00035 m	
Total layer height: 1.25 m, for Wall Lower Downstream: 0.625 m	
Layer growth rate: 1.3	
Boundary layer elements type: Tetrahedron	

Wall-Step does not need a boundary layer because it is not expected to have attached flow. The step edge has been resolved with a fine mesh because it is the location of separation.

Results from this mesh can be seen to have a proper representation of all of the features of interest for this case. The recirculation zone is properly represented and the location of the reattachment point can be easily identified.

The reattachment point for this mesh is observed to be at a distance of 5.73 m downstream of the step.

Mesh 5 – image (e)

Having refined all critical areas of the domain, further improvement in the solution may be achieved by using a smaller element size. Mesh topology does not need to be changed from this point forward.

For this study, the following settings were used to generate a fine mesh with similar topology as the Mesh 4:

- Global anisotropic mesh size: X, Y element size: 1 m, 0.2 m

- Recirculation zone mesh size: 0.05 m, Shear Layer Zone: 0.005 m

Wall Lower Downstream, Wall Lower Upstream, Wall Upper	**Wall - Step**
Mesh Type: Absolute Anisotropic	Mesh Type: Absolute
X, Y element size: 1 m, 0.2 m	Element size: 0.05 m
Boundary layer type: Full control	Boundary layer: No
Resolve type: Number of layers	
First element height: 0.0001 m	
Total layer height: 1.25 m, for Wall Lower Downstream: 0.625 m	
Layer growth rate: 1.2	
Boundary layer elements type: Tetrahedron	

The reattachment point for this mesh is observed to be at a distance of 5.73 m downstream of the step.

The table below gives a summary of the refinement process discussed above along with the mesh size generated in each case.

Table 6: Summary of the Mesh Refinement Process

Mesh Number	**Number of Nodes**	**Number of Elements**	**Refinement over previous mesh**
1	688	1,737	
2	4,508	12,981	Reduced element size
3	51,056	152,049	Refinement zone in recirculation zone

Mesh Number	Number of Nodes	Number of Elements	Refinement over previous mesh
4	68,014	202,329	Boundary layers on the walls
5	207,492	619,551	Reduced element size further

The table below shows the results achieved using five different meshes. Listed in the table is the variation of the location of the reattachment point for each mesh.

Table 7: Reattachment Point Location as Observed for Each of the Different Meshes

Mesh Number	Number of Nodes	Reattachment Point distance downstream of the step (m)
1	688	No reattachment happens
2	4,508	8.44
3	51,056	7.42
4	68,014	5.73
5	207,492	5.73

It is evident that refining the mesh in the shear layer, recirculation zone and the near wall area where the velocity gradients are highest leads to a change in the solution between meshes one through four. However, it is interesting to note that as the mesh is further refined between grids four and five there is no change seen in the solution. This implies that the solution error associated with grid refinement has been minimized and you have reached an asymptotically grid converged solution with the mesh density and topology utilized in mesh four. All of the critical regions have been refined at this stage and suitable mesh topology as well as sufficient mesh resolution has been achieved. Further refinement of the mesh did not change the solution quantity of interest. A review of the table above indicates that the separation location changed by almost 50 percent between mesh one and the final grid converged solution of mesh four. If no grid sensitivity study was performed the engineer could have made very poor conclusions about the location of the pressure tap.

Appropriate grid refinement is one of the most important aspects of obtaining accurate CFD results. Unfortunately, there is currently no reliable method of automatically generating appropriate meshes for all applications. Additionally, different numerical methods will require different levels of mesh refinement, that is, each code will be different. Ensuring the suitability of a mesh for a given application is your responsibility. The level of accuracy required from a CFD analysis depends on the desired use of the results. A conceptual design effort may be content with general depiction of the flow features, whereas a detailed design may require accurate determination of the flow field. Each quantity to be determined generally has its own accuracy requirement. Levels of effort invested into the CFD model

may vary according to the information required. It is often recommended that a minimum of three different meshes are constructed that cover a wide range of refinement and differ significantly in mesh density and resolution. For applications that require high levels of accuracy this number may be more depending on the number of mesh refinements it takes to achieve a grid converged solution. This allows you to evaluate the sensitivity of the solution quantity of interest to mesh density. Some CFD practitioners endorse the use of a Grid Convergence Index, or GCI, to estimate the level to which a simulation has reached a grid independent solution. More information about the GCI metric is available in the book by Patrick J. Roache, listed in reference [1].

Boundary Condition Sensitivity

This section discusses and illustrates the effects of the location of your model boundaries and the boundary conditions you apply on your CFD solution.

Boundary conditions specify the set of constraints on the solution of a CFD problem at the bounds of the modeled domain. There are many different types of boundary conditions that exist. The available set of constraints and conditions under which they should be used is specific to each CFD solver. However, you should consider the following points when applying boundary conditions.

Proximity of the boundary conditions with respect to the results of interest from the simulation.

In the discussion of the geometric sensitivity of the model it is mentioned that the boundaries must be modeled far away from the region of interest to prevent any interference on the results due to proximity to the boundary. To understand the possible reasons behind this interference it is important to understand that the boundary conditions impose a constraint on the solution. This constraint is an assumption about the behavior of the flow. If the boundary is placed too close to a location in which the results are of interest it is possible that the solution will be impacted drastically by the constraint applied at the boundary.

Realism of the constraints.

Determining appropriate boundary conditions to apply to CFD simulations is often very challenging. This is particularly true when considering inflow conditions. You should consider the suitability of the constraints that are applied to the simulation. For example, analysts need to evaluate the suitability of applying constant values for velocity and turbulence variables at inlet conditions as opposed to specifying boundary layer profiles. These types of decisions can have a significant impact on the realism of the model and introduce errors into the simulation. If there is a separation location downstream of the inlet, the thickness of the incoming boundary layer is a critical parameter and needs to be considered when assigning the location and constraints to apply.

Presence of reverse flow at outlet conditions.

When modeling complex flows it is important to take into consideration the behavior of the flow at the outlet. Most CFD codes do not apply any constraints at outflow conditions that force the flow to exit the domain. If the flow is recirculating and entering back into the domain it is indicative that the boundary is poorly located. If repositioning the boundary is not possible you need to ensure that any flow quantities re-entering the domain are properly bounded. For example, in the case of a turbulent thermal flow that is re-entering the domain at an outlet boundary, it is necessary to assign a constraint on the temperature and turbulence quantities that are being convected back into the domain. Each CFD solver may handle this situation differently, so it is up to you to determine if this situation is acceptable.

The Backward Facing Step Case

This section revisits each of the boundary condition related aspects discussed above in context of the backward facing step case.

- Proximity of the boundary conditions with respect to the results of interest from the simulation. If the boundaries in the backward step facing case are placed too close to the step it will have an adverse effect on the solution. If the outlet is too close to the step the presence of outlet constraints may interfere with the solution, preventing accurate representation of the recirculation zone and the reattachment point.
- Realism of the constraints. Two cases are presented to demonstrate the effect of inlet condition sensitivity on the solution of the backward facing step problem. The first case uses a constant value of velocity and turbulent eddy viscosity at the inlet. This case is derived from Mesh_4 from Mesh Sensitivity uses the same setup as mentioned in that section. The second case provides the inlet variables as a profile similar to the one used in an experimental study of the same problem. Figure 51 shows the profiles with boundary layer definition for the second case.

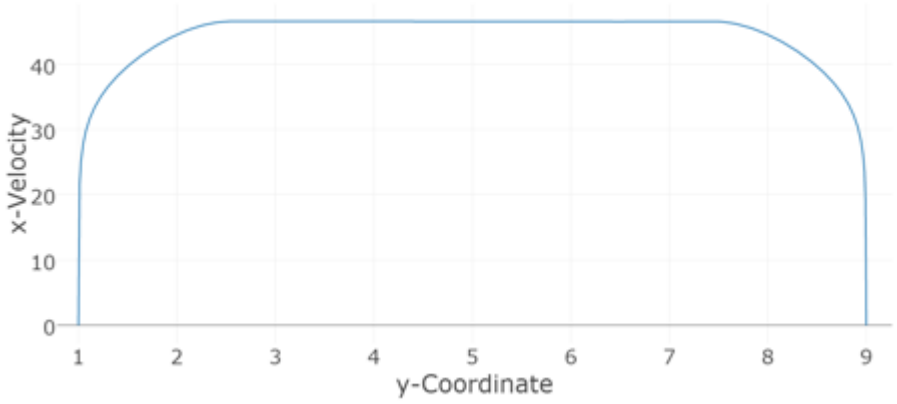

Figure 51: Inlet Velocity Profile

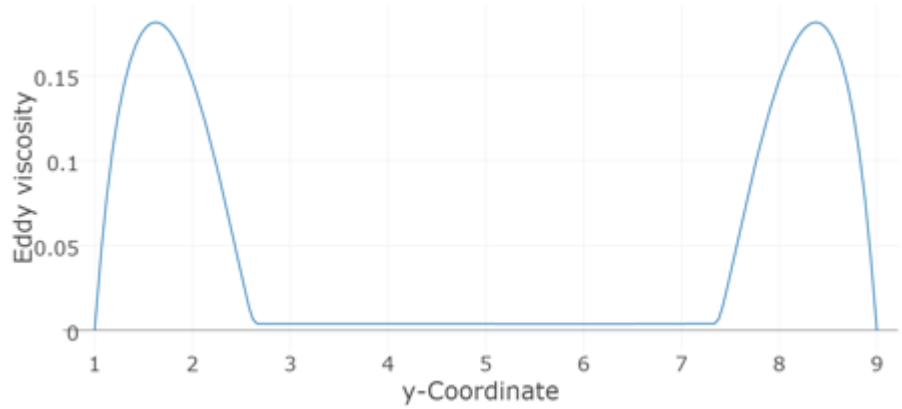

Figure 52: Inlet Turbulent Eddy Viscosity Profile for Inlet Boundary Condition Definition

The inlet velocity profile shows the presence of boundary layers at the edges while the eddy viscosity profile shows a concentrated presence of eddy viscosity in the boundary layer.

When comparing the results of the simulations run with the boundary conditions described above you can see that the profiled inlet condition reflects the experimental data much more accurately. The following plot compares the velocity profiles for both of the cases mentioned above with experimental measurements at the location four times of step height upstream of the step.

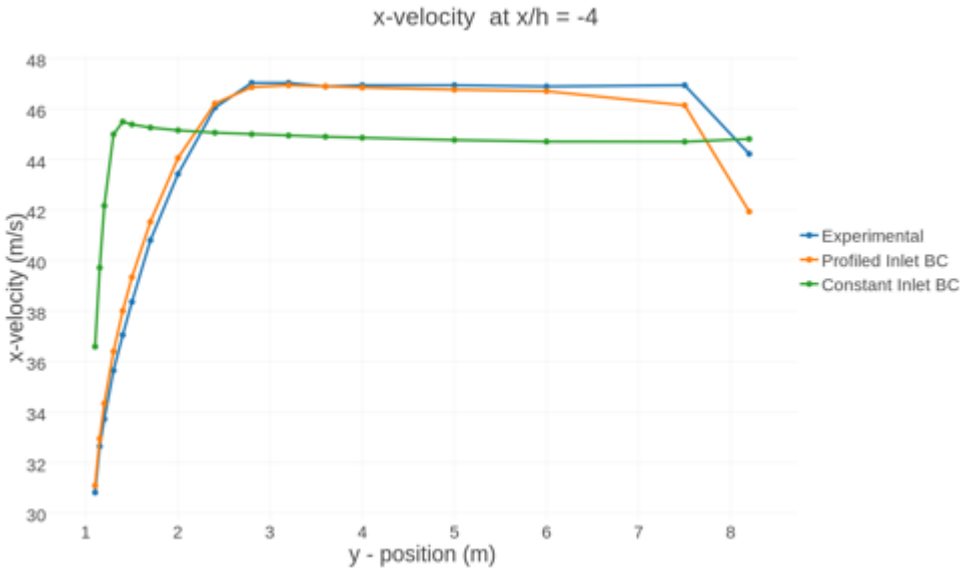

Figure 53: Velocity Profiles at x/h=-4 for Profiled and Constant Inlet Boundary Conditions Compared Against Experimental Data at the Same Location

You can see from the above comparison that using a boundary condition specification that resembles the real physics is much more likely to provide a correct solution to the problem.

The table below shows the difference between the reattachment length observed in the backward facing step problem when a profile similar to the one in the experiment is provided at the inlet, rather than using a constant value for the variables.

Table 8: Inlet Conditions Sensitivity for Backward Facing Step Simulation

Inlet condition type	**Reattachment Length (m)**
Constant	5.73
Velocity profile with boundary layer definition	5.96

Presence of reverse flow at outlet conditions. Figure 54 shows three candidate locations for an outlet boundary in the backward facing step model. The location represented by the white line falls in a region of recirculating flow and would cause inaccurate results as well as numerical difficulties due to the flow re-entering the domain. The location represented by the blue line falls outside of the recirculation zone, but there is still a significant amount of flow non-uniformity and falls fairly close to the recirculation region. To minimize the impact of the outflow conditions on the solution it should be moved further downstream, as shown by the green line.

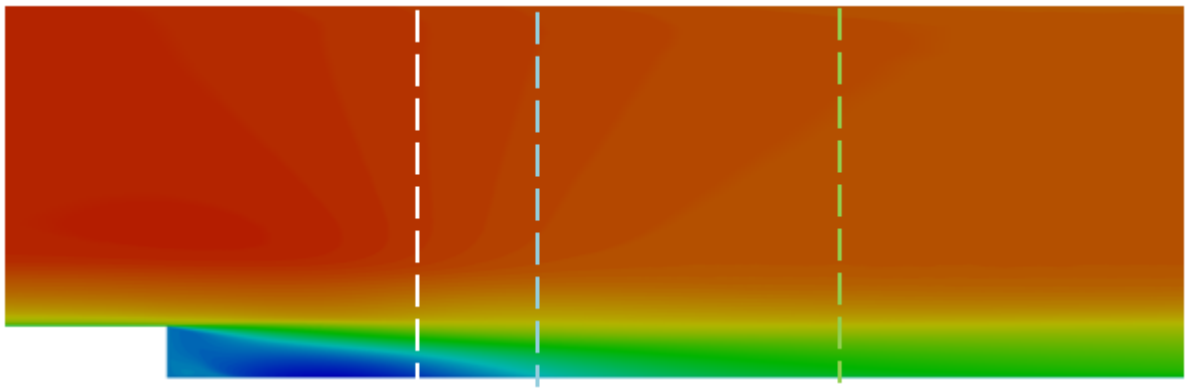

Figure 54: Candidate Locations for an Outlet Boundary on the Backward Facing Step Model

Physical Model Sensitivity

This section discusses and illustrates the effects of the mathematical models you choose to represent the problem physics, flow type, material properties, and so on, in your problem.

Setting up a CFD simulation requires the selection of a number of physical models. The purpose of the physical model is to mathematically represent the physics of a process that occurs in the simulation. One of the first steps in defining the simulation is the identification of the relevant physics that need to be modeled. Once this is done, a suitable model needs to be selected for each aspect of the simulation. Because various models exist for different characteristics of a simulation, it is important to investigate the sensitivity of the results to each of them. The following list mentions some of the possible physical models that need to be considered.

Flow Physics and Modeling

Flows can exhibit different physics under different conditions which must be carefully considered when setting up a simulation. A few variations of these are discussed below.

Steady and unsteady flows

In steady flows, flow properties, such as velocity and pressure, at a given point do not depend upon time.

In unsteady flows, flow properties at a point are functions of time.

Steady flow model is actually a simplification, and it is valid only when the time period over which the flow is observed is large. For modeling a steady flow, the time dependent terms in the Navier-Stokes governing equations are dropped.

Compressible and incompressible flows

Flows with Mach number up to 0.3 at room temperature are said to have weakly compressible behavior, and for the purpose of simulation can be considered incompressible flows, assuming the density to be constant.

Flows with Mach number greater than 0.3 are compressible where the fluid flow should account for the variation of fluid density.

Viscous and inviscid flows

Viscous flows are those in which frictional effects between fluid layers and fluid layers and surfaces are significant. All real flows are viscous flows.

Inviscid fluid flow model is a simplification that can be applied in cases when viscosity effects are expected to be small in comparison to inertial forces. High Reynolds number flows in large size domains where viscosity effects are limited to the small regions close to the boundaries can be considered as inviscid flows for bulk of the domain.

Single-phase and multi-phase flows

Single-phase flows are those in which the flow domain contains only one fluid material in a single state throughout the domain.

In case this condition is not satisfied the flow may be considered multiphase. Multiphase flows can contain a single material in different states or a mixture of two or more different materials in the same or different states. Examples of multiphase flows include solid or liquid particles immersed in a liquid medium or liquid droplets in gaseous medium.

Some common methods for dealing with multiphase flows are Volume of Fluid (VOF) method and Level Set method. Often the multiphase methods are not standalone methods to solve the complete flow field but track the interface between the existing phases.

Laminar and turbulent flows

Laminar flows are characterized by a highly ordered fluid flow where fluid flows in smooth non intersecting layers.

Turbulent flow is characterized by its irregular flow regime where fluid layers are not easily distinguished. Rapid changes are experienced in a turbulent flow regime. Instead of layers turbulent flows are made up of eddies of various sizes. These eddies constantly form and dissipate as they interact with each other in a rather chaotic manner.

The characterization between the laminar and turbulent nature of a flow is usually done on the basis of the Reynolds number (Re) for the flow. Pipe flows with Re < 2300 are laminar. Flows with Re > 4000 are considered turbulent. For flows with Re-value between these ranges the flow is said to be in a transition state.

If the problem is identified as a case of turbulent flow you must decide on the turbulence model to use for the problem. There are a number of choices available for this and not all models behave similarly in all situations. The following discussion is about making the choice of the turbulence model for the problem.

Turbulence Physics and Modeling

Turbulent flows have eddies of various scales. These eddies interact with each other causing rapid changes in flow properties. The highly chaotic nature of the flow makes modeling it a challenge.

The smallest turbulence eddies occurring in flows can have extremely small length scales. Direct simulation of these eddies requires mesh and temporal resolution which exceeds the computational capabilities of most modern computers. The computationally effective way is to model the behavior of the turbulent eddies in a time averaged flow field.

Turbulence models are used to predict the effects of turbulence in the fluid flow without resolving all of the small scales of motion that are associated with a turbulent flow. This reduces the amount of computing time necessary to obtain a solution to a fluid flow problem.

Most CFD solvers contain a broad selection of different turbulence models. The most commonly employed models in the industry are based on the Reynolds-averaged Navier-Stokes (RANS) equations.

Among RANS models there are eddy viscosity and Reynolds Stress formulations that need to be considered. Alternative approaches such as Detached Eddy Simulation (DES), Large Eddy Simulation (LES) and Direct Numerical Simulation (DNS) are also available in many CFD solvers. DNS approach, as the name suggests, is the approach that directly solves for eddies of all scales and does not involve any kind of modeling. It is mostly employed only for research purposes. Accuracy and computational requirements for these approaches is as follows.

RANS < DES < LES < DNS

When setting up a simulation it is your responsibility to select a suitable turbulence model for your application. Many models provide a reasonable level of accuracy for a broad range of applications while others are formulated specifically for certain flows. Among the most popular general purpose models are the one equation Spalart-Allmaras (SA) model and the two equation Shear Stress Transport (SST), and k-omega (k – ω) models.

Even while using general purpose turbulence models the choice of the model is important with respect to the problem being analyzed. Some models are better suited to some flows than others. The accuracy of a given turbulence model is highly case dependent and there are no established rules that can ensure correctness of the chosen model for a specific application. You must always proceed with caution and choose a turbulence model only after verifying its suitability to previously benchmarked problems of a similar nature.

In addition to the selection of a turbulence model it is also important to consider whether the flow is fully turbulent or transitional. If the flow is transitional it is important to include a transition model to properly account for this effect.

Wall modeling for turbulent flows	The use of a wall model is common practice when simulating high Reynolds Number viscous flows. The wall model relaxes the near wall meshing requirement to resolve the turbulent boundary layer and results in a reduction in required overall mesh count. Most wall models are formulated for simple boundary layer flows with no adverse pressure gradient. The application of these wall functions to non equilibrium boundary layers may impact accuracy.

Material Physics and Modeling

Setting up material properties is an important aspect of setting up a CFD simulation. Typically, CFD allows two types of materials, solids and fluids. Gases and liquids are both classified as fluids.

Setting up a solid model requires specification of density, specific heat and conductivity.

It is not required for a CFD model to have a solid material in the domain. These should be added only as required when an interaction between the fluid and the solid is present. Of the properties mentioned the specific heat and the conductivity are required only when energy equation is being solved.

Setting up a fluid model requires specification of the following properties:

- Density
- Viscosity
- Specific Heat
- Conductivity

- Viscoelastic properties, if fluid exhibits viscoelastic behavior
- Diffusivity for mass diffusion problems
- Porosity for porous materials

Of the properties mentioned above specific heat and the conductivity are required only when energy equation is being solved.

The material properties in a CFD simulation can be defined in a number of ways. The simplest definition is specifying the properties as a constant value. Once specified these constant values do not change during the simulation. For solids, the conductivity can also be specified as constant, but anisotropic. That is a different but constant conductivity in each normal direction.

For some cases, however, specifying a constant value of properties is not exactly representative of the actual material behavior. For example, for highly compressible flows specifying a constant density will lead to inaccurate results. For such flows it is prudent to use the ideal gas model for the fluid density, which uses the ideal gas law to calculate density at a given time step.

There are various options available to specify the different properties for the materials. You should choose the option that resembles the actual conditions as closely as possible. Some options are as follows:

- Linear or polynomial dependent on another variable (typically pressure, temperature or species)
- A user-defined function
- Ideal gas law for modeling density for compressible flows
- Boussinesq model for density in naturally convected flows in which small density variations encountered in such flows can be neglected in all but the buoyancy terms. This approach should not be used if large density variations are expected.

Heat Transfer Physics and Modeling

When temperature field variations are expected to have a significant impact on the flow properties, or the temperature distribution is of interest in the analysis, the energy equation must be included in the governing equations.

The heat transfer modes available are conduction, convection (natural and forced) and radiation.

For highly viscous flows viscous heating of the fluid must be taken into account. An example of flows where viscous heating can have a significant effect are the internal flows in microchannels.

For simulating processes where the fluid undergoes adiabatic compression compression heating of the fluid must be taken into account as well.

Prandtl number (Pr) is an important parameter when heat transfer within the boundary layer is being studied. Prandtl number can, in simple terms, be described as being proportional to the rate of growth of the velocity and thermal boundary layers. Smaller values of Pr indicate that thermal diffusion is more prominent than momentum diffusion. Thermal boundary layer grows faster than the velocity boundary layer.

When temperature effects are being studied and the flow is turbulent it is also critical to take into account the additional effect of turbulence on heat transfer properties. The turbulent Prandtl number is an important parameter in this case. Experiments show the average value to be 0.85 for most applications, but the actual value can vary between 0.7 and 0.9 depending on the specific problem.

If radiation effects are present in the problem you must choose the radiation parameters accordingly. In case of enclosure radiation view factor computation between the enclosure surfaces is critical. In case of external incident radiation, for example solar radiation, solar flux vector should be specified.

Chemistry Models

Selection of chemistry models can play a critical role in the results of simulations of combusting and reacting flows. When selecting a chemistry model you need to consider the rate of the chemical reaction in comparison to the times scales of other events in the flow. Some models are geared specifically towards turbulent flows where the turbulent time scale is much slower than the chemical reaction. Others are intended for the opposite scenario.

The Backward Facing Step Case

For the backward facing step case you will be solving the RANS equation, which includes terms for viscous effects. The flow field can be considered incompressible and single phase, as the Mach number is below 0.3 (it is actually about 0.13), and air is the only fluid present in the domain. The flow within the domain is turbulent, as the inlet Reynolds number is 36000. The flow can be solved for a steady state solution as the inlet conditions or the fluid properties are not time varying.

In the solver setups used in previous sections the backward facing step case was solved using the SA turbulence model. To illustrate the sensitivity of the solution to the selection of turbulence model, the results from two models, the one equation SA model and the two-equation SST turbulence model, are shown in the table below. For this application, experimental data shows a reattachment length of 6.26 m. The results show that the SST model has a lower deviation from the experimental observation indicating that it is more suitable for this flow than the SA model.

Table 9: Turbulence Model Sensitivity for Backward Facing Step Simulation

Turbulence model	Reattachment length (m)	Percent difference from experiment
SA	5.96	4.8 percent
SST	6.40	2.2 percent

Convergence Sensitivity

This section discusses and illustrates the effects of the level of convergence tolerance you provide to the solver, and also stresses on the need to look for other solution parameters before accepting a solution.

The convergence of the CFD solver gives an indication of how well it has solved the discretized equation set for the application of interest. Most CFD solvers measure convergence by monitoring the residuals, which represent the imbalance of terms in the governing equations at each iteration. As a general rule, the lower the residuals the lower the error due to imbalance in the terms in the equation. Some solvers also monitor the degree to which the solution is changing between iterations. As the simulation progresses, the residuals should fall and also the solutions to the equations should reach a stabilized value. It is a good practice to measure a solution quantity which may also capture the behavior of other solution variables to determine convergence. A converged solution means that the solver has done its job and produced the best solution it can for the given setup. However, that does not guarantee that the solution is correct in comparison to test or physics. The accuracy of the solution is a function of many other characteristics, some of which are described above.

CFD solver packages typically set default convergence criteria that are suitable for many applications. However, if high levels of accuracy are important it is necessary to monitor the impact of convergence on the solution for the application of interest. For steady state simulations this means monitoring the solution quantity of interest as the simulation is converged further. For transient applications it is also necessary to evaluate the convergence at each time step to see how it impacts the overall transient.

The Backward Facing Step Case

The backward facing step example is revisited to illustrate this point. Consider a steady state simulation of this flow. Figure 55 shows how the reattachment length estimated by the solver varies with each time step as the solver iterates over the equations to reach the desired residual levels. The target residual level has been set at 0.0001 for this solution. Using this criteria the converged solution for the location of reattachment point is determined to be 6.55 m downstream of the step.

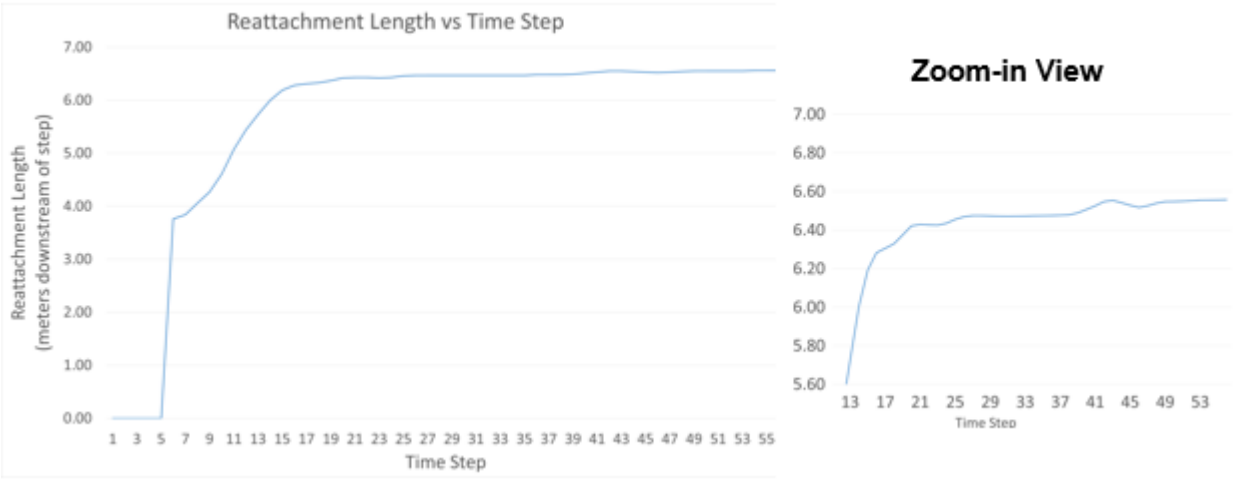

Figure 55: Convergence of Backward Facing Step Model

A closer inspection of the reattachment length convergence history in the second plot shows that the size of the separation zone does not stabilize until about time step 42. Therefore, the level of convergence necessary to obtain a high level of accuracy for the separation location corresponds to the levels corresponding to step 42 of the simulation. This value may or may not coincide with the solver's default convergence tolerance settings.

The solution can also be visualized to further inspect the convergence of the flow. The image below shows the solution at various time steps as the solution approaches convergence. Inspection of these figures indicates very little change in the flow after time step 20 when observed visually. However, as seen in the plot of reattachment length, the results change until stabilizing at time step 42. The decision of desired convergence tolerance thus depends on accuracy required from the CFD solution.

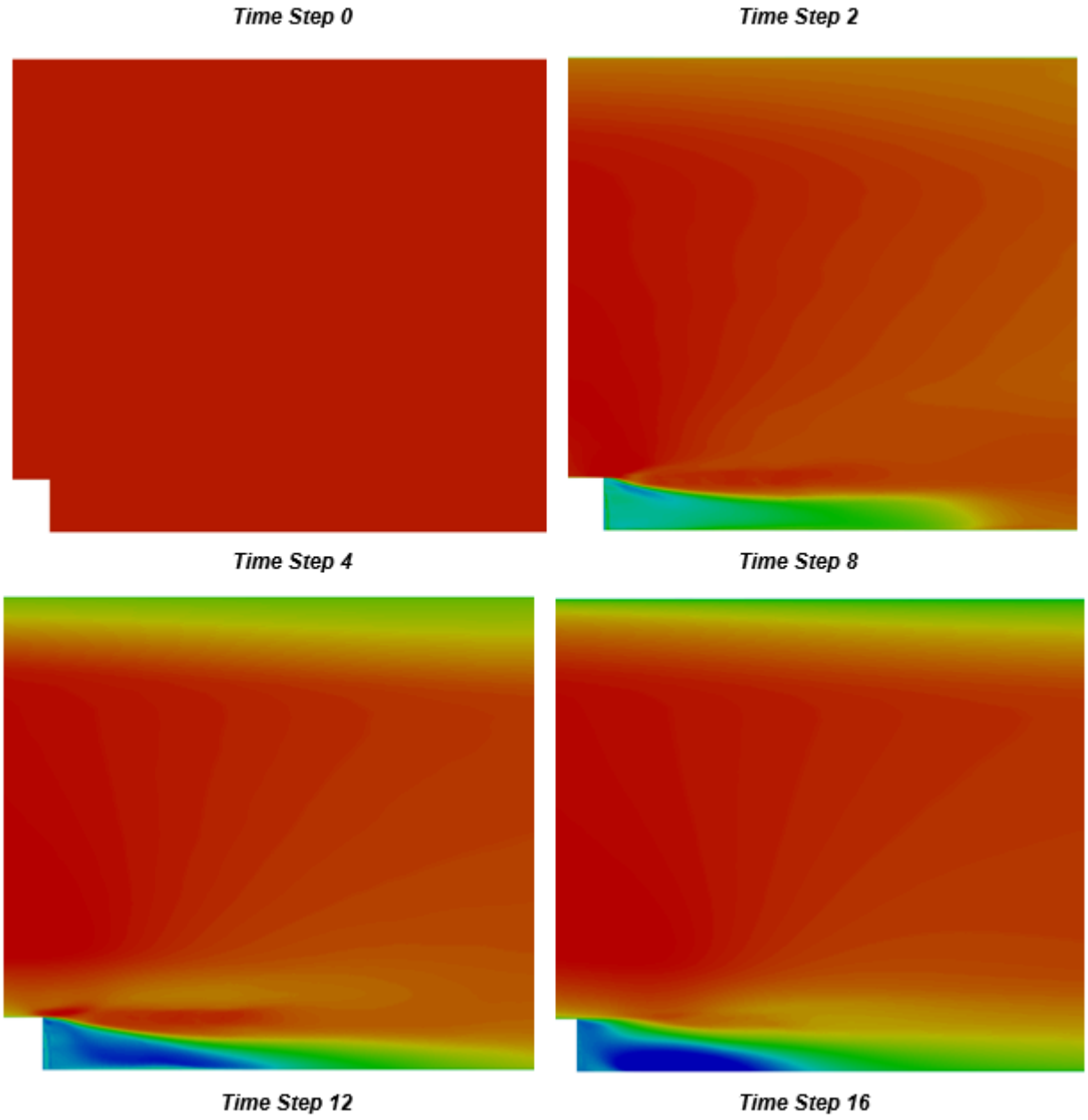

Figure 56: Convergence Behavior of the Backward Facing Step Simulation using the Shear Stress Transport (SST) Turbulence Model

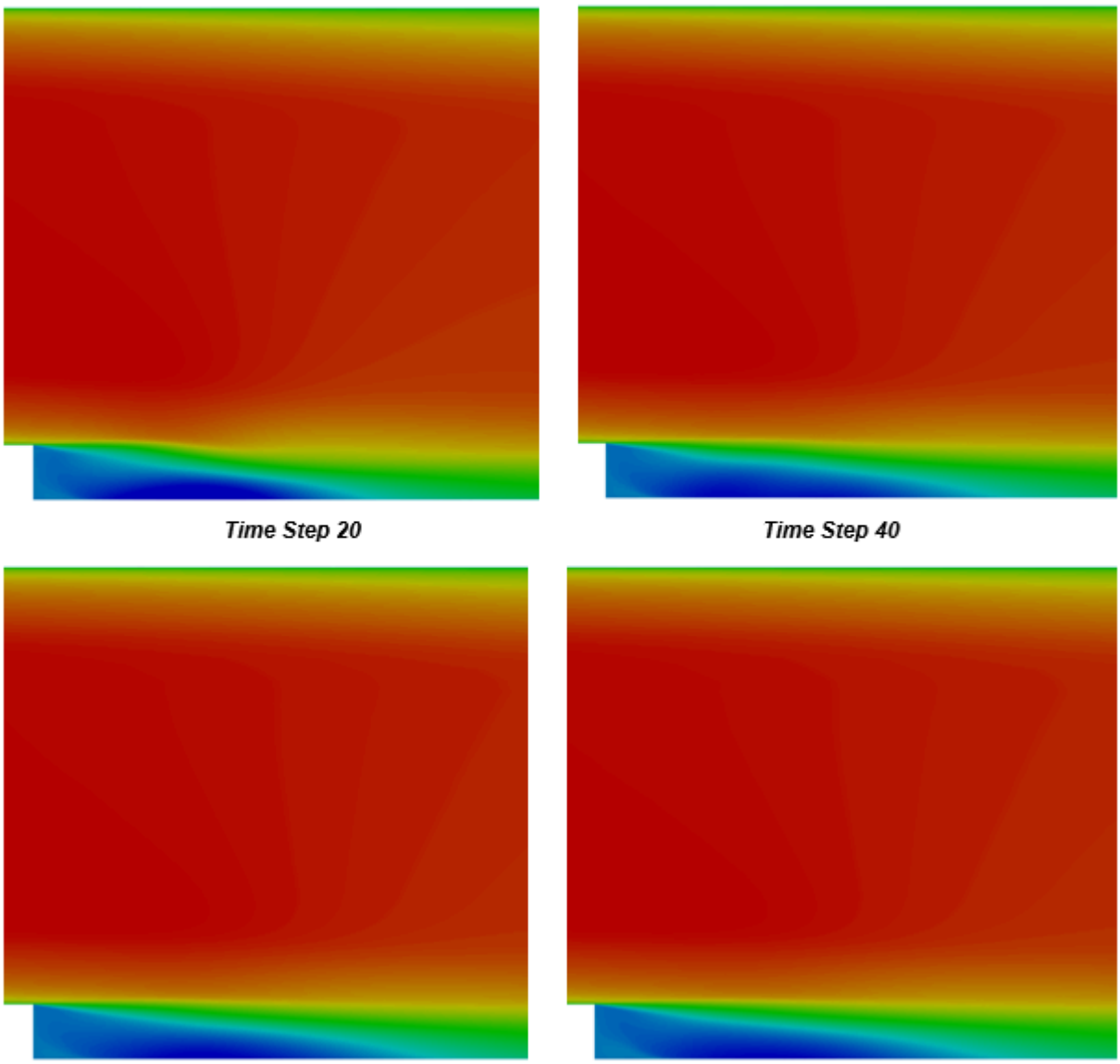

Figure 57: Convergence Behavior of the Backward Facing Step Simulation using the SST Turbulence Model

Each solver will be different and will perform differently on each application. It is up to you to investigate the proper convergence levels for your application. It should also be noted that convergence cannot be gauged by the residual metrics alone. Judging suitable convergence levels involves monitoring the convergence metrics, the solution quantity of interest, as well as looking at momentum and mass balances within the flow field when possible.

Conclusion

The modeling aspects described in this section are by no means complete for all of the flow simulations that can be imagined. This discussion is intended only to convey some of the common sources of variability among CFD model results.

A rigorous CFD analysis involves investigating all of the items described in this section. However, it is acknowledged that in practice it is necessary to rely on engineering judgment to reach a balance between producing results in a reasonable amount of time and performing a suitable level of quality assurance on the model. You should always consider the desired level of accuracy of the CFD model when deciding how much effort needs to be invested in quality assurance efforts.

An important observation to be made here is that this CFD solution may not be the true physical solution to the backward facing step problem. Over the course of this study, an attempt has been made to minimize the uncertainties by careful optimization of the problem setup with reference to each of the aspects discussed in the beginning of the section. It is meaningful now to go back to that discussion and recall that although these uncertainties can be minimized it is nearly impossible to eliminate them completely. At this stage, through optimization of all the critical aspects of your model, the uncertainties associated with these modeling aspects have been minimized. The solution at this stage can be deemed as the best possible CFD solution with respect to the aspects of the model discussed in this section. The difference observed between this numerical solution and the true physical solution can be attributed to the following factors:

- Mathematical modeling: The mathematical models which are used to represent the physical processes are not an exact representation of the physical phenomena. Even the best available models are based on certain approximations and simplifications.
- Input errors: These are the errors due to uncertainties of certain inputs such as the boundary condition specification. For example, even when the boundary conditions are specified as equivalent to the available experimental values there might be some interpolation errors when these values are projected on to the CFD domain.
- Uncertainties in experimental results and measurements: This discussion focused on a few guidelines to setup the CFD simulation model for a given problem. However, one key aspect that cannot be overlooked while comparing CFD results with experimental results of a problem is the uncertainties present in the experiment. An experiment, just like CFD analysis, is a controlled simulation of the problem. There are various sources of errors and uncertainties in the experiments such as uncertainties in the setup and environmental conditions in which the experiment is conducted, uncertanties in the measurement instruments used in the experiment and uncertainties in the post-processing equipment.

Due diligence is required to carry out an experiment with application of refined experimental methods to achieve a reliable set of results. A similar diligence, when applied to carrying out a CFD simulation, will help achieve a reliable set of results from CFD. An analysis completed with the above mentioned guidelines supporting the procedure will provide a result which for most purposes can be used as a substitute of the true value of the solution.

References

[1] Roache, P.J., Verification and Validation in Computational Science and Engineering, Hermosa Publishers, Albuquerque, New Mexico, 1998.

Index

Special Characters

A

B

C

D

F

G

H

I

K

L

M

N

O

P

Q

R

S

T

V

W

Z